

## Review Article

# Computation of MHD Equilibrium of Tokamak Plasma

TATSUOKI TAKEDA AND SHINJI TOKUDA

*Japan Atomic Energy Research Institute,  
Naka-Machi, Naka-Gun, Ibaraki-Ken, Japan 311-01*

Received January 1, 1989; revised January 5, 1990

Computation of the MHD equilibrium of a tokamak plasma is reviewed as comprehensively as possible. The basic equation of this problem is the Grad-Shafranov equation. General remarks on this equation and related issues are, first, summarized with historical survey of the MHD equilibrium solution, where some mathematical discussions on the numerical analysis of the problem are also presented. Distinguishing features of this problem are seen in treatment of the boundary condition and constraining conditions and we describe them in a rather detailed manner. In the main part of this review paper we present a concrete description on the numerical procedures of the MHD equilibrium solvers which are classified into two groups, that is, the real space solvers and the inverse equilibrium solvers. We also describe topics on more general equilibrium models, that is, the equilibrium with steady flow, anisotropic equilibria, equilibria with specified current sources, and equilibrium evolution. Brief comments on three-dimensional equilibrium solvers are also presented. As for application of the MHD equilibrium solvers we present only a small part, that is, beta limit optimization, design of external coils, analysis of positional instability, and analysis of experimentally obtained data from electromagnetic measurement. It is concluded that among various kinds of numerical solution methods we can usually find most adequate ones for the present problem.

© 1991 Academic Press, Inc.

## CONTENTS

1. *Introduction.*
2. *General remarks on tokamak equilibrium.* 2.1. Historical survey of MHD equilibrium solution. 2.2. Grad-Shafranov equation and magnetic flux function. 2.3. Flux coordinate system. 2.4. Flux surface average. 2.5. Quantities characterizing a tokamak equilibrium. 2.6. Integral relation. 2.7. Approximation of the Grad-Shafranov equation. 2.8. Mathematical remarks on the Grad-Shafranov equation.
3. *Boundary conditions and constraining conditions.* 3.1. Boundary conditions and vacuum field. 3.2. Nonlinear eigenvalue problem. 3.3. FCT equilibrium and GDE.
4. *Numerical methods for inversion of the Grad-Shafranov operator.* 4.1. Real space solution methods. 4.1.1. Finite difference method. 4.1.2. Finite element method. 4.1.3. Other methods. 4.2. Inverse equilibrium methods. 4.2.1. Iterative reconstruction of metrics. 4.2.2. Direct solution of inverse equilibrium equation. 4.2.3. Methods of expansion in poloidal angle. 4.3. Numerical mapping to flux coordinates. 4.4. Numerical technique for vector processor.

5. *More general equilibrium models.* 5.1. Equilibrium with steady flow. 5.2. Anisotropic equilibria. 5.3. Equilibria with specified current sources. 5.4. Equilibrium evolution. 5.5. Comments on three-dimensional equilibrium solvers.
6. *Applications.* 6.1. Beta limit optimization. 6.2. Engineering applications. 6.3. Experimental analyses.
7. *Summary and discussion.*

## 1. INTRODUCTION

As the first candidate of the fusion reactor many tokamak-type devices [1–3] are being studied extensively. With the fusion devices becoming larger and more complicated and also with more detailed experiments being carried out needs for further quantitative analyses are increased. Consequently, the role of computations in the field of the tokamak fusion research becomes very large [4–6]. In various kinds of computation the solution of an MHD equilibrium equation of a toroidal plasma (the Grad-Shafranov equation) [7, 8] is necessary frequently and plays a fundamental role. There are a variety of MHD equilibrium codes developed depending on different applications.

One of the engineering applications of the MHD equilibrium solvers is to calculate the external magnetic field and to design an external magnetic field coil system by giving a set of plasma parameters and geometrical parameters. Here the determination of a configuration of external conductors is the aim, and only global or averaged equilibrium quantities such as the total plasma current and averaged pressure are necessary. In such cases the requirement for accuracy of the equilibrium calculation is not usually so stringent but intelligibility of a numerical code is considered to be more essential. In applications for experimental analyses a plasma equilibrium is conjectured from a limited number of parameters and the results are utilized for further analyses of the plasma behavior. In this case a unique correspondence between the experimentally observed data and the input data for the numerical calculation is desirable. On the other hand, in theoretical analysis extremely high resolution is required and a wide range of variation of the parameters is usually considered. If one uses the equilibrium solution for the linear MHD stability analyses derivatives of various quantities such as current density and magnetic field should be obtained with a very high accuracy. A high accuracy calculation is pursued by using a special numerical scheme or by increasing the mesh number. Usually, however, in the stability calculation only the information inside the plasma is important and the concrete configuration of external coil system consistent with engineering requirements is not important.

The above description is for a scalar pressure equilibrium without a plasma flow. However, tensor pressure (anisotropic pressure) and flow of a plasma should, sometimes, be taken into account for the equilibrium analysis of an intensely heated plasma. In the above-described “conventional” equilibrium codes the plasma current distribution is given somewhat arbitrarily and consistency between the current distribution and a transport process is not assured generally. Therefore, an equilibrium code with self-consistently determined current distribution, and an

equilibrium evolution code made of a combination of a two-dimensional equilibrium code and a one-dimensional tokamak transport code are important for experimental and theoretical analyses. Though the tokamak plasma is essentially axisymmetric, the three-dimensional feature becomes important sometimes. Three-dimensional codes developed for non-axisymmetric systems are useful for these purposes.

In this article we review the MHD equilibrium computation of a tokamak plasma as comprehensively as possible. We are mainly concerned with numerical schemes and algorithms for solving the Grad-Shafranov equation developed for the various applications. The general MHD theory which the problems in this article are based on are described in Refs. [9–15]. In Section 2 we summarize properties of the MHD equilibrium of a tokamak plasma and some general remarks necessary for the computation of the equilibrium. We also give a brief description of approximate methods for the Grad-Shafranov equation based on the inverse aspect ratio expansion and some mathematical remarks on the equation. In Section 3, we discuss the boundary conditions and the constraining conditions imposed on the Grad-Shafranov equation. Here two main algorithms developed to solve the Grad-Shafranov equation for a tokamak plasma are described, i.e., the nonlinear eigenvalue method and the FCT (flux conserving tokamak) algorithm. Section 4 is the core of this review article. We describe numerical methods developed so far for solving the Grad-Shafranov equation, which are classified into two groups, i.e., the real space solution methods and the inverse equilibrium methods. In this section we also describe a numerical method to construct a flux coordinate system from a numerically computed equilibrium (numerical mapping). A numerical technique concerning the use of a vector processor to solve the Grad-Shafranov equation is also mentioned. Section 5 is devoted to more general equilibrium models. These are equilibria with anisotropic pressure or flow, an equilibrium with self-consistently given current sources, and equilibrium evolution. Comments on the three-dimensional equilibrium solvers are also given in this section. In Section 6 we describe applications of the equilibrium solvers from various viewpoints. In this section we describe beta limit optimization, determination of external magnetic fields, positional instability analyses, and determination of tokamak equilibria from experimentally obtained electromagnetic signals. Section 7 gives a summary and a discussion.

## 2. GENERAL REMARKS ON TOKAMAK EQUILIBRIUM

### 2.1. *Historical Survey of MHD Equilibrium Solution*

As described later in detail, the basic equation of the axisymmetric toroidal equilibrium is the second-order elliptic partial differential equation of the magnetic flux function  $\psi$ . This equation was derived independently by Grad [16], Shafranov [17], and Schlüter [18], and it is called the Grad-Shafranov equation or the Grad-Schlüter-Shafranov equation. Throughout this review article we call it the

Grad-Shafranov equation. The right-hand side of the Grad-Shafranov equation represents the plasma current and if it is a linear function of  $\psi$  or constant, one can obtain an exact analytical solution of the equation [19–21]; otherwise one should rely on approximate solutions derived by some kind of expansion or on numerical solutions described in this article. In the early stage of the tokamak research, analytical equilibria were studied extensively. Many works in this stage are still important as the basis of the inverse equilibrium solvers which became powerful means to analyze the three-dimensional equilibrium as well as the two-dimensional one in 1980s. In this category of the analytical solutions two different approaches were generally taken. One is based on the expansion of metrics by the plasma radius (the near-axis expansion) [22–24] and the other is based on the expansion of the solution  $\psi$  by the inverse aspect ratio  $\epsilon$  (defined in 2.5). The latter approach is further subdivided into the method based on the low beta tokamak ordering [25–27], and the method based on the high beta tokamak ordering [12, 15, 28–30].

Though several numerical equilibrium codes for other types of devices [31] were developed earlier, a numerical equilibrium code for the analysis of a tokamak plasma was first published by Callen and Dory [32]. This code solves a fixed boundary equilibrium of a tokamak with a circular cross section by using the FDM (finite difference method) on the  $(r, z)$  rectangular mesh and the SOR (successive overrelaxation) algorithm. Throughout the 1970s various numerical methods were developed, investigated, and applied to various numerical equilibrium codes to solve the Grad-Shafranov equation [7, 33–38]. Among them the nonlinear eigenvalue method [7, 37], the semi-fixed boundary method [7, 38], employing the least square fitting of the plasma surface [7] played crucial roles in the subsequent progress of the equilibrium analyses. The efficient solvers based on the DCR (double cyclic reduction) method and the FACR (Fourier analysis cyclic reduction) method described later were made realizable by application of these methods. Numerical schemes, such as the FDM and the FEM (finite element method), the Green's function method, and the expansion method were also applied to develop equilibrium solvers. As for the algorithms to solve the resulting matrix equations from the FDM discretization, initially the iterative methods such as the SOR and the ADI (alternative direction implicit iteration) method [31] were favourably employed. Before the nonlinear eigenvalue method was established, combination of the ADI and the Marder-Weitzner's three-step iteration method [34] was one of the most useful solution methods [39] to cope with the nonlinearity arising from the free-boundary equilibrium problem. Afterward, with the progress of the computer system, the direct method became more favourable and solvers based on the cyclic reduction methods become standard. Recently, however, iterative methods such as the MGM (multi-grid method) are again being used because they are generally more favourable than the direct method for parallel processors. Equilibrium codes based on the Green's function method, in which the Green's function of the Grad-Shafranov operator is directly integrated, were also developed [40, 41]. This method is simple and intelligible. However, as it takes much

computing time in comparison with other more efficient codes and there is a difficulty associated with the inherent singularity, the code is not used widely at present. Application of the toroidal multipolar expansion to the MHD equilibrium solvers was proposed by Feneberg and Lackner [36] and several codes were developed [42, 43]. But they could not become widely used codes, too. The FEM equilibrium solvers are less efficient than the FDM solvers but they seem useful for some special purposes such as the analyses of the flow equilibria [44, 45]. And mathematically strict analysis of the solution method itself is carried out concerning the FEM solvers. The conformal mapping method developed by Goedbloed [46] is not also the widely used one but it is still useful for some stability problems because of its mathematical sophistication.

In parallel with the development of the above-described real space equilibrium solvers, studies of the inverse equilibrium solutions advantageous for the subsequent processing based on the flux coordinate system and for the analysis of the three-dimensional equilibria have been continued. Because usual MHD stability codes are developed on the flux coordinate system mapping procedure is required by which various quantities are mapped from the  $(r, z)$  space to the  $(\psi, \chi)$  space in the flux coordinate system where  $\chi$  is a poloidal angle. The equilibrium solution given by the inverse equilibrium solver is, therefore, directly used for such stability analyses. Several types of the inverse equilibrium solvers, i.e., the iterative metric methods, the direct inverse solution methods, and the methods of expansion in poloidal angle, were developed [47–51]. But at present the numerical codes based on the methods of expansion in poloidal angle [50] are used most widely among them for various purposes. This method was used also to develop an efficient compact equilibrium solver run on a small personal computer [52].

With the progress of the tokamak research interest in the high beta tokamak equilibria was increased in order to realize an efficient fusion reactor. Correspondingly, the FCT concept was proposed and the FCT equilibrium was studied extensively by many authors [53–56]. Clarke and Sigmar [54] derived several fundamental relations among the equilibrium quantities in the high beta region by solving the integral relation for the circular cross sectional tokamak with a high aspect ratio under the FCT condition. This result was extended by Mizoguchi *et al.* to include the case of the equilibrium with the elliptical cross section [55]. Dory and Peng [53] formulated the numerical procedure to solve the Grad–Shafranov equation under the FCT condition and obtained numerically equilibria with very high beta value as about 30%. Several issues concerning the boundary conditions of the FCT equilibrium were discussed by Nelson [57] and Albert [58]. Spies showed that the entropy density (adiabatic pressure)  $\mu$  is more appropriately used for the expression of the FCT condition rather than the pressure  $p$  [56]. Owing to these basic studies it became easy to solve the high beta tokamak equilibrium by the FCT algorithm, and afterward the FCT equilibrium solvers play main roles in the stability analyses of a high beta tokamak [59, 60], analyses of the adiabatic compression [58], and equilibrium analyses subject to resistive diffusion [61]. Typical numerical procedures are summarized in Table I.

TABLE I  
Summary of Numerical Procedures for Equilibrium Solution

| Issues  | Authors   | Other references                              |
|---|---|---|
| a. Basic Contributions                            |   |   |
| Derivation of the Grad-Shafranov equation         | H. Grad and H. Rubin [16],<br>V. D. Shafranov [17],<br>R. Lüst and A. Schlüter [18] | [91]  |
| Low beta tokamak ordering and inverse equilibrium | J. M. Greene <i>et al.</i> [27]   | [25, 26]                                      |
| High beta tokamak ordering                        | H. R. Strauss [28], F. A. Hass [29]   | [12, 15, 30]                                  |
| Nonlinear eigenvalue formulation                  | K. Lackner [7]  | [37, 48, 93–96, 98–101]                       |
| FCT concept                                       | J. F. Clarke and D. J. Sigmar [54]  | [55]  |
| FCT algorithm                                     | R. A. Dory and Y.-K. M. Peng [53]   | [56–61]                                       |
| Algorithms  | Authors   | Remarks                                       |
| b. Real Space Solvers                             |   |   |
| ADI + three-step iteration                        | B. Marder and H. Weitzner [34]  | Free boundary,<br>old method                  |
| FDM + SOR   | J. D. Callen and R. A. Dory [32]  | Fixed boundary                                |
| FDM + MGM   | B. J. Braams [112]  |   |
| FDM + DCR   | J. L. Johnson <i>et al.</i> [38]  | Semi-fixed boundary with least square fitting |
| FEM   | S. Semenzato <i>et al.</i> [44],<br>W. Kerner and O. Jandl [45]                     | Equilibrium with flow                         |
|   |   | [48, 85, 86]                                  |
| c. Inverse Equilibrium Solvers                    |   |   |
| Iterative metric method                           | J. DeLucia <i>et al.</i> [49]   |   |
| Direct inverse method                             | P. N. Vabishchevich <i>et al.</i> [47]  |   |
| Expansion in poloidal angle                       | L. L. Lao <i>et al.</i> [50]  | Variational moment method, 3D equilibrium     |
|   |   | [52, 123, 180–183]                            |
| d. Other Solvers                                  |   |   |
| Green's function method                           | H. Ninomiya <i>et al.</i> [40]  | Simple, inefficient                           |
| Expansion with orthogonal functions               | S. Seki <i>et al.</i> [42],<br>F. Alladio <i>et al.</i> [43]                        |   |
| Conformal mapping method                          | J. P. Goedbloed [46]  | Use of fast Hilbert transform                 |

## 2.2. Grad-Shafranov Equation and Magnetic Flux Function

The basic equations of the ideal MHD equilibrium of a plasma with scalar pressure and without flow are

$$\nabla p = \mathbf{J} \times \mathbf{B}, \quad (2.1)$$

$$\nabla \times \mathbf{B} = \mu_0 \mathbf{J}, \quad (2.2)$$

$$\nabla \cdot \mathbf{B} = 0, \quad (2.3)$$

where  $\mathbf{J}$  and  $\mathbf{B}$  are the current density and magnetic flux density, respectively, and  $\mu_0$  is the magnetic permeability of the vacuum. Throughout this review article, we adopt SI units unless otherwise specified. For an axisymmetric system such as a tokamak plasma we can define a magnetic flux function  $\psi$  from the toroidal component of vector potential  $A_\phi$  as

$$\psi = -rA_\phi. \quad (2.4)$$

By using this single scalar function  $\psi$  in a cylindrical coordinate system  $(r, z, \phi)$  (Fig. 2.1) the magnetic field  $\mathbf{B}$  is represented by

$$\mathbf{B} = \nabla\phi \times \nabla\psi + F\nabla\phi, \quad (2.5)$$

where toroidal field function (poloidal current function)  $F$  is expressed by using the toroidal field  $B_t$ , as

$$F = rB_t. \quad (2.6)$$

Then the set of the equilibrium equations, Eqs. (2.1)–(2.3), is reduced to a second-order partial differential equation called Grad-Shafranov equation [16–18] as

$$\Delta^*\psi \equiv \frac{\partial^2\psi}{\partial r^2} - \frac{1}{r} \frac{\partial\psi}{\partial r} + \frac{\partial^2\psi}{\partial z^2} = f(\psi, r), \quad (2.7)$$

$$f(\psi, r) \equiv \mu_0 r J_\phi, \quad (2.8)$$

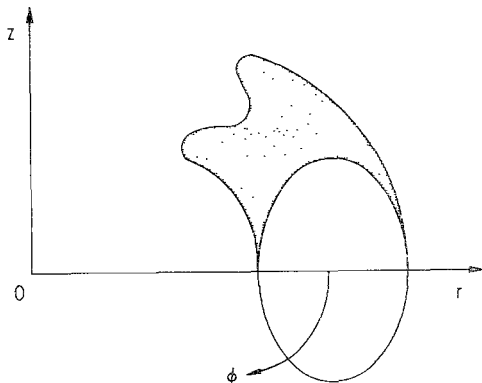


FIG. 2.1. A cylindrical coordinate system  $(r, z, \phi)$  used for the equilibrium calculation.

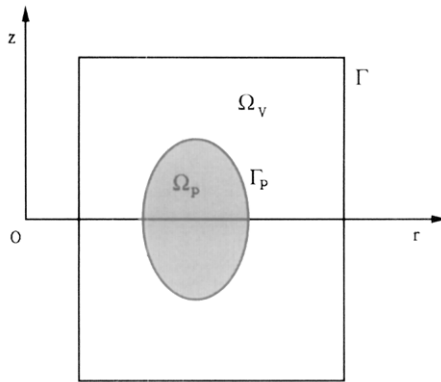


FIG. 2.2. Region for the equilibrium calculation.  $\Omega_p$ : plasma,  $\Omega_v$ : vacuum,  $\Gamma_p$ : plasma-vacuum boundary,  $\Gamma$ : computational boundary.

where the toroidal component of the plasma current  $J_\phi$  is given by

$$J_\phi = -r \frac{dp}{d\psi} - \frac{1}{\mu_0 r} \frac{F}{d\psi} \frac{dF}{d\psi}. \quad (2.9)$$

The above Grad-Shafranov equation is solved in a two-dimensional region as shown in Fig. 2.2, where  $\Omega_p$ ,  $\Omega_v$ ,  $\Gamma_p$ , and  $\Gamma$  denote the plasma region, vacuum region, plasma-vacuum surface, and the computational boundary.

It is easily seen that the pressure function  $p$  and toroidal field function  $F$  are functions of only  $\psi$ . The magnetic flux function  $\psi$  has an ambiguity of shift of constant value and, hereafter, we define the  $\psi$  value at the plasma surface to be zero; inside the surface the value of the magnetic flux function is negative unless otherwise

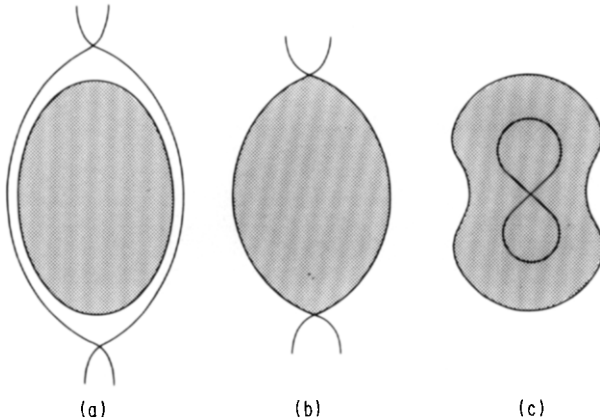


FIG. 2.3. Classification of the equilibria according to topology of magnetic surfaces. (a) Separatrix magnetic surface is located outside the plasma. (b) Separatrix magnetic surface coincides the plasma surface. (c) Separatrix magnetic surface is located inside the plasma surface.

remarked. In the case of an axisymmetric toroidal equilibrium the structure of nested magnetic surfaces is clearly defined by the contours of the magnetic flux function  $\psi$ . From the practical viewpoint of equilibrium computation the structures of the magnetic surfaces are classified topologically into three groups as shown in Fig. 2.3. In the case (a), the separatrix magnetic surface is outside the plasma region and the magnetic surfaces inside the plasma region are nested tori made of simply connected contours of the magnetic flux function. There is only one elliptic singular point of the magnetic flux function inside the plasma region, which is called a magnetic axis. When the separatrix magnetic surface coincides with the plasma surface we call it the case (b) equilibrium. In this case hyperbolic singularities ( $X$ -points) appear on the plasma surface and multiplet plasma equilibrium with several magnetic axes may be observed. This kind of configuration is also found in a divertor tokamak. From the viewpoint of numerical calculation difficulty may be found because some metric quantities diverge at the  $X$ -point on the separatrix and usually stability calculation is carried out by assuming the plasma surface is located just inside the separatrix. If the separatrix magnetic surfaces exist inside the plasma region it is classified as the case (c) equilibrium. In this case there may appear several magnetic axes and magnetic islands inside the plasma region. An example of this type is an equilibrium of the doublet tokamaks [62].

In this article we mainly describe the case (a) equilibrium. It should be noted that a finite toroidal current inside the plasma region is needed to realize the above equilibria as the following integral of the poloidal magnetic field strength  $B_p$  yields a finite value,

$$I_p = \frac{1}{\mu_0} \oint B_p dl. \quad (2.10)$$

In other words the above axisymmetrically nested magnetic surfaces cannot be realized by the current flowing in external coils alone. Plasma current or current in internal conductors is necessary for the above axisymmetric toroidal equilibria as in the case of a tokamak and an RFP [63] or in the case of a multipole [64], a levitron [65], and a spherator [66], respectively.

### 2.3. Flux Coordinate System

Plasma behaviors along the magnetic surfaces and across them are extremely different. It is, therefore, desirable or, sometimes, inevitable to employ a flux coordinate system [10, 11] based on the contours of the magnetic flux function to analyze instabilities or transport. In the previously described case (a) equilibrium the  $\psi$  contours have a topologically same structure with concentric circles and a flux coordinate system similar to a toroidal coordinate system is easily defined.

In this article we adopt a flux coordinate system  $(\psi, \theta, \phi)$ , where  $\phi$  is the toroidal angle defined in a real space and  $\theta$  is an arbitrarily chosen poloidal angle (Fig. 2.4).

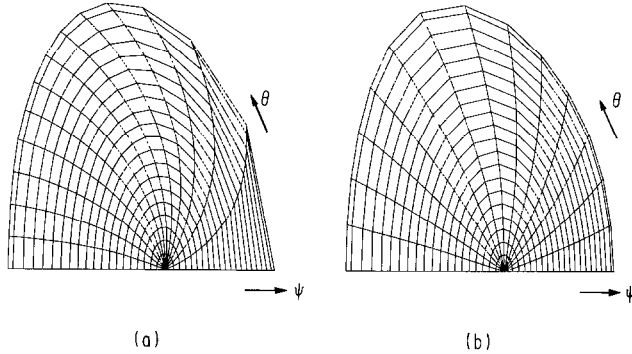


FIG. 2.4. A flux coordinate system  $(\psi, \theta)$  used for the stability calculation: (a) An example of the coordinate system with straight field lines; and (b) an example of the coordinate system with constant arc length is presented. In both coordinate systems the coordinate in the toroidal direction is the usual toroidal angle.

In general this system is a nonorthogonal coordinate system and the line element is given as

$$dl^2 = g_{\psi\psi} d\psi^2 + 2g_{\psi\theta} d\psi d\theta + g_{\theta\theta} d\theta^2 + g_{\phi\phi} d\phi^2, \quad (2.11)$$

$$g_{\psi\psi} = \frac{\mathcal{J}^2}{r^2} |\nabla\theta|^2, \quad g_{\psi\theta} = -\frac{\mathcal{J}^2}{r^2} \nabla\psi \cdot \nabla\theta, \quad g_{\theta\theta} = \frac{\mathcal{J}^2}{r^2} |\nabla\psi|^2, \quad g_{\phi\phi} = r^2, \quad (2.12)$$

$$\mathcal{J} = [(\nabla\psi \times \nabla\theta) \cdot \nabla\phi]^{-1}. \quad (2.13)$$

Because  $\theta$  is the angular coordinate with modulus of  $2\pi$  the following constraint is imposed to the Jacobian  $\mathcal{J}$ ,

$$\oint \frac{dl}{\mathcal{J} B_p} = 2\pi. \quad (2.14)$$

By choosing an appropriate  $\mathcal{J}$  we can specify a coordinate system. For example, the coordinate system with straight field lines,

$$\left( \frac{\partial\theta}{\partial l} \right)_\psi = \frac{F}{q} \frac{1}{r^2 B_p}, \quad (2.15)$$

which is often adopted for stability analyses is constructed by choosing a Jacobian as

$$\mathcal{J} = \frac{r^2}{F} q(\psi), \quad (2.16)$$

where the safety factor  $q(\psi)$  is defined as

$$q(\psi) \equiv \frac{F}{2\pi} \oint \frac{dl}{r^2 B_p} = \frac{F}{2\pi} \oint \frac{dl}{r |\nabla\psi|}. \quad (2.17)$$

Any quantity expressed as a function of only a magnetic surface label (such as the safety factor, the poloidal/toroidal magnetic flux functions, flux surface averages in the next subsection) is called a surface quantity.

#### 2.4. Flux Surface Average

The flux surface average  $\langle X \rangle$  of a variable  $X$  is defined as

$$\langle X \rangle \equiv \lim_{\Delta V \rightarrow 0} \frac{1}{\Delta V} \int_{\Psi}^{\Psi + \Delta \Psi} X dV = 2\pi \int_0^{2\pi} \frac{X \mathcal{J} d\theta}{(dV/d\Psi)} = 2\pi \oint \frac{(X/B_p) dl}{(dV/d\Psi)}, \quad (2.18)$$

$$\frac{dV}{d\Psi} = 2\pi \int_0^{2\pi} \mathcal{J} d\theta = 2\pi \oint \frac{dl}{B_p}, \quad (2.19)$$

where  $V(\Psi)$  is a volume inside a magnetic surface specified by an arbitrarily chosen label  $\Psi$ , such as, the poloidal magnetic flux  $\psi \equiv \int \mathbf{B} \cdot \nabla \theta dV/(2\pi)^2$ , the toroidal magnetic flux  $\chi \equiv \int \mathbf{B} \cdot \nabla \phi dV/(2\pi)^2$ , and so on. In the following we adopt the poloidal flux coordinate  $\psi$  as the magnetic surface label unless otherwise specified. It is needless to say that a surface quantity itself is also a label of a magnetic surface. Many important quantities appearing in the MHD stability analyses [67, 68] and transport analyses [69] are represented by the flux surface average. In the following we describe two important expressions derived by using the surface averaged quantities.

First, we describe the parallel component of the plasma current and discuss the consequence of the quasi-neutral condition. The quasi-neutral condition is expressed as

$$\operatorname{div} \mathbf{J} = 0, \quad (2.20)$$

where

$$\mathbf{J} = \mathbf{J}_\perp + J_\parallel \frac{\mathbf{B}}{B}, \quad (2.21)$$

$$\mathbf{J}_\perp = \frac{\mathbf{B} \times \nabla p}{B^2}. \quad (2.22)$$

From the above equations we get the divergence of the perpendicular current as

$$\operatorname{div} \mathbf{J}_\perp = -\frac{2F}{\mathcal{J}} \frac{\partial B}{\partial \theta} \frac{1}{B^3} \frac{dp}{d\psi}. \quad (2.23)$$

As  $\partial B/\partial \theta \neq 0$  in general, the divergence of the perpendicular current has a finite value, which means that the parallel component of the current always exists in an axisymmetric toroidal equilibrium. If we rewrite the expression for the current  $\mathbf{J}$  as

$$\mathbf{J} = K \mathbf{B} + J_\phi \nabla \phi, \quad (2.24)$$

with the coefficient  $K$  being a function of only  $\psi$  and for the case of a scalar pressure it is represented as

$$K(\psi) = -\frac{1}{\mu_0} \frac{dF}{d\psi}. \quad (2.25)$$

After some manipulations the parallel current  $J_{||}$  is derived as

$$J_{||} = -\frac{F}{B} \frac{dp}{d\psi} \left( 1 - \frac{B^2}{\langle B^2 \rangle} \right) + \frac{\langle \mathbf{J} \cdot \mathbf{B} \rangle}{\langle B^2 \rangle} B. \quad (2.26)$$

The current of the first term of this equation is the well-known Pfirsch–Schlüter current which maintains the quasi-neutral condition. This current originates from the charge separation due to the toroidicity. The divergence-free current of the second term assures the momentum balance along the magnetic lines of force and it is essential for confining the tokamak plasma.

The second example of the flux surface average is the surface averaged Grad–Shafranov equation, which is important in relation with the FCT algorithm [53] and the equilibrium evolution. By averaging the Grad–Shafranov equation on the magnetic surface we obtain the equation

$$\frac{1}{dV/d\psi} \frac{d}{d\psi} \left( \frac{dV}{d\psi} \langle B_p^2 \rangle \right) = -\mu_0 \frac{dp}{d\psi} - F \frac{dF}{d\psi} A, \quad (2.27)$$

where

$$A \equiv \left\langle \frac{1}{r^2} \right\rangle = \left( \frac{2\pi}{(dV/d\psi)} \right) \oint \frac{dl}{r |\nabla \psi|} = \frac{4\pi^2}{F} \frac{q}{(dV/d\psi)}. \quad (2.28)$$

After integrating the equation with respect to  $\psi$  we again average it over the whole volume, and obtain the equation

$$\beta_p = 1 + \int_{\psi_0}^{\psi_s} \frac{V(\psi)}{\langle B_p^2 \rangle_s V_s} \left\{ 2F \frac{dF}{d\psi} A + \langle B_p^2 \rangle \frac{d}{d\psi} \left[ \ln \frac{(dV/d\psi) \langle B_p^2 \rangle}{V} \right] \right\} d\psi, \quad (2.29)$$

where the suffix  $s$  denotes the values at the plasma surface and the poloidal beta  $\beta_p$  is defined as

$$\beta_p \equiv 2\mu_0 \frac{1}{V_s} \int \frac{p dV}{\langle B_p^2 \rangle_s}. \quad (2.30)$$

From Eq. (2.29) it is shown that  $dF/d\psi < 0$  (paramagnetic) corresponds to  $\beta_p < 1$  and  $dF/d\psi > 0$  (diamagnetic) corresponds to  $\beta_p > 1$ , because the second term of the integrand is a small quantity.

### 2.5. Quantities Characterizing a Tokamak Equilibrium

In this section we summarize the quantities characterizing a tokamak plasma and ranges of values of these parameters. First, several geometrical parameters should be mentioned. Because the tokamak plasma is of toroidal shape there are major radius  $R_0$  and minor radius  $a$  which characterize the size of the torus. Inverse aspect ratio  $\varepsilon$  is defined as

$$\varepsilon = \frac{a}{R_0}. \quad (2.31)$$

Usually the value of the aspect ratio  $\varepsilon^{-1}$  is larger than 3 for a tokamak but sometimes a very fat tokamak with a low aspect ratio as  $\varepsilon^{-1} \approx 2$  is considered. An earlier tokamak has a plasma cross section of a circular shape but a noncircular cross sectional tokamak is preferred because higher plasma current and higher beta value are attainable. For such a tokamak an ellipticity  $\kappa$  and a triangularity  $\delta$  of the plasma cross section are defined as shown in Fig. 2.5. The following definition of the noncircularity is also widely used:

$$r = R_0 + a \cos(\theta - \delta \sin 2\theta), \quad (2.32)$$

$$z = \kappa a \sin \theta. \quad (2.33)$$

When the ellipticity  $\kappa$  is very large the plasma suffers from the vertical positional instability (see 6.2) and the range of the ellipticity is usually between 1 and approximately 2.

The value of the safety factor defined by Eq. (2.17),  $q_\psi$  (flux  $q$ ), is known only after the equilibrium is solved. Therefore a simpler definition of the safety factor,  $q_J$  (current  $q$ ) is often employed for the purpose of rough calculation of experimental analyses and design of a tokamak device. The current safety factor  $q_J$  is defined as

$$q_J \equiv \frac{B_{t0}}{R_0 \mu_0} \frac{1}{I_p} \frac{\pi a^2 (1 + \kappa^2)}{I_p}, \quad (2.34)$$

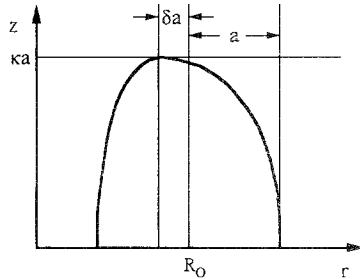


FIG. 2.5. Definition of the geometrical parameters of a plasma cross section:  $\kappa$ , ellipticity;  $\delta$ , triangularity.

where  $B_{t0}$  is the toroidal magnetic field at the plasma center  $R_0$ . Practically, in addition to this definition, several kinds of different expressions for the current safety factor are defined as

$$q_{J1} \equiv \frac{2\bar{a}^2 B_{t0}}{R_0 I_p (MA)}, \quad (2.35)$$

$$q_{J2} \equiv \frac{2ka^2 B_{t0}}{R_0 I_p (MA)}, \quad (2.36)$$

where

$$\bar{a} \equiv \sqrt{D/\pi}, \quad (2.37)$$

$$k \equiv \frac{1 + \kappa^2}{2}, \quad (2.38)$$

and  $D$  is the area of the cross section. It should be noted that the difference between the flux  $q$  and current  $q$  becomes considerably large when the cross section is shaped too much and/or the beta value becomes large (Fig. 2.6). The safety factor was originally defined as a margin to the stability limit observed at  $q_J = 1$  in an early circular tokamak (Kruskal-Shafranov limit) [17, 70]. But tokamaks are rarely operated in the parameter range with such a low value of the safety factor. Low  $q$  discharge with  $q < 2$  is very difficult because of strong external kink mode instability. Usual experiments are carried out between  $q \approx 2$  and  $q \approx 5$  or 6.

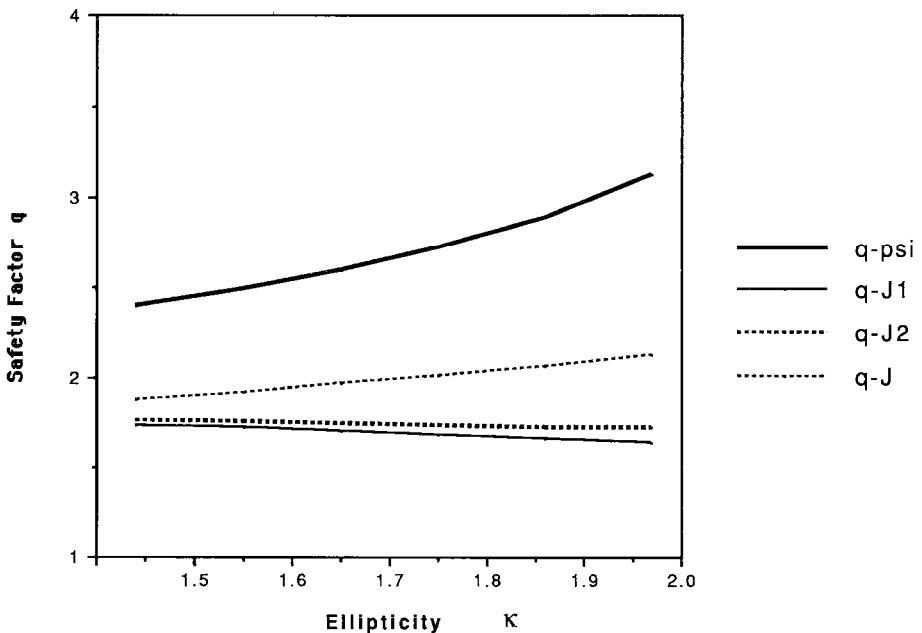


FIG. 2.6. Various definitions of the safety factor,  $q_\psi$ ,  $q_J$ ,  $q_{J1}$ , and  $q_{J2}$ .

A beta value is defined as a ratio of the plasma pressure to the magnetic pressure. In addition to the poloidal beta defined by Eq. (2.30), beta values  $\beta_r$ , current poloidal beta value  $\beta_J$ , are defined, where two different definition of the current poloidal betas,  $\beta_{J1}$  and  $\beta_{J2}$  are presented, as

$$\beta_r \equiv \frac{2\mu_0 \bar{p}}{B_{r0}^2}, \quad (2.39)$$

$$B_{J1} \equiv \frac{4\mu_0 \bar{p} V_s}{R_0 [\mu_0 I_p]^2}, \quad (2.40)$$

and

$$\beta_{J2} \equiv \frac{2\mu_0 \bar{p}}{\hat{B}_p^2}, \quad (2.41)$$

where

$$\bar{p} \equiv \frac{1}{V_s} \int p dV, \quad (2.42)$$

$$\hat{B}_p \equiv \mu_0 I_p / \oint_{\text{surface}} dl. \quad (2.43)$$

Under the constant plasma current condition the maximum poloidal beta value is limited [3, 32] as

$$\varepsilon \beta_J < 1. \quad (2.44)$$

To characterize the current profile of “normalized internal inductance per unit length”  $l_i$  is defined as

$$l_i \equiv \frac{4}{\mu_0 (I_p)^2 R_0} \int \frac{B_p^2}{2\mu_0} dV. \quad (2.45)$$

The following several parameters are also often used for stability analyses, i.e., shear,  $S$ , mean radius of the magnetic surface,  $\rho$ , local poloidal beta,  $\alpha$ , and average parallel current  $I_{||}$ ,

$$S \equiv \frac{2V}{q} \frac{dq}{dV} = \frac{\rho}{q} \frac{dq}{d\rho}, \quad (2.46)$$

where

$$\rho \equiv \sqrt{\frac{V}{2\pi^2 R_0}}, \quad (2.47)$$

$$\alpha \equiv -\frac{\mu_0}{2\pi^2} \frac{dp}{d\psi} \frac{dV}{d\psi} \sqrt{\frac{V}{2\pi^2 R_0}}, \quad (2.48)$$

$$I_{||} \equiv \frac{\langle \mathbf{J} \cdot \mathbf{B} \rangle}{\langle B^2 \rangle} = -\frac{F}{\langle B^2 \rangle} \frac{dp}{d\psi} - \frac{1}{\mu_0} \frac{dF}{d\psi}. \quad (2.49)$$

### 2.6. Integral Relation

In this section some useful relations [71, 72] among integrals of the equilibrium magnetic field, plasma current, plasma pressure, and another arbitrary vector are derived. First the equilibrium magnetic field is decomposed into two parts,  $\mathbf{B}_1$  and  $\mathbf{B}_2$ , as

$$\mathbf{B} = \mathbf{B}_1 + \mathbf{B}_2, \quad (2.50)$$

where

$$\text{rot } \mathbf{B}_1 = \mu_0 \mathbf{J}, \quad (2.51)$$

$$\text{rot } \mathbf{B}_2 = 0. \quad (2.52)$$

It should be noted that this decomposition is not unique. Next we consider the following vector identity which holds for arbitrarily chosen vectors,  $\mathbf{Q}$  and  $\mathbf{A}$ , as

$$\mathbf{Q}[\text{rot } \mathbf{A} \times \mathbf{A}] = \text{div} \left[ (\mathbf{Q} \cdot \mathbf{A}) \mathbf{A} - \frac{A^2}{2} \mathbf{Q} \right] + \frac{A^2}{2} \text{div } \mathbf{Q} - \mathbf{A}[(\mathbf{A} \cdot \nabla) \mathbf{Q}]. \quad (2.53)$$

By letting  $\mathbf{A}$  equal  $\mathbf{B}_1$  and using Eq. (2.1) we obtain an integral of the above equation over the volume, including the plasma volume, as

$$\begin{aligned} & \int_V \left\{ \left( p + \frac{B^2}{2\mu_0} \right) \text{div } \mathbf{Q} - \frac{1}{\mu_0} \mathbf{B}_1[(\mathbf{B}_1 \cdot \nabla) \mathbf{Q}] \right\} dV \\ &= \oint \left[ \left( p + \frac{B_1^2}{2\mu_0} \right) \mathbf{Q} \cdot d\mathbf{S} - \frac{1}{\mu_0} (\mathbf{Q} \cdot \mathbf{B}_1)(\mathbf{B}_1 \cdot d\mathbf{S}) \right] - \frac{1}{\mu_0} \int \mathbf{Q} \cdot (\mathbf{J} \times \mathbf{B}_2) dV. \end{aligned} \quad (2.54)$$

This equation is called the integral relation [73]. As one of the examples of application of the integral relation, the following virial theorem is derived from the previous vector identity by letting  $\mathbf{B}_2 = 0$  and  $\mathbf{Q} = \mathbf{r} = r\mathbf{e}_r + z\mathbf{e}_z$ ,

$$\int_V \left( 3p + \frac{B^2}{2\mu_0} \right) dV = \oint_S \left[ \frac{B^2}{2\mu_0} \mathbf{r} \cdot d\mathbf{S} - \frac{1}{\mu_0} (\mathbf{B} \cdot \mathbf{r})(\mathbf{B} \cdot d\mathbf{S}) \right], \quad (2.55)$$

where  $\mathbf{e}_r$  and  $\mathbf{e}_z$  are the unit vectors in the  $r$ - and  $z$ -directions, respectively,  $S$  is an arbitrarily chosen surface located outside of the plasma surface where  $p = 0$ . When the magnetic field  $B$  is generated only by the plasma current it scales as  $B \propto 1/r^3$  in the distance, which means the right-hand side of the equation vanishes in the distance. In this way we can get an important conclusion that the plasma equilibrium is only attainable in the existence of external magnetic field.

From Eq. (2.54) we can derive two important relations which are used to express macroscopic parameters of a confined plasma by a set of experimentally measurable quantities. To obtain the first relation we decompose the magnetic field  $\mathbf{B}$  into the

poloidal and the toroidal components as  $\mathbf{B} = \mathbf{B}_p + \mathbf{B}_t$ , and carry out the integration of the virial theorem (Eq. (2.55)) at the plasma surface. Then the equation

$$\int_V \left( 3p + \frac{B_p^2}{2\mu_0} + \frac{B_t^2 - B_{te}^2}{2\mu_0} \right) dV = \oint_S \frac{B_p^2}{2\mu_0} \mathbf{r} d\mathbf{S} \quad (2.56)$$

is derived, where  $B_{te}$  is the toroidal magnetic field at the plasma surface. On the other hand, by letting  $\mathbf{Q} = \mathbf{e}_r$  in Eq. (2.54), the second relation is derived as

$$\int_V \frac{1}{r} \left( p + \frac{B_p^2}{2\mu_0} - \frac{B_t^2 - B_{te}^2}{2\mu_0} \right) dV = \oint_S \frac{B_p^2}{2\mu_0} \mathbf{e}_r d\mathbf{S}, \quad (2.57)$$

where the pressure at the plasma surface is assumed as  $p = 0$ . Expressing the plasma surface as  $\mathbf{r} = R_0 \mathbf{e}_r + \rho \mathbf{e}_\rho$  in the quasi-cylindrical coordinates  $(\rho, \omega, \phi)$  system (Fig. 2.7), and defining the current beta,  $\beta_J$ , and the diamagnetic parameter  $\mu_J$  as

$$\beta_J \equiv \beta_{J1}, \quad (2.58)$$

$$\mu_J \equiv \frac{4}{\mu_0 (I_p)^2 R_0} \int \frac{B_{te}^2 - B_t^2}{2\mu_0} dV \cong 4\pi R_0 B_0 \Delta\Phi, \quad (2.59)$$

where  $\Delta\Phi$  is the increment of the toroidal magnetic flux, we can transform these relations to the form convenient for the experimental analysis as

$$\beta_J = \mu_J + S_1 + \delta_R S_2, \quad (2.60)$$

$$\beta_J + \frac{1}{2} l_i = \frac{1}{2} S_1 + S_2 \left( 1 - \frac{\delta_R}{2} \right). \quad (2.61)$$

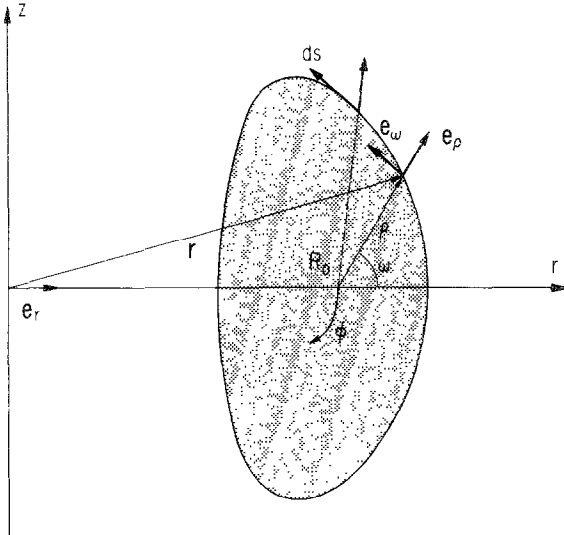


FIG. 2.7. A quasi-cylindrical coordinate system  $(\rho, \omega, \phi)$ .

In the above equations  $S_1$  and  $S_2$  are expressed by the integrals at the plasma surface as

$$S_1 = \frac{2}{\mu_0 I_p^2} \frac{1}{R_0} \oint \frac{B_p^2}{2\mu_0} \rho \mathbf{e}_\rho d\mathbf{s}, \quad (2.62)$$

$$S_2 = \frac{2}{\mu_0 I_p^2} \frac{1}{R_0} \oint \frac{B_p^2}{2\mu_0} \mathbf{e}_r d\mathbf{s}, \quad (2.63)$$

where

$$\delta_R \equiv \frac{R_0 - R_T}{R_0}, \quad (2.64)$$

$$R_T \equiv \int \tilde{f} dV / \int \frac{\tilde{f}}{r} dV, \quad (2.65)$$

$$\tilde{f} \equiv p + \frac{B_p^2}{2\mu_0} - \frac{B_t^2 - B_{te}^2}{2\mu_0}, \quad (2.66)$$

and for a usual tokamak,  $\delta_R$  is sufficiently small in comparison with unity. When the plasma cross section is circular and the inverse aspect ratio  $\varepsilon$  is sufficiently small,  $S_1$  becomes nearly unity and Eq. (2.61) becomes the well-known Shafranov's equilibrium relation [9, 74]. Equations (2.60) and (2.61) are used for determination of  $\beta_J$  from the experimentally obtained electromagnetic signals, and usually the current beta,  $\beta_J$ , determined from Eq. (2.60) is called the "diamagnetic" current beta ( $\beta_J^{\text{dia}}$ ) and that determined from Eq. (2.61) is called "MHD" current beta ( $\beta_J^{\text{MHD}}$ ). To calculate these betas, identification of the position of the plasma surface and measurement of poloidal magnetic field at the surface, diamagnetic flux, and the internal inductance are necessary. These issues will be described in 6.3 in detail.

### 2.7. Approximation of the Grad-Shafranov Equation

In this subsection we describe two representative approximate solution methods used for calculation of the tokamak equilibrium, i.e., the low beta tokamak ordering and the high beta tokamak ordering. Other approximations based on, such as, the near-axis expansion [22–24] were preferably applied to analytical solution of the equilibrium in the early stage of the tokamak research but, with the progress of computer systems and computational techniques, large-scale numerical solutions have been substituted for the analytical solutions. By employing the inverse aspect ratio,  $\varepsilon$ , as the expansion parameter we normalize the magnetic flux function,  $\psi$ , coordinates,  $r$  and  $z$ , the pressure function,  $p$ , and the toroidal field function,  $F$ , as

$$\psi = \frac{a^2 B_0}{\alpha} \Psi, \quad (0 \leq \Psi \leq 1), \quad (2.67)$$

$$r = R_0(1 + \varepsilon x), \quad z = R_0 \varepsilon y, \quad (2.68)$$

$$p = \varepsilon^n B_0^2 P(\Psi), \quad F^2 = (R_0 B_0)^2 [1 + \varepsilon^n \hat{F}(\Psi)], \quad (2.69)$$

where  $\alpha$  is a parameter relating to the magnetic flux function at the plasma surface,  $B_0$  is the typical value of the toroidal magnetic field, and the following ordering of the magnetic field is considered:

$$rB_p = |\nabla\psi| \approx \frac{\psi}{a}, \quad (2.70)$$

$$B_p \approx \varepsilon B_0. \quad (2.71)$$

By using the above-described normalized quantities the original Grad-Shafranov equation is rewritten as

$$\mathcal{A}_\perp \Psi - \frac{\varepsilon}{1 + \varepsilon x} \frac{\partial \Psi}{\partial x} = -\alpha^2 \varepsilon^{n-2} \left\{ \frac{dG}{d\Psi} + \varepsilon x(2 + \varepsilon x) \frac{dP}{d\Psi} \right\}, \quad (2.72)$$

where

$$\mathcal{A}_\perp \Psi \equiv \left( \frac{\partial^2}{\partial x^2} + \frac{\partial^2}{\partial y^2} \right) \Psi, \quad (2.73)$$

$$\frac{dG}{d\Psi} \equiv \frac{dP}{d\Psi} + \frac{1}{2} \frac{dF}{d\Psi}. \quad (2.74)$$

Then we expand the normalized coordinates  $x$  and  $y$  as

$$x \equiv x(\Psi, \theta) = x^{(0)}(\Psi, \theta) + \varepsilon x^{(1)}(\Psi, \theta) + \dots, \quad (2.75)$$

$$y \equiv y(\Psi, \theta) = y^{(0)}(\Psi, \theta) + \varepsilon y^{(1)}(\Psi, \theta) + \dots \quad (2.76)$$

In order that the equilibrium equation (Eq. (2.72)) is satisfied in each order of  $\varepsilon$ , the following two cases of  $n=2$  (low beta tokamak ordering) and  $n=1$  (high beta tokamak ordering) are possible.

(1) *Low beta tokamak ordering* [27, 75]. In this case the beta value,  $\beta$ , and the poloidal beta value,  $\beta_p$ , are  $O(\varepsilon^2)$  and  $O(\varepsilon^0)$ , respectively, and the following equations hold for the orders of  $\varepsilon^0$  and  $\varepsilon^1$ , in the respective order:

$$\mathcal{A}_\perp \Psi = -\alpha^2 \frac{dG}{d\Psi}, \quad (2.77)$$

$$(\mathcal{A}_\perp \Psi)^{(1)} = -\alpha^2 x^{(0)} \frac{dP}{d\Psi} + x^{(0)} \left( \frac{\partial \Psi}{\partial x} \right)^{(0)}. \quad (2.78)$$

Toroidal effect is not included in the equation of  $O(\varepsilon^0)$  (Eq. (2.77)) and the first term of Eq. (2.78) represents the toroidal shift arising from the finite- $\beta$  effect. The second term represents the toroidal shift due to the self-force of the plasma current. Above equations (Eqs. (2.77) and (2.78)) can be solved only numerically except for special cases such as an equilibrium of a circular cross-sectional tokamak.

(2) *High beta tokamak ordering* [28, 29]. In this case  $\beta$  and  $\varepsilon\beta_p$  are quantities of  $O(\varepsilon^1)$  and  $O(\varepsilon^0)$ , respectively, and we expand the current function  $dG/d\Psi$  as

$$\frac{dG}{d\Psi} = \varepsilon \frac{dG_1}{d\Psi} + \varepsilon^2 \frac{dG_2}{d\Psi} + \dots, \quad (2.79)$$

from which the following equation is derived:

$$F^2 = (R_0 B_0)^2 \{1 - 2\varepsilon[P(\Psi) - P(1)] + 2\varepsilon^2[G(\Psi) - G(1)] + \dots\}. \quad (2.80)$$

By using the above expansion, the following equations valid up to the first order of  $\varepsilon$  are obtained:

$$\mathcal{A}_\perp \Psi = -\alpha^2 \frac{dG_1}{d\Psi} - 2\alpha^2 x^{(0)} \frac{dP}{d\Psi}, \quad (2.81)$$

$$(\mathcal{A}_\perp \Psi)^{(1)} = \left( \frac{\partial \Psi}{\partial x} \right)^{(0)} - \alpha^2 \frac{dG_2}{d\Psi} - \alpha^2 (x^{(0)})^2 \frac{dP}{d\Psi}. \quad (2.82)$$

Equation (2.81) includes only a toroidal effect due to the plasma pressure and coincides with Eq. (2.77) in the limit of null beta. Though by the tokamak ordering a slightly simpler equation (Eq. (2.81)) is derived in comparison with the original Grad-Shafranov equation, analytical solutions can be obtained only for the functions  $dG_1/d\Psi$  and  $dP/d\Psi$  with linear dependence on  $\Psi$ , and numerical calculation is necessary for other cases.

## 2.8. Mathematical Remarks on the Grad-Shafranov Equation

In this section we summarize some basic remarks on the mathematical aspects of the Grad-Shafranov equation, which are closely related to numerical solutions of the equation. From the mathematical viewpoint the distinctive feature of the MHD equilibrium problem is that this problem is often formulated as a nonlinear eigenvalue problem with a free boundary condition. The mathematical issues to be clarified for such a problem are to prove existence and uniqueness of the solution and the error estimation of a numerical solution method. Among them, existence of the solution was proved by Temam [76] and Berestycki and Brézis [77] on the basis of the variational approach [78, 79] and by Kikuchi [80], Rappaz [81], and Kikuchi *et al.* [82] on the basis of the principle of contraction mappings [83].

Existence of the equilibrium solution for a rather general case was proved by Temam [76]. In this case the equilibrium problem is formulated in  $R^2$  ( $x = (x_1, x_2) \in R^2$ ) as

$$Lu = \lambda \hat{f}(u, x) \quad \text{in } \Omega_p, \quad (2.83)$$

$$Lu = 0 \quad \text{in } \Omega_V, \quad (2.84)$$

$$u = 0 \quad \text{on } \Gamma_p, \quad (2.85)$$

$$u = d \quad \text{on } \Gamma. \quad (2.86)$$

$$\int \frac{1}{x_1} \frac{\partial u}{\partial n} d\Gamma = I, \quad (2.87)$$

where the normal derivative of  $u$ ,  $\partial u / \partial n$ , is continuous on  $\Gamma_p$ ,  $d$  is an unknown constant,  $I$  is a given constant representing the plasma current, the variable  $u$  corresponds to the flux function  $\psi$  with a positive value in the plasma region  $\Omega_p$  and does not vanish in  $\Omega_p$ ,  $\hat{f}(u, x) = b(x)u$  ( $0 < b_0 \leq b(x) \leq b_1$ ;  $b_0$  and  $b_1$  are appropriately chosen constants), and

$$Lu \equiv \mathcal{A}^* u = \sum_{i=1}^2 \frac{\partial}{\partial x_i} \left( \frac{1}{x_1} \frac{\partial u}{\partial x_i} \right). \quad (2.88)$$

For this problem, the plasma region  $\Omega_p$  and eigenvalue  $\lambda$  as well as the dependent variable  $u = u(x)$  are to be determined. The operator  $L$  is not necessarily restricted to the above form and in general it is an arbitrary second-order self-adjoint elliptic operator. If the function  $\hat{f}(u, x)$  is given as  $b(x)u$ , we can set  $d = 1$  without losing generality. Then the original problem can be reduced to the problem of finding the critical point of the functional,

$$k_1(u) = \frac{1}{2} \int_{\Omega} \frac{1}{x_1} |\nabla u|^2 dx, \quad (2.89)$$

with the constraint

$$k_2(u) = \int_{\Omega} \frac{b}{2} [(u + 1)_-]^2 dx = \text{const}, \quad (2.90)$$

where  $u$  satisfies  $u = 0$  on  $\Gamma$ ,  $u_- = \max(-u, 0)$ , and  $\lambda$  is the corresponding critical value. Temam showed that  $k_1(u)$  is bounded from the lower side and existence of the critical point of the functional  $k_1(u)$  is proved by using the weak lower semi-continuity of  $k_1(u)$  [84]. For a more general form of the function  $\hat{f}$  as

$$\hat{f}(u, x) = \frac{\partial g(u, x)}{\partial u}, \quad (2.91)$$

$$\hat{f}(x, 0) = 0, \quad \hat{f}(x, u) > 0, \quad \text{for } u > 0, \quad (2.92)$$

existence of the equilibrium solution is also proved by using the same variational method, provided the function  $\hat{f}$  is bounded from both the upper and lower sides as

$$b_1(|u|^\beta - 1) \leq \hat{f}(u, x) \leq b_2(|u|^\beta + 1), \quad (2.93)$$

with  $\beta > 1$ ,  $b_1, b_2 > 0$ . Existence of the solution to the problem treated in 4.1.2 is assured by the above proof.

On the other hand, Kikuchi proved both existence and uniqueness of the equilibrium solution by considering a concrete procedure for application to the FEM formulation. In the following we summarize the results heuristically for a cylindrical tokamak equilibrium with  $\hat{f}(u) = u_+ = \max(u, 0)$ . First, the problem is formulated as finding a pair of  $\{\lambda, u\}$  which satisfies the following nonlinear eigenvalue problem in  $R^2$ ,

$$-\Delta u = \lambda \hat{f}(u) \quad \text{in } \Omega, \quad (2.94)$$

$$u = -1 \quad \text{on } \Gamma. \quad (2.95)$$

It should be noted that the trivial solution of this problem is  $u(x) = -1$ , where the eigenvalue  $\lambda$  is arbitrary. Next, instead of solving the above problem directly we consider solving the following fixed-boundary problem, that is, finding a pair  $\{\lambda_0, \phi\}$  of the linear eigenvalue problem,

$$-\Delta \phi = \lambda \phi \quad \text{in } \Omega, \quad (2.96)$$

$$\phi = 0 \quad \text{on } \Gamma. \quad (2.97)$$

There is one and only one solution of this problem which satisfies

$$(\phi, \phi) = 1 \quad \text{and} \quad \phi(x) > 0, \quad (2.98)$$

and the corresponding eigenvalue  $\lambda_0$  is simple and positive, where the inner product of two functions,  $X$  and  $Y$ , is defined as

$$(X, Y) = \int XY dS. \quad (2.99)$$

Then, by considering a transformation,

$$u^* = \varepsilon u, \quad (2.100)$$

where  $\varepsilon$  is a small positive definite parameter, the original problem is reduced to

$$-\Delta u^* = \lambda \hat{f}(u^*) \quad \text{in } \Omega, \quad (2.101)$$

$$u^* = -\varepsilon \quad \text{on } \Gamma. \quad (2.102)$$

Though we assumed that  $\varepsilon$  is positive definite the above equation is meaningful even for  $\varepsilon \leq 0$ . And if we set  $\varepsilon = 0$ ,  $u^* = \phi$  becomes a solution of the above equation. Then, we solve the original equation starting from the solution of the linear eigenvalue problem  $\phi$ . The solution is expressed as

$$u^* = \phi + \varepsilon \psi + w, \quad (2.103)$$

$$(\psi, \phi) = 0, \quad (2.104)$$

$$(w, \phi) = 0. \quad (2.105)$$

If we consider a neighborhood of  $\{\lambda_0, \phi\}$ ,  $u^*$  and  $\lambda$  can be expressed approximately as  $\phi + \varepsilon\psi$  and  $\lambda_0 + \varepsilon\mu$  with very small  $\varepsilon$ . In this case the problem is reduced to find a pair  $\{\mu, \psi\}$  which satisfies

$$-\Delta\psi - \lambda_0\psi = \mu\phi \quad \text{in } \Omega, \quad (2.106)$$

$$\psi = -1 \quad \text{on } \Gamma. \quad (2.107)$$

From the solvability condition, Eq. (2.104), the eigenvalue of  $\mu$  is given by

$$\mu = \lambda_0(1, \phi) \quad (2.108)$$

and the unique solution  $\psi$  can be obtained from the above linear boundary problem. The equation for  $w$  is given by

$$-\Delta w - \lambda_0 w = \lambda \hat{f}(u^*) - \lambda_0 u^* - \varepsilon \lambda_0(1, \phi) \phi. \quad (2.109)$$

From the solvability condition, Eq. (2.105), the eigenvalue  $\lambda$  is expressed as

$$\lambda = \lambda_0 \frac{(u^*, \phi) + \varepsilon(1, \phi)}{(\hat{f}(u^*), \phi)}. \quad (2.110)$$

A concrete iteration procedure to determine the solution as well as the proof of convergence was given by Kikuchi *et al.* [82] as

$$\lambda^{(i)} = \lambda_0 \frac{(w^{(i-1)}, \phi) + \varepsilon(1, \phi)}{(\hat{f}(w^{(i-1)}), \phi)}, \quad (2.111)$$

$$-\Delta w^{(i)} - \lambda_0 w^{(i)} = \lambda^{(i)} \hat{f}(w^{(i-1)}) - \lambda_0 w^{(i-1)} - \varepsilon \lambda_0(1, \phi) \phi. \quad (2.112)$$

This procedure can be directly applied to analysis of the solution by finite element approximation [85, 86] as shown in 4.1.2.

### 3. BOUNDARY CONDITIONS AND CONSTRAINING CONDITIONS

#### 3.1. Boundary Conditions and Vacuum Field

There are several possible ways to impose the boundary condition at the plasma surface. From the practical viewpoint four types of treatments of the plasma-vacuum boundary are considered (Fig. 3.1). The simplest is the fixed boundary condition, where the plasma-vacuum boundary is replaced by a surface of a perfect conductor. In this case the Grad-Shafranov equation is solved only in the plasma region at first and the whole system including the vacuum region is calculated, if necessary, on the basis of the virtual casing principle by Shafranov and Zakharov [87], in which the external magnetic field is calculated so that the magnetic field is continuous at the surface [88]. Details of the procedure will be described in 6.2 in relation to the design of the external magnetic field coils. The

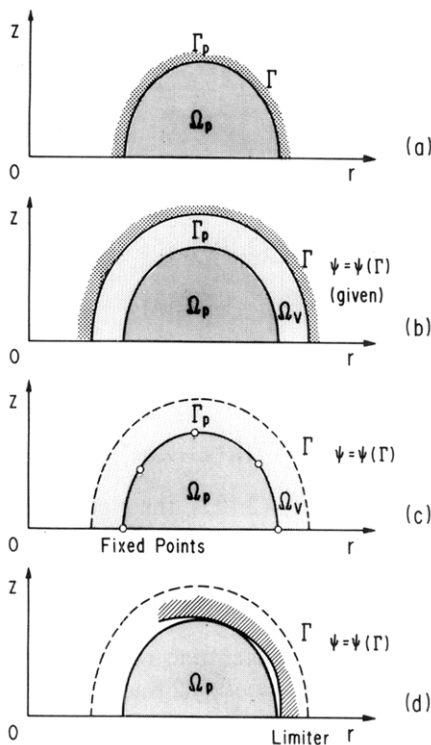


FIG. 3.1. Four types of treatment of the plasma-vacuum boundary: (a) fixed boundary problem; (b)-(d) free boundary problems of types (1)-(3).

other three are free boundary treatments in some sense. In the first type of free boundary problem, the shape of the plasma surface is not known beforehand and the boundary values  $\psi$  on  $\Gamma$  are given as was described in 2.8. In the second type of free boundary problem, which is also called a semi-fixed boundary problem, the approximate plasma shape is prescribed by giving several fixed points on  $\Gamma_p$ . In the third type of free boundary problem, the equilibrium is solved under the given external magnetic field by imposing a constraint such as a fixed contact point of the plasma with the limiter. These four types of boundary conditions are chosen in correspondence with the applications.

For the first type of free boundary problem it is convenient to introduce a form factor  $S(\psi)$  which unifies the plasma and vacuum equations for the plasma and vacuum regions; the boundary condition on the plasma-vacuum interface is automatically satisfied and, if only the boundary condition on the shell or at infinity is given, the plasma shape is determined self-consistently. The unified Grad-Shafranov equation for the plasma and the vacuum regions is given as

$$\mathcal{A}^* \psi + S(\psi)(\Lambda^2 r^2 + M)\psi = 0, \quad (3.1)$$

where

$$S(\psi) = 1, \quad \text{for } \psi < 0, \text{ inside the plasma}, \quad (3.2)$$

$$S(\psi) = 0, \quad \text{for } \psi > 0, \text{ outside the plasma}, \quad (3.3)$$

and for simplicity  $p(\psi)$  and  $F^2(\psi)$  are often expressed in terms of quadratic forms of  $\psi$  with constant coefficients. The boundary condition on the conducting shell surface is

$$\psi = C(\text{const}), \quad (3.4)$$

from the condition that the normal component of the magnetic field vanishes there. As in present day tokamaks the role of the external control magnetic field is important to maintain the MHD equilibrium in comparison with the conducting shell, this kind of equilibrium solver becomes less important, except for its interesting mathematical properties as shown in 2.8.

Next we describe how to determine the external magnetic field for the second type of free boundary problem. In this type of free boundary treatment, the total magnetic flux,  $\psi$ , i.e., the sum of the flux due to the plasma contribution  $\psi_p$  and that of the vacuum contribution  $\psi_v$ , is determined iteratively by adjusting the vacuum flux  $\psi_v$ . Moreover, in this type and also in the third type, the problem in the original infinite computational domain is transformed into a Dirichlet boundary value problem in a rectangular domain by using the Green's function of the Grad-Shafranov operator  $\Delta^*$  (the Green's function formulation) [7, 37, 38]. The

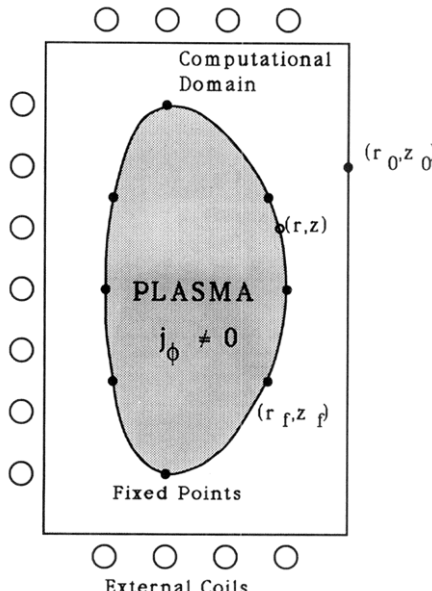


FIG. 3.2. A computational domain and fixed points for the second type free boundary problem.

poloidal flux  $\psi_p(r_0, z_0)$  produced by the plasma current  $j_\phi$  at the point  $(r_0, z_0)$  on the boundary of the computational domain (Fig. 3.2) is given by the Green's function formula as

$$\psi_p(r_0, z_0) = \frac{1}{\mu_0} \oint_{\psi=0} G(r, z; r_0, z_0) \frac{|\nabla \psi(r, z)|}{r} dl, \quad (3.5)$$

where  $\psi(r, z)$  is composed of the magnetic fluxes due to the plasma current and the external current as

$$\psi(r, z) = \psi_p(r, z) + \psi_V(r, z). \quad (3.6)$$

In the above equation,  $G(r, z; r_0, z_0)$  is the Green's function of the Grad-Shafranov operator given as

$$G(r, z; r_0, z_0) = -\frac{\mu_0}{2\pi} \sqrt{rr_0} \frac{1}{k} [(2 - k^2) K(k) - 2E(k)], \quad (3.7)$$

$$k^2 = \frac{4rr_0}{(r + r_0)^2 + (z - z_0)^2}, \quad (3.8)$$

where  $K(k)$  and  $E(k)$  are the first and the second complete elliptic integrals, respectively. In this way the value of the magnetic flux  $\psi$  on the boundary of the computational domain is given as

$$\psi(r_0, z_0) = \psi_p(r_0, z_0) + \psi_V(r_0, z_0). \quad (3.9)$$

For this process it is convenient to decompose the vacuum contribution  $\psi_V$  into  $J$  multipolar components  $\psi_V^j$ ,

$$\psi_V = \sum_{j=0}^{J-1} a_j \psi_V^j, \quad (3.10)$$

and the coefficients  $a_j$ 's are determined so that the  $\psi = 0$  contour contains the  $J$  prescribed fixed points as

$$\psi_p(r_f, z_f) + \sum_{j=0}^{J-1} a_j \psi_V^j(r_f, z_f) = 0. \quad (3.11)$$

The main advantage of this method is that the problem is reduced to a Dirichlet boundary value problem in a rectangular computational domain, which can be solved easily by applying rapid direct solvers such as the DCR (double cyclic reduction method) and the FACR (Fourier analysis cyclic reduction method), described later. The basis functions of the multipolar components  $\psi_V^j$ 's are derived by using linear combinations of the vacuum solution represented by the associated Legendre

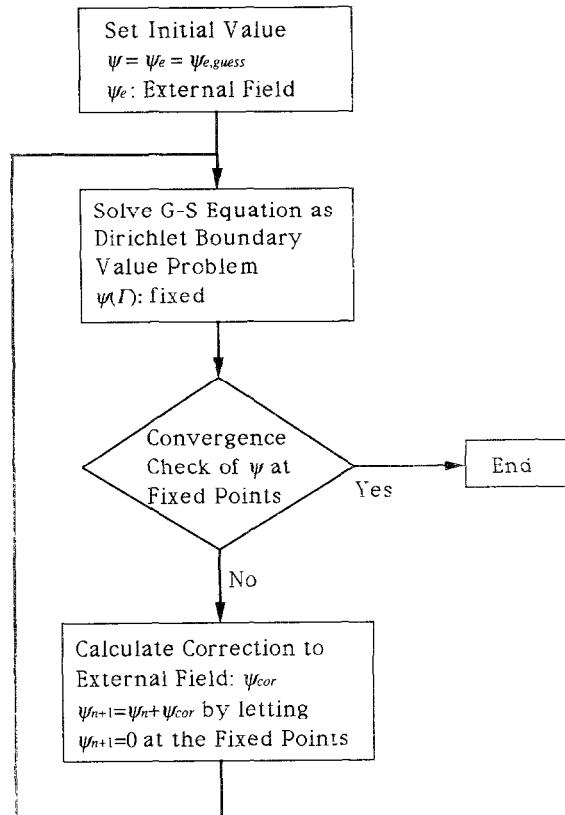


FIG. 3.3. Flow diagram of the type-2 free boundary calculation.

functions. The flow diagram for this process is shown in Fig. 3.3. The concrete forms of the multipole solution up to  $n=5$  components are shown as

$$\psi_\nu^0 = 1, \quad (3.12)$$

$$\psi_\nu^1 = \frac{1}{R_0 a} (r^2 - R_0^2), \quad (3.13)$$

$$\psi_\nu^2 = -\frac{1}{(R_0 a)^2} \left[ r^2 z^2 - \frac{1}{4} (r^2 - R_0^2)^2 \right], \quad (3.14)$$

$$\psi_\nu^3 = \frac{1}{(R_0 a)^3} \left[ r^2 z^4 - \frac{3}{2} (r^2 - R_0^2) r^2 z^2 + \frac{1}{8} (r^2 - R_0^2)^3 \right], \quad (3.15)$$

$$\begin{aligned}\psi_V^4 = & -\frac{1}{5(R_0 a)^4} \left[ r^2 z^6 - \frac{5}{4} (3r^2 - 2R_0^2) r^2 z^4 \right. \\ & \left. + \frac{15}{8} (r^2 - R_0^2)^2 z^2 - \frac{5}{64} (r^2 - R_0^2)^4 \right],\end{aligned}\quad (3.16)$$

$$\begin{aligned}\psi_V^5 = & \frac{4}{7} \frac{1}{(R_0 a)^5} \left[ r^2 z^8 - \frac{7}{2} (2r^2 - R_0^2) r^2 z^6 + \frac{35}{8} (2r^2 - R_0^2)(r^2 - R_0^2) r^2 z^4 \right. \\ & \left. - \frac{35}{16} (r^2 - R_0^2)^3 r^2 z^2 + \frac{7}{128} (r^2 - R_0^2)^5 \right].\end{aligned}\quad (3.17)$$

This kind of expression becomes extremely complicated as the number of components  $J$  increases. Therefore, magnetic fields by an appropriately chosen set of coils are more easily used as the basis functions in the case of a tokamak with a strongly shaped cross section. When the coil system is approximated by a set of filament currents the flux  $\psi_V$  in the computational domain produced by a unit current flowing in a coil at  $(r_c, z_c)$  is derived by solving the boundary value problem,

$$\Delta^* \psi = 0, \quad \text{for the current outside the domain,} \quad (3.18)$$

$$\Delta^* \psi = \mu_0 r \delta(r - r_c) \delta(z - z_c), \quad \text{for the current inside the domain,} \quad (3.19)$$

where

$$\psi_0(r_0, z_0) = \mu_0 G(r_0, z_0; r_c, z_c). \quad (3.20)$$

By this kind of boundary condition, the approximate plasma shape is prescribed as a set of input parameters. Generally it is very convenient to analyze the plasma properties for the given conditions and this boundary condition is preferred for theoretical stability analyses. It should, however, be noted that this type of problem is an ill-posed one and it is rather difficult to calculate an equilibrium with an extremely shaped cross section or with a separatrix at the plasma surface. To cope with this difficulty, modification of this method based on the least square method is often effective [38]. In this method the coil current  $I_j$ 's are obtained by minimizing an appropriately chosen object function such as

$$\Xi = \sum_{k=1}^N w_k \left| \frac{\psi_p(r_k, z_k) + \sum_{j=1}^M I_j \psi_V^j(r_k, z_k)}{\psi_{\text{axis}}} \right|^2 + \gamma \sum_{j=1}^M \frac{I_j^2}{I_p^2} + \lambda \sum_{j=1}^M \frac{I_j}{I_p}, \quad (3.21)$$

where  $N$  and  $M$  are the number of fixed points and the number of independent coils (usually  $N > M$ ). The regularization parameter  $\gamma$  is introduced to stabilize the procedure against large unreal oscillations of the current  $I_j$ 's. The last term can be used to constrain the total current in all the coils to zero.

On the other hand, the third type of free boundary problem often appears in an actual experimental situation when one wishes to conjecture the realized equilibrium for a given magnetic field and limiter position because the shape of the

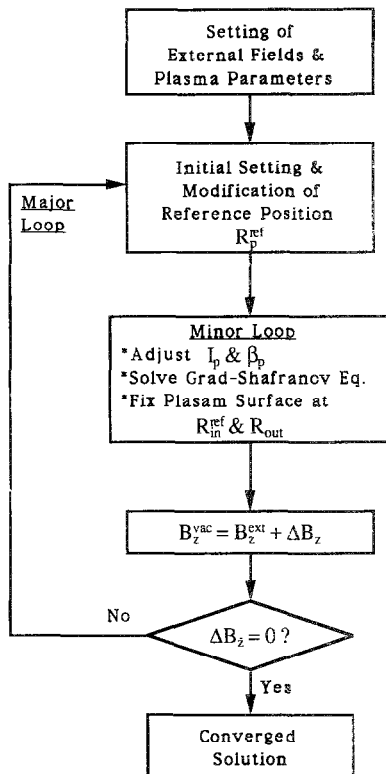


FIG. 3.4. Flow diagram of the type-3 free boundary calculation [89]. The major loop which modifies a reference position  $R_p^{\text{ref}}$  in accordance with the vacuum field  $\Delta B_z$  is added to the minor iteration loop.

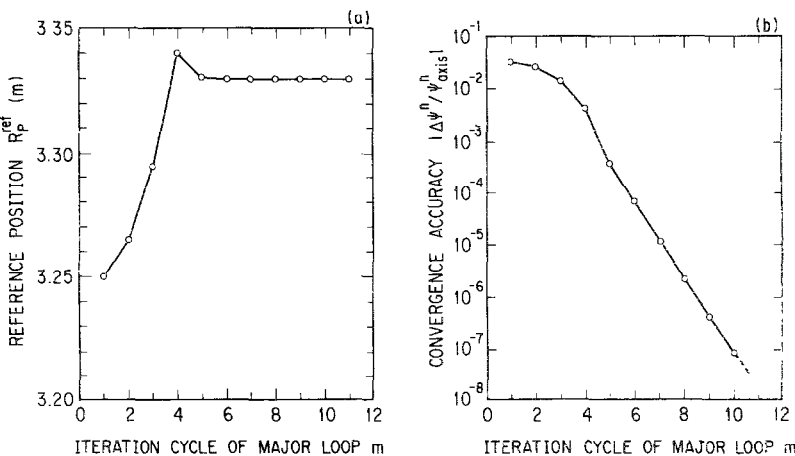


FIG. 3.5. An example of convergence curve for the type-3 free boundary calculation [89]. The reference position and convergence are shown as functions of the iteration number of the major loop.

plasma cross section is not prescribed. In this type of boundary condition, however, the standard iteration scheme fails to calculate the equilibrium when the constraint is given by an outboard limiter [36]. During iterations the plasma expands or shrinks infinitely in correspondence with the larger or smaller initial plasma radii compared with the equilibrium one. To overcome this difficulty several ideas [89, 90] were proposed and successfully applied to actual problems. One of the ideas to suppress this numerical instability is to stop the plasma movement by applying a virtual magnetic field during the iteration and to bring the plasma into a equilibrium state by decreasing the virtual field. The flow diagram of this algorithm and an example of the convergence curve are shown in Figs. 3.4 and 3.5, respectively [89].

### 3.2. Nonlinear Eigenvalue Problem

In general a careful treatment is required to solve the Grad–Shafranov equation as it includes two differentiation operators  $\nabla$  and  $d/d\psi$  defined in the two different spaces [91]. For this purpose two kinds of formulations dependent on constraining conditions are possible. One is the nonlinear eigenvalue problem in which the functional forms of pressure  $p(\psi)$  and toroidal field function  $F(\psi)$  are prescribed and the absolute value of them are determined from the eigenvalue of the system [7, 33]. The other is the flux conserving tokamak (FCT) equilibrium, where the problem is formulated so that the magnetic flux  $\psi$  is conserved and the safety factor profile  $q(\psi)$  is also given [53, 56, 58, 59, 92]. In this subsection we describe the formulation of the nonlinear eigenvalue problem.

We rewrite the Grad–Shafranov equation (Eq. (2.7)), as the nonlinear eigenvalue problem

$$\mathcal{A}^* \psi = \lambda f(\psi, r), \quad (3.22)$$

where

$$f(\psi) \equiv \mu_0 r J_{\phi 0} = \mu_0 r J_{\phi} / \lambda. \quad (3.23)$$

First, the above equation is solved with some appropriate numerical method and eigenvalue  $\lambda$  is obtained. In this calculation the variable range of  $\psi$  is fixed as  $[-1, 0]$  in the plasma and the following iteration scheme is adopted:

- (1) Prepare initial values,  $\psi^0, \lambda^0$ ;
- (2) Solve the following equation for  $\psi^{n+1}$ ,

$$\psi^{n+1} = \mathcal{A}^{*-1} \lambda^n f(\psi^n, r); \quad (3.24)$$

- (3) Normalize the  $\psi$  values by the value at the magnetic axis and obtain  $(n+1)$ th eigenvalue  $\lambda^{n+1}$ ,

$$\lambda^{n+1} = \frac{1}{\psi_{\text{axis}}^{n+1}} \lambda^n; \quad (3.25)$$

- (4) Repeat the above iteration procedure.

In the above calculation the range of the variable  $\psi$  is restricted within  $[-1, 0]$  and it is necessary to transform the variable into an appropriate range if the physical quantities, such as the total plasma current, maximum plasma pressure, etc., are to be adjusted to the prescribed values. For this purpose the following scaling of equilibrium quantities is carried out:

$$\begin{aligned}\hat{\psi} &= \sigma\psi, & \hat{B}_\rho &= \sigma B_\rho, & \hat{J}_\phi &= \sigma J_\phi, & \hat{p} &= \sigma^2 p, & \widehat{\left(F \frac{dF}{d\psi}\right)} &= \sigma F \frac{dF}{d\psi}, \\ \widehat{F^2} &= F_a^2 + \sigma^2(F^2 - F_a^2), & \widehat{q^2} &= q^2 \frac{\widehat{F^2}}{F^2 \sigma^2},\end{aligned}\quad (3.26)$$

where the quantities with hats are new quantities and  $\sigma$  is the scaling factor. If one wishes to adjust the total plasma current with the prescribed current  $I_p$ , the scaling factor  $\sigma$  is calculated as

$$\sigma^{-1} = \left( \frac{\lambda}{I_p} \right) \iint J_{\phi 0} dS. \quad (3.27)$$

It is easily seen from Eq. (3.26) that there are several iteration processes equivalent to the above one, e.g., an iteration under the constraint of constant current instead of the constant range of the  $\psi$  variation adopted in the above iteration [36].

From a practical viewpoint the convergence of the above iteration procedure of the nonlinear eigenvalue problem is very good and it is used widely for various applications. Detailed mathematical discussions on this problem are given in Ref. [93–96].

### 3.3. FCT Equilibrium and GDE

In contrast with the nonlinear eigenvalue approach, where the functional forms of  $p(\psi)$  and  $F(\psi)$  are given beforehand, in the FCT equilibrium approach the safety factor  $q(\psi)$  and adiabatic pressure  $\mu(\psi)$  defined in the following equation are given to solve the Grad-Shafranov equation,

$$\mu(\psi) = p \left( \frac{dV}{d\psi} \right)^\gamma, \quad (3.28)$$

where  $\gamma$  is the ratio of specific heats. The FCT equilibrium was devised to attain a higher beta state. As shown in Eq. (2.44) the maximum beta value of a tokamak plasma is determined by an equilibrium beta limit when the pressure is raised under the fixed plasma current condition. Shafranov [97] suggested that the limit will be overcome by appropriately adjusting the plasma current distribution, which was numerically demonstrated by Peng *et al.* [92]. As the equilibrium beta limit is imposed by the condition that the topological structure of the magnetic surfaces should be conserved, a high beta tokamak equilibrium can be obtained by calculating an equilibrium sequence with a constant  $q$ -profile, i.e., with conserved

toroidal and poloidal magnetic fluxes (FCT: flux conserving tokamak). By assuming a high beta tokamak ordering for the equilibrium of this sequence some asymptotic scaling laws among the normalized plasma current  $\hat{I}_p$ , total beta  $\beta_t$ , poloidal beta  $\beta_p$ , current beta  $\beta_{J1}$ , safety factor at the plasma surface  $q_s$ , and inverse aspect ratio  $\varepsilon$  are given [54] as

$$2q_s \hat{I}_p \approx \left( \frac{\beta_t}{\varepsilon} q_s^2 \right)^{1/3} + \text{const}, \quad (3.29)$$

$$\varepsilon \beta_p \approx \left( \frac{\beta_t}{\varepsilon} q_s^2 \right)^{2/3} + \text{const}, \quad (3.30)$$

$$\varepsilon \beta_{J1} \approx \left( \frac{\beta_t}{\varepsilon} q_s^2 \right)^{1/3} + \text{const}, \quad (3.31)$$

where

$$\hat{I}_p \equiv I_p / \left( \frac{4\pi a^2 B_{t0}}{R_0} \right). \quad (3.32)$$

By a numerical solution without any assumption the above approximate scaling laws are modified a little as shown in Fig. 3.6. There is a limit at  $\beta_J \sim \varepsilon^{-1}$ , whereas the total beta has no limit up to  $\beta_t \approx 1$  when the plasma pressure is raised in an appropriate manner. Concrete expressions of the Grad-Shafranov equation for the FCT equilibrium are derived as follows.

By using  $q$ ,  $\mu$ , and  $V$  the Grad-Shafranov equation is rewritten as follows:

$$A^* \psi = -r^2 \left[ \frac{d\mu}{dV} \left( \frac{d\psi}{dV} \right)^\gamma + \gamma \left( \frac{d\psi}{dV} \right)^{\gamma-1} \frac{d^2\psi}{dV^2} \right] - 16\pi^4 \frac{q}{A} \frac{d}{dV} \left( \frac{q}{A} \frac{d\psi}{dV} \right). \quad (3.33)$$

The left-hand side of the equation has the elliptic partial differential operator for the function  $\psi(r, z)$  and the right-hand side has the second order ordinary differential operator. This kind of equation is called the “generalized differential equation” (GDE) [91]. There are various kinds of solution methods devised for the above equation and the following method is convenient for solution of the equilibrium of a tokamak plasma. First, we derive an equilibrium equation (Eq. (2.27)) by taking an average of the Grad-Shafranov equation on a magnetic surface, and from this equation the ordinary differential equation of  $F(\psi)$ ,

$$\frac{1}{F} \frac{dF}{d\psi} = -D \quad (3.34)$$

is obtained, where

$$D = \frac{v A \dot{K} + (A/2\pi)^\gamma \dot{\mu} F^{\gamma-2}}{v A K + \gamma \mu (A/2\pi)^\gamma F^{\gamma-2} + A}, \quad (2.35)$$

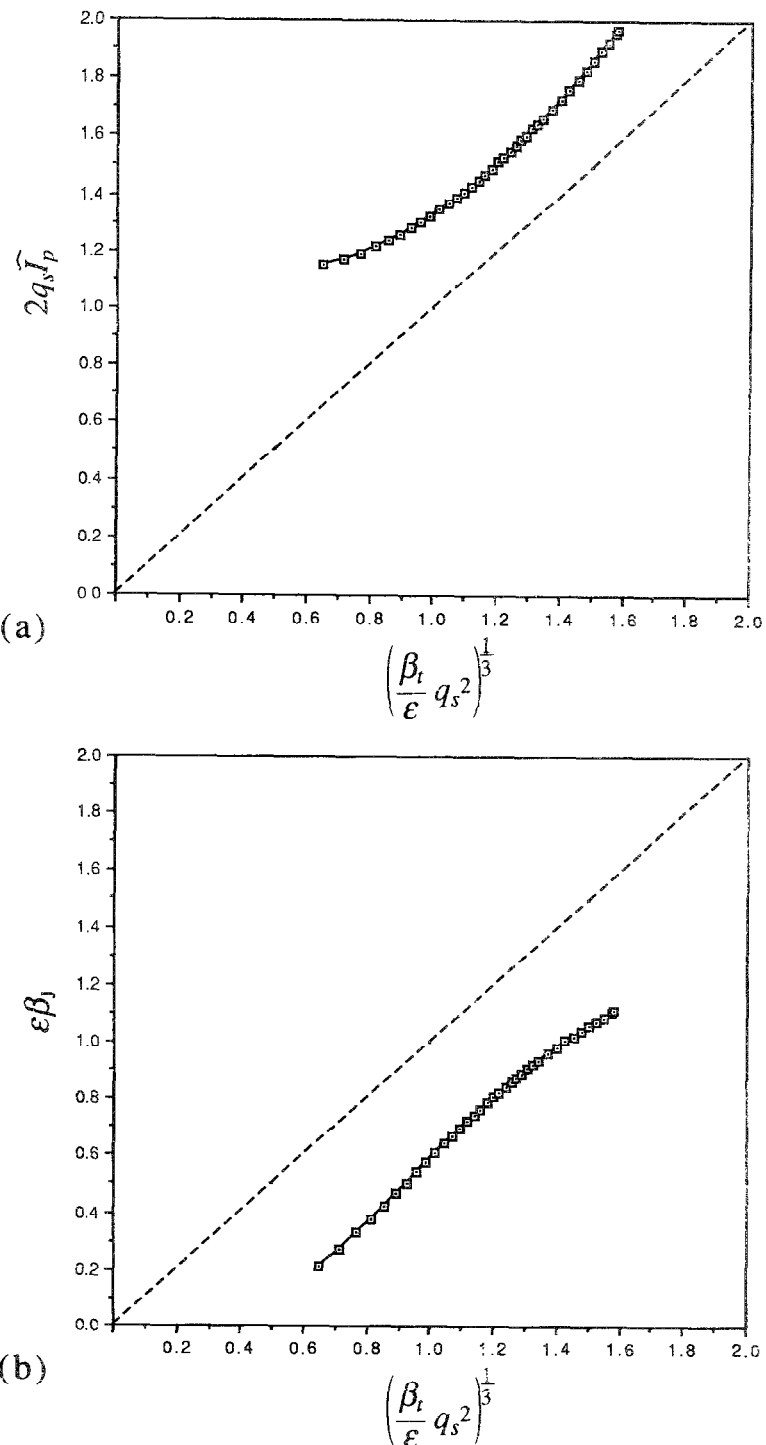


FIG. 3.6. Scaling laws of  $I_p$  and  $\beta_j$  with  $\beta_t$  for the FCT sequence.

$$v \equiv \frac{1}{4\pi^2 q}, \quad (3.36)$$

$$K \equiv \frac{1}{F} \dot{V} \langle B_\vartheta^2 \rangle = \frac{1}{q} \left[ \oint dl \frac{1}{r |\nabla \psi|} \right] \left[ \oint r dl \frac{1}{|\nabla \psi|} \right], \quad (3.37)$$

$$T = 4\pi^2 \frac{q}{A \dot{V}}, \quad (3.38)$$

and the dot denotes the differentiation with respect to  $\psi$ . The present problem is to solve this equation under the boundary condition,  $\psi(V=0)=0$ , and  $\psi(V=V_S)=\psi_S=\text{const}$ . It should be noted, however, that the magnetic surface  $\psi(r, z)$  should be determined beforehand in order to perform the surface integrals contained in  $A$  and

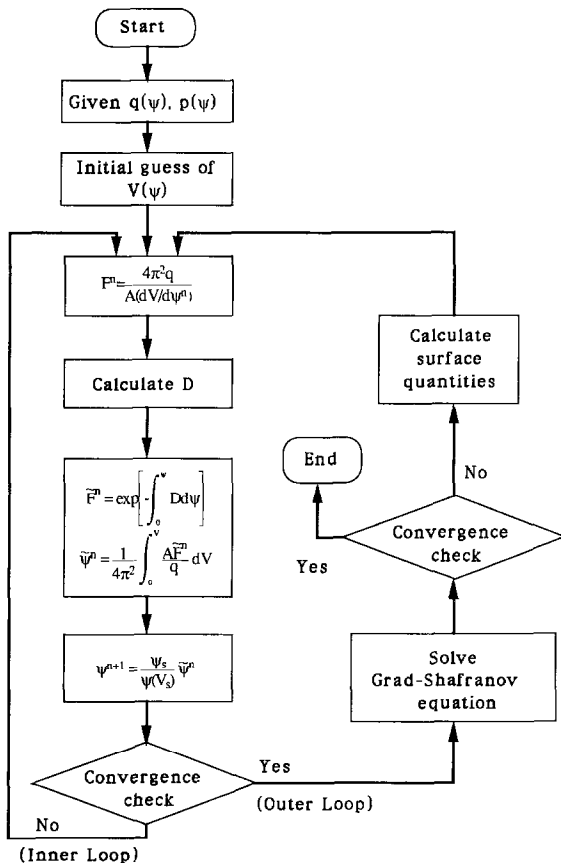


FIG. 3.7. Flow diagram for an FCT equilibrium solver.

*K.* For this purpose Eq. (3.34) should be solved iteratively with the original Grad-Shafranov equation as shown in the flow chart (Fig. 3.7). The above procedure is used for solving the equilibrium inside the plasma. When the equilibrium is extended to the vacuum region it should be noted that the toroidal magnetic field strength increases at the plasma surface with raising the plasma pressure. As a natural consequence, skin current appears at the surface to cancel the jump of the vacuum toroidal magnetic field, which is unrealistic, or to increase the plasma volume and decrease the surface magnetic field (Fig. 3.8). The increment of the plasma volume obeys the following scaling law in the case of a circular cross-sectional tokamak:

$$\frac{\delta V}{V} = \frac{1}{2} \beta. \quad (3.39)$$

Therefore, the numerical procedure should be carefully constructed to remove this skin current when one solves a free boundary equilibrium under the FCT condition.

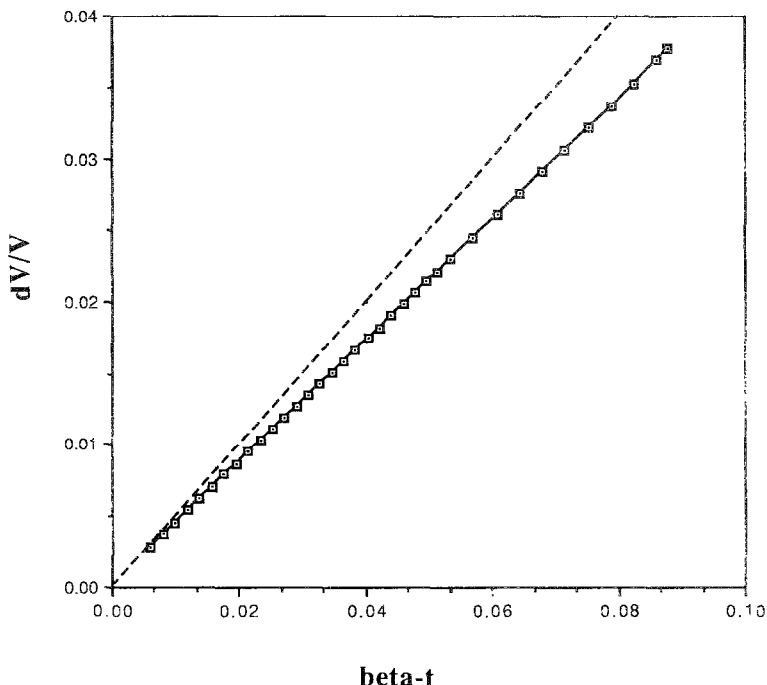


FIG. 3.8. Increase of the plasma volume with raising the beta value for a free boundary FCT calculation.

## 4. NUMERICAL METHODS FOR INVERSION OF GRAD–SHAFRANOV OPERATOR

### 4.1. Real Space Solution Method

#### 4.1.1. Finite Difference Method

A lot of equilibrium solvers have been developed on the basis of the finite difference method (FDM). Regular rectangular meshes with a five-points difference formula are usually employed for the finite difference discretization of these equilibrium solvers and the distinction of a solver is mainly displayed in the algorithms to solve the resulting simultaneous linear equations rather than in the discretization schemes. From this viewpoint we classify the FDM equilibrium solvers according to the algorithms into those based on the direct methods and the iterative methods, and we describe in detail the cyclic reduction methods and the multigrid method as the representative algorithms of the direct methods and the iterative methods, respectively.

(1) *The direct solution method.* In principle, various direct methods can be used to develop equilibrium solvers with the finite difference discretization. However, the cyclic reduction method overwhelmed other direct methods of the FDM formalism and it became one of the standard algorithms for the MHD equilibrium codes [38, 98]. The reasons are: first, this is a very efficient algorithm; second, a large memory space becomes available in a present-day computer; and third, because of good feedback control of a tokamak plasma it is not always necessary to solve a pure free boundary problem but it is sufficient, in many cases, to solve a semi-fixed boundary problem to which the cyclic reduction method is easily applicable. The cyclic reduction methods are described in a fairly detailed manner by Hockney [99] and Christiansen and Hockney [100]. Embodiment of the cyclic reduction methods as the algorithms for the equilibrium solvers was carried out by many authors [38, 98] on the basis of the double cyclic reduction (DCR) method by Buneman [101] and the Fourier analysis cyclic reduction (FACR) method by Hockney [99]. Although both the DCR and the FACR algorithms were originally designed to invert the Laplacian,  $\Delta$ , efficiently, here we give a detailed description of algorithms for inversion of the Grad–Shafranov operator,  $\Delta^*$ .

We consider a rectangular mesh with constant spacing  $\Delta r$  in the  $r$ -direction and  $\Delta z$  in the  $z$ -direction. Each mesh point is labeled by the mesh numbers  $i=0, 1, 2, \dots, M$ , and  $j=0, 1, 2, \dots, N$ , in the  $r$ - and  $z$ -directions, respectively, where  $M$  and  $N$  are chosen as the power of 2, i.e.,  $M=2^m$  and  $N=2^n$ . It was a stringent constraint when one solved an equilibrium on a small computer but recently it is not so serious because one can solve a large-scale problem by a large computer system. The Grad–Shafranov equation (Eq. (2.7)) is discretized on this mesh by a five-points formula as

$$\frac{\psi_{i-1,j} - 2\psi_{i,j} + \psi_{i+1,j}}{(\Delta r)^2} + \frac{1}{r_i} \frac{\psi_{i-1,j} - \psi_{i+1,j}}{2\Delta r} + \frac{\psi_{i,j-1} - 2\psi_{i,j} + \psi_{i,j+1}}{(\Delta z)^2} = g_{i,j}, \quad (4.1)$$

where  $\psi_{i,j} \equiv \psi(r_i, z_j)$  and  $g_{i,j} \equiv g(r_i, z_j)$ . In the following discussion we assume that  $\psi$  values at the boundary are given beforehand (the Dirichlet boundary condition). By introducing vectors,  $\phi$ 's, defined as

$$\phi_j = \begin{pmatrix} \psi_{0,j} \\ \vdots \\ \psi_{i,j} \\ \vdots \\ \psi_{M,j} \end{pmatrix}, \quad (4.2)$$

the vector equations

$$\phi_{j-1} - B\phi_j + \phi_{j+1} = \mathbf{p}_j, \quad j = 1, \dots, M-1, \quad (4.3)$$

are derived from Eq. (4.1), where  $B$  and  $\mathbf{p}_j$  are a tridiagonal matrix  $(M+1) \times (M+1)$  and a vector with  $(M+1)$  elements, respectively, defined as

$$B = \begin{pmatrix} 1 & 0 & 0 & & & & & 0 \\ \alpha_1 & \beta & \gamma_1 & & & & & \\ 0 & \alpha_2 & \beta & \gamma_2 & & & & \\ \cdot & \cdot & \cdot & \cdot & & & & \\ & \alpha_i & \beta & \gamma_i & & & & \\ \cdot & \cdot & \cdot & \cdot & & & & \\ 0 & & \alpha_{M-2} & \beta & \gamma_{M-2} & 0 & & \\ & & & \alpha_{M-1} & \beta & \gamma_{M-1} & & \\ & & & 0 & 0 & 1 & & \end{pmatrix}, \quad (4.4)$$

$$\alpha_i = (\Delta z)^2 \left[ \frac{1}{(\Delta r)^2} + \frac{1}{2r_i \Delta r} \right], \quad \beta = -2 \left[ \frac{(\Delta z)^2}{(\Delta r)^2} + 1 \right], \quad \gamma_i = (\Delta z)^2 \left[ \frac{1}{(\Delta r)^2} - \frac{1}{2r_i \Delta r} \right], \quad (4.5)$$

$$\mathbf{p}_j = (\Delta z)^2 \begin{pmatrix} g_{0,j} \\ \vdots \\ g_{i,j} \\ \vdots \\ g_{M,j} \end{pmatrix}. \quad (4.6)$$

By using the above representations we, next, consider the DCR algorithm. Because the Grad-Shafranov operator is uniform in the  $z$ -direction as the usual Laplacian and consequently the matrix  $B$  is independent of the index  $j$ , we can

apply cyclically the odd/even reduction with respect to the index  $j$ . After  $i$  reductions the vector equations (Eq. (4.3)) are reduced to the equations

$$\phi_{j-2^i} - B^{(i)}\phi_j + \phi_{j+2^i} = \mathbf{p}_j^{(i)}. \quad (4.7)$$

In the above equation the matrix  $B^{(i)}$  and the vector  $\mathbf{p}_j^{(i)}$  are given as

$$B^{(i)} = [B^{(i-1)}]^2 - 2I = (B^{(i-1)} - \sqrt{2} I)(B^{(i-1)} + \sqrt{2} I), \quad (4.8)$$

$$\mathbf{p}_j^{(i)} = \mathbf{p}_{j-2^{i-1}}^{(i-1)} + B^{(i-1)}\mathbf{p}_j^{(i-1)} + \mathbf{p}_{j+2^{i-1}}^{(i-1)}, \quad (4.9)$$

$$\phi_{j-2^i} = (B^{(i)})^{-1} [\phi_{j-2^{i+1}} + \phi_j - \mathbf{p}_j^{(i)}], \quad (4.10)$$

$$\phi_{j+2^i} = (B^{(i)})^{-1} [\phi_j + \phi_{j+2^{i+1}} - \mathbf{p}_{j+2^i}^{(i)}], \quad (4.11)$$

where  $I$  is the  $(M+1) \times (M+1)$  unit matrix. Finally, the vector equations (Eq. (4.7)) are reduced to a single vector equation as

$$\phi_0 - B^{(L)}\phi_{N/2} + \phi_N = \mathbf{p}_{N/2}^{(L)} \quad (L = \log_2 N - 1 = n - 1), \quad (4.12)$$

where

$$\phi_0 = \begin{pmatrix} \psi_{0,0} \\ \vdots \\ \psi_{i,0} \\ \vdots \\ \psi_{M,0} \end{pmatrix}, \quad \phi_N = \begin{pmatrix} \psi_{0,N} \\ \vdots \\ \psi_{i,N} \\ \vdots \\ \psi_{M,N} \end{pmatrix} \quad (4.13)$$

are given as the boundary condition. The solution of Eq. (4.12) is derived as

$$\phi_{N/2} = [B^{(n-1)}]^{-1} [\phi_0 + \phi_N - \mathbf{p}_{N/2}^{(n-1)}]. \quad (4.14)$$

In the above equations it should be noted that the matrix  $B^{(i)}$  is not tridiagonal although the initial matrix  $B^{(0)} = B$  (Eq. (4.4)) is a tridiagonal matrix. However, the final  $B$ -matrix,  $B^{(n-1)}$ , as well as  $B^{(i)}$  in Eq. (4.11), is easily factorized as

$$B^{(n-1)} = (B - b_1 I)(B + b_1 I) \cdots (B - b_{n-1} I)(B + b_{n-1} I), \quad (4.15)$$

where each elementary matrix,  $B_k - b^k I$ , is tridiagonal. Therefore, the simultaneous linear equations (Eq. (4.14)) can be solved by  $n-1$  inversions of the tridiagonal matrices, which is carried out by the one-dimensional cyclic reduction. In the case of the Grad-Shafranov equation, however, off-diagonal elements of the above elementary tridiagonal matrix are not constant and it is not so advantageous to apply the cyclic reduction to the solution in the  $r$ -direction. Solutions of the other vectors are synthesized by using Eqs. (4.10) and (4.11). It should be noted that, during the construction of the matrices,  $B^{(i)}$ , overflow will occur. But it can be overcome by changing the recurrence relation (Eq. (4.9)) to one that is algebraically equivalent, with multiplication by the inverse of the  $B^{(i)}$ -matrices, which brings about underflow in place of the overflow [99].

As for the FACR method, we express the flux function at the mesh point  $\psi_{i,j}$  by the finite Fourier series in the  $z$ -direction as

$$\psi_{i,j} = \frac{1}{2}\psi_{i,0}^c + \frac{1}{2}(-1)^j\psi_{i,N/2}^s + \sum_k \psi_{i,k}^c \cos \frac{2\pi k j}{N} + \sum_k \psi_{i,k}^s \sin \frac{2\pi k j}{N}. \quad (4.16)$$

For the usual Laplacian operator the cyclic reduction can be applied efficiently in both the  $r$ - and the  $z$ -directions, and application of the odd/even reduction before the Fourier analysis reduces the count of the numerical operations considerably. In the case of the Grad-Shafranov operator, however, good efficiency of the cyclic reduction method is exhibited only in the  $z$ -direction, and the Fourier analysis is applied to the solution directly from the beginning. By substituting the above Fourier series into Eq. (4.7) we obtain

$$\mu_i \psi_{i-1,k} + \lambda_k \psi_{i,k} + v_i \psi_{i+1,k} = g_{i,k}^*, \quad (4.17)$$

$$g_{i,k}^* = g_{i,k}(\Delta z)^2, \quad (4.18)$$

$$\mu_i = \left( \frac{\Delta z}{\Delta r} \right)^2 + \frac{(\Delta z)^2}{2r_i \Delta r}, \quad (4.19)$$

$$v_i = \left( \frac{\Delta z}{\Delta r} \right)^2 - \frac{(\Delta z)^2}{2r_i \Delta r}, \quad (4.20)$$

$$\lambda_k = -2 \left[ \left( \frac{\Delta z}{\Delta r} \right)^2 + 1 - 2 \cos \left( \frac{2\pi k}{N} \right) \right], \quad (4.21)$$

$$\psi_{i,k} = \psi_{i,k}^c, \quad \text{or} \quad \psi_{i,k}^s; \quad (4.22)$$

$$g_{i,k} = g_{i,k}^c, \quad \text{or} \quad g_{i,k}^s, \quad (4.23)$$

$$\psi_{i,k} = \psi_{i,k}^c, \quad g_{i,k} = g_{i,k}^c \quad \text{for } k = 0 \text{ or } N/2. \quad (4.24)$$

In the original FACR algorithm Eq. (4.17) is solved by the cyclic reduction method, which is extremely advantageous in the case of the usual Laplacian operator. For the Grad-Shafranov equation, however, necessary counts of the numerical operations to solve Eq. (4.17) are about the same among the cyclic reduction method, the method of recursive formula [102], and the LU decomposition method [103], because all the matrix elements are to be calculated at each step. As for the comparison between the DCR and the FACR methods the above situation is not altered. But in a large computer the FACR program is more preferable because it is not necessary to save the memory space so tightly and, moreover, high vector efficiency is difficult to attain for the DCR program in comparison with the FACR program. This issue will be discussed in 4.4.

(2) *The iterative solution method.* As the direct solution methods of the linear equations have been well developed to a sophisticated level and farther development seems difficult, some good iterative methods were looked for. Detailed

descriptions of representative classical iterative methods such as the SOR method, the ADI method, and the CG (conjugate gradient) method are found in monographs and review papers [104–106]. In the equilibrium solvers of the early stage of tokamak research such kinds of numerical methods were often used (e.g., [31, 32]) but recently these are not considered to be efficient for the purpose. However, the progress of computers in the fields of vector and parallel processors again stimulated the investigation of the iterative methods because the iterative algorithms are more easily adaptable to vector or parallel processors than direct methods. In general the iterative procedure [104] to solve a simultaneous linear equation,

$$\mathbf{A}\mathbf{u} = \mathbf{f}, \quad (4.25)$$

is represented by the iteration of the equation,

$$\mathbf{S}\mathbf{u}^{(n+1)} = \mathbf{T}\mathbf{u}^{(n)} + \mathbf{f}, \quad (4.26)$$

where the matrix  $\mathbf{A}$  is divided into two matrices as

$$\mathbf{A} = \mathbf{S} - \mathbf{T}. \quad (4.27)$$

The error of the solution,  $\mathbf{e}^{(n)} \equiv \mathbf{u}^{(n)} - \mathbf{u}$ , develops as

$$\mathbf{e}^{(n+1)} = \mathbf{M}\mathbf{e}^{(n)}, \quad (4.28)$$

where

$$\mathbf{M} = \mathbf{S}^{-1}\mathbf{T}. \quad (4.29)$$

From the above equations criteria to design an efficient iterative algorithm is summarized as: (1)  $\mathbf{S}^{-1}$  should be calculated as easily as possible and (2) the spectral radius,  $\rho(\mathbf{M})$ , of the matrix  $\mathbf{M}$  should be as small as possible in comparison with unity, where  $\rho(\mathbf{M})$  is the maximum of the absolute values of the eigenvalues of the matrix  $\mathbf{M}$ . In order to meet the above antipodal requirements the multi-grid method (MGM) was devised and applied to the solution of various linear problems [107–110]. This method can be applied not only to the linear equations but also to singular equations and eigenvalue problems [110, 111].

The basic idea of the MGM algorithm is that, by choosing an appropriate simple iterative procedure, the eigenvalues of  $\mathbf{A}$  for the short wavelength modes are made relatively small and converge rapidly enough for a given mesh resolution, and the rapid convergence of eigenvalues of longer wavelength modes (smoother modes) can be attained by the subsequent choice of coarser meshes. According to the above basic idea, the calculation of the MGM algorithm is carried out at each level from the level  $l=L$  with the finest mesh to the level  $l=0$  with the coarsest mesh (smoothing and restriction processes) and afterward the calculated data are transferred from the lower levels to the higher levels (prolongation process). To be

more precise on the process at the level  $l$ , first we consider the  $l$ -level equation of the vector  $\mathbf{u}_l$ ,

$$\mathbf{A}_l \mathbf{u}_l = \mathbf{f}_l. \quad (4.30)$$

Then, by the simple iteration method, e.g., the Gauss-Seidel method, we solve the above equation and obtain an approximate solution,  $\mathbf{U}_l$ , which is called the “smoothing” process, because this process derives a lower level equation for a smoother solution. Thus the  $(l-1)$ -level equation is given as

$$\mathbf{A}_{l-1} \mathbf{u}_{l-1} = \mathbf{f}_{l-1}, \quad (4.31)$$

by calculating the  $l$ -level defect,  $\mathbf{d}_l$ , and introducing the restriction operator,  $\mathbf{R}$ , as

$$\mathbf{d}_l = \mathbf{A}_l \mathbf{U}_l - \mathbf{f}_l, \quad (4.32)$$

$$\mathbf{f}_{l-1} = \mathbf{R} \mathbf{d}_l, \quad (4.33)$$

where “restriction,”  $\mathbf{R}$ , means to get data on the  $(l-1)$ -level mesh from the data on

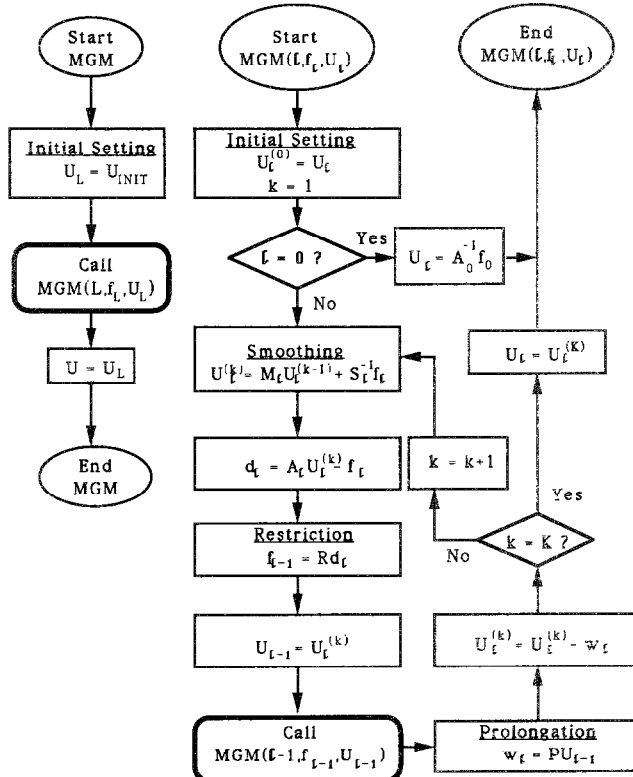


FIG. 4.1. Flow diagram of the MGM algorithm.

the  $l$ -level mesh. On the other hand, “prolongation,”  $\mathbf{P}$ , is the interpolation process from the data,  $\mathbf{U}_{l-1}$ , on the coarser mesh to the data,  $\mathbf{w}_l$ , on the finer mesh as

$$\mathbf{w}_l = \mathbf{P} \mathbf{U}_{l-1}. \quad (4.34)$$

After the lower level solution  $\mathbf{U}_{l-1}$  is transferred and prolonged, the  $l$ -level solution is constructed as

$$\mathbf{U}_l = \mathbf{U}_l^{(\text{old})} - \mathbf{w}_l. \quad (4.35)$$

If it is necessary, the smoothing process is repeated for  $K$  times in each level before the solution is transferred to the higher level. The MGM cycles with  $K=1$  and  $K=2$  are called  $V$ -cycle and  $W$ -cycle, respectively. The flow diagram of the MGM algorithm is shown in Fig. 4.1. In order to visualize the recursive operations among the levels, the path diagrams of the MGM algorithm for two cases with  $L=4$  and  $K=1, 2$  are shown in Fig. 4.2.

There are a few examples of the application of the MGM algorithm to the MHD equilibrium solvers. Braams developed an axisymmetric MHD equilibrium code and gave some speculations on the application of the MGM algorithm to the problems on axisymmetric equilibrium solver in the inverse coordinate system and the three-dimensional equilibrium calculations [112]. As for the axisymmetric equilibrium problem in the usual coordinate system the author succeeded in developing an efficient code which is about three times faster than a code with the well optimized Buneman algorithm. Real-time interpretation and control of an experiment on a time scale of about 10 ms or less were expected to be a promising

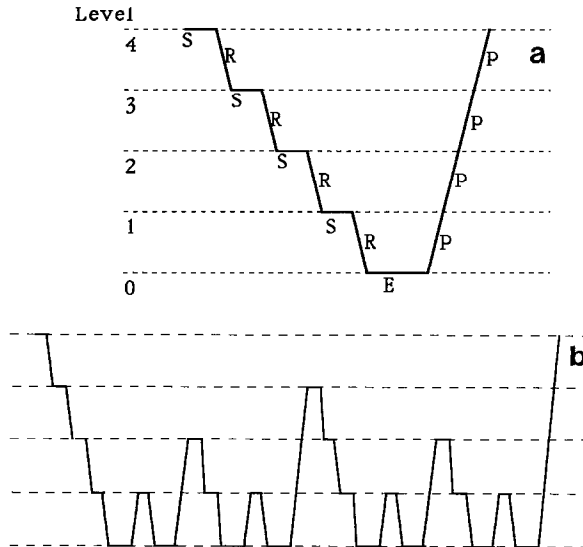


FIG. 4.2. Path diagrams of the MGM algorithm for  $L=4$  and  $K=1$  (a) and 2 (b).

application field of the MGM equilibrium code. The author speculated that the MGM algorithm plays an important role in development of the inverse equilibrium solver because there are no competing algorithms as the DCR algorithm in the case of the real-space equilibrium solvers. Application of the MGM algorithm to the three-dimensional equilibrium problem has been initiated by the author but satisfactory results have not been reported yet and the development of appropriate adaptive method to adjust the grid to the magnetic configuration is required before the MGM algorithm is fully utilized for this problem.

#### 4.1.2. Finite Element Method

When one solves a system with a complicated geometrical shape the finite element method is more advantageous than the finite difference method because of the flexibility of choice of a mesh shape. In contrast with this advantage the matrix generated by the finite element method is, generally, more dense and more arithmetic operations are required to calculate the matrix elements in comparison with the finite difference method. From the viewpoint of the geometrical shape the computational object of MHD equilibrium in a fusion device is extremely simple among the engineering calculations and one cannot, usually, take advantage of the finite element method in the calculation of MHD equilibrium. For limited problems

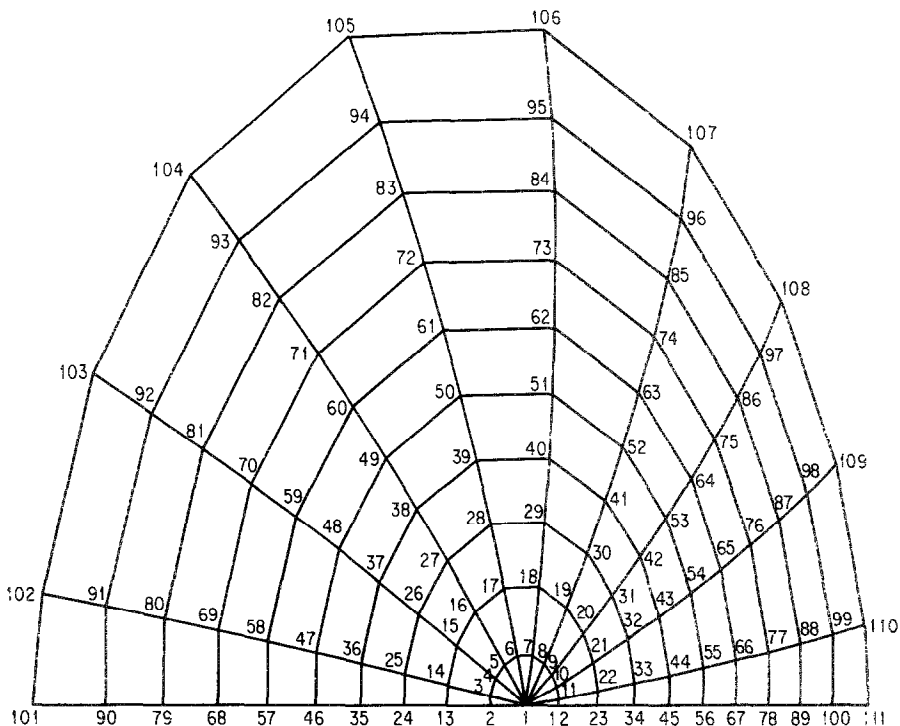


FIG. 4.3. An example of the FEM mesh structure for an equilibrium calculation.

of MHD equilibrium the finite element method is more advantageous than the finite difference method. Examples of these cases are the inverse equilibrium solver and some other applications where information on the magnetic flux surfaces should be explicitly used during the calculation process, such as the analyses of MHD equilibrium with flow. In the following we describe the finite element formulation of the MHD equilibrium problem and some related topics. To define the problem clearly we treat the nonlinear eigenvalue problem described in Section 3.2. First we derive the objective function of the finite element formalism as a weak form of Eq. (3.24) as

$$L(\psi^{n+1}) = (\Delta^* \psi^{n+1}, \psi^{n+1}) - 2(f(\psi^n), \psi^{n+1}), \quad (4.36)$$

$$f(\psi^n) = -\lambda^n \mu_0 J_{\phi 0}(-\psi^n / \psi_0^n). \quad (4.37)$$

By executing a partial integration the objective function  $L(\psi)$  is rewritten as

$$L(\psi^{n+1}) = - \int r dr dz \left\{ \left( \frac{1}{r} \frac{\partial \psi^{n+1}}{\partial r} \right)^2 + \left( \frac{1}{r} \frac{\partial \psi^{n+1}}{\partial z} \right)^2 - \frac{2\lambda^n}{r} J_{\phi 0}(\psi^n) \psi^{n+1} \right\}. \quad (4.38)$$

By using an appropriate set of linear basis functions, the functional  $L$  is represented by  $N$  parameters  $(\psi_1^{n+1}, \psi_2^{n+1}, \dots, \psi_N^{n+1})$ , where  $N$  is the number of nodes (Fig. 4.3). Simultaneous linear equations with respect to  $\psi_i^{n+1}$  are immediately derived as

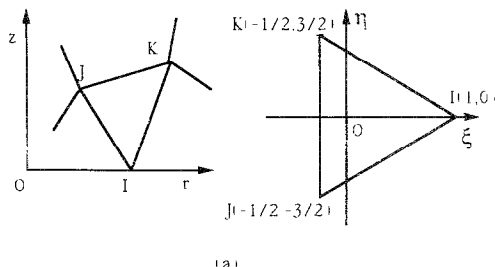
$$\mathbf{A} \Psi^{n+1} = \mathbf{B}^n, \quad (4.39)$$

$$\Psi^{n+1} = \begin{pmatrix} \psi_1^{n+1} \\ \psi_2^{n+1} \\ \vdots \\ \psi_N^{n+1} \end{pmatrix}, \quad (4.40)$$

$$\mathbf{B}^n \Psi^{n+1} = -2 \int f(\psi^n) \psi^{n+1} dS, \quad (4.41)$$

where the matrix  $\mathbf{A}$  and vector  $\mathbf{B}^n$  are derived according to the standard procedure of the FEM formulation.

There are several possibilities for the choice of the expansion of the function  $\psi$  and the finite elements. Usual choice of two-dimensional fintic elements for the MHD equilibrium calculation of the plasma are 3-node triangular and 4-node rectangular elements with linear and bilinear basis functions (Fig. 4.4), respectively, which were employed by Takeda and Tsunematsu for the SELENE code [48]. Application of 8-node isoparametric elements (Fig. 4.5) to the problem of flow equilibrium instead of the 4-node elements was carried out by Kerner and Jandl [45]. In this code a technique for storing the stiffness matrix and solving the system of linear equation is used where only the non-zero elements are processed. They found no remarkable difference under the same computational condition between the



(a)

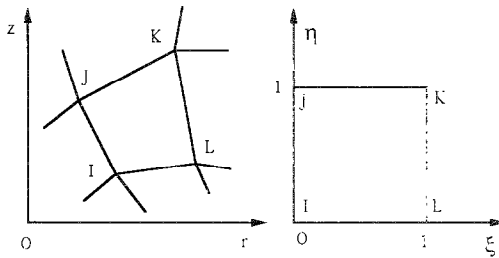


FIG. 4.4. Triangular and rectangular elements with linear and bilinear basis functions, respectively, and corresponding isoparametric transformations: (a) a triangular element; (b) a rectangular element.

4-node (bilinear) elements and the 8-node (biquadratic) elements. Also the effect of the mesh rearrangement was investigated and it was concluded that the mesh rearrangement causes an interpolation error but finally a set of sufficiently accurate magnetic surfaces is recovered (Fig. 4.6). By assuming that a  $21 \times 21$  finite element net is sufficient for most applications they estimated that accurate solution is computed after 20 iterations in 5 to 10 s of Cray 1 CPU time. Another extension of the method is to employ higher order elements. By using a higher order basis function, such as those by Felippa [113] and by Melosh [114] one can obtain directly the derivatives of the magnetic flux function,  $\partial\psi/\partial r$  and  $\partial\psi/\partial z$  as well as the function  $\psi$  itself. If one uses a linear basis function for a triangular element and combination

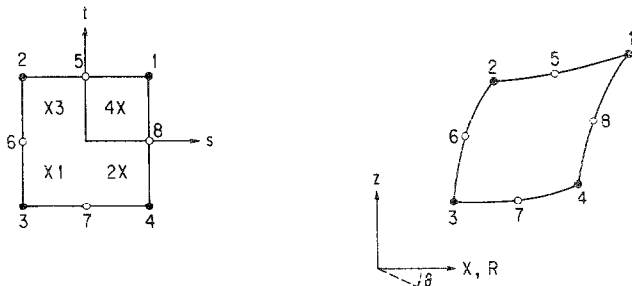


FIG. 4.5. Isoparametric mapping between the local and global systems for the 8-node rectangular element [45].

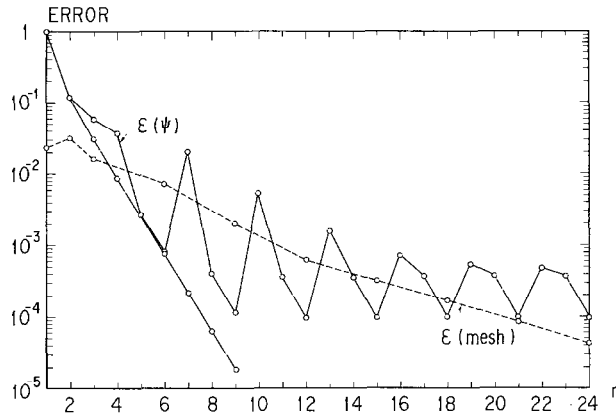


FIG. 4.6. An example of the convergence curves of the FEM code by Kerner and Jandl [45]. The steep curve is for the case without the mesh rearrangement.

of a bilinear basis function and isoparametric transformation for the rectangular element the solution becomes continuous on the edges of the elements. On the other hand, for the higher order elements not only the derivatives,  $\partial\psi/\partial r$  and  $\partial\psi/\partial z$  but also the flux function  $\psi$ , can be made continuous on the edge of the elements.

The FEM solution of the first type of free boundary problem was formulated by Kikuchi [80] with mathematical strictness. The procedure is described for the model equations (2.94) and (2.95) (see [86] for the more general case), as follows: Let  $X_0^h$  be a set of piecewise linear polynomial functions  $u_h$  such that  $u_h = 0$  on  $\Gamma$  ( $h$ : the maximum length of finite elements in  $R^2$ ). In this functional space approximation of the weak form (Eqs. (2.94) and (2.95)) given by

$$\langle u_h, v_h \rangle = \lambda_h(\hat{f}(u_h), v_h), \quad \forall v_h \in X_0^h, \quad (4.43)$$

$$u_h + 1 \in X_0^h, \quad (4.44)$$

where

$$\langle u, v \rangle \equiv \sum_{i=1}^2 \int_r \frac{\partial u}{\partial x_i} \frac{\partial v}{\partial x_i} dx. \quad (4.45)$$

The corresponding linear equation (Eqs. (2.96) and (2.97)) are also approximately expressed by the equations

$$\langle \phi_h, v_h \rangle = \lambda_{h0}(\phi_h, v_h), \quad \forall v_h \in X_0^h \quad (4.46)$$

$$(\phi_h, \phi_h) = 1, \quad (4.47)$$

which have a simple eigenvalue  $\lambda_{h0} > 0$  and a unique solution  $\phi_h > 0$ . From Eqs. (2.101) to (2.102), the equation for  $u_h^*$  is derived as

$$\langle u_h^*, v_h \rangle = \lambda_h (\hat{f}(u_h^*), v_h), \quad (4.48)$$

$$u_h^* + \varepsilon \in X_0^h, \quad (4.49)$$

and  $u_h^*$  is decomposed as

$$u_h^* = \phi_h + \varepsilon \psi_h + w_h, \quad (4.50)$$

$$(\psi_h, \phi_h) = 0, \quad (4.51)$$

$$(w_h, \phi_h) = 0, \quad (4.52)$$

where the equations for  $\psi_h$  and  $w_h$  are

$$\langle \psi_h, v_h \rangle - \lambda_{h0} (\psi_h, v_h) = \lambda_{h0} (1, \phi_h) (\phi_h, v_h), \quad (4.53)$$

$$\langle w_h, v_h \rangle - \lambda_{h0} (w_h, v_h) = (\lambda_h \hat{f}(u_h^*) - \lambda_{h0} u_h^* - \varepsilon \lambda_{h0} (1, \phi_h) \phi_h, v_h) \quad (4.54)$$

and the eigenvalue  $\lambda_h$  is given by

$$\lambda_h = \frac{(u_h^*, \phi_h) + \varepsilon (1, \phi_h)}{(\hat{f}(u_h^*), \phi_h)}. \quad (4.55)$$

The solution  $\psi_h$  of Eq. (4.53) can be obtained from the linear algebraic equation. The iteration of Eqs. (4.54) and (4.55) is contracting, and  $u_h$  derived from Eq. (4.50) gives the unique solution of Eq. (4.43) for sufficiently small  $|\varepsilon|$  which corresponds to an approximate solution of Eqs. (2.93) and (2.94) for sufficiently small  $h$ .

#### 4.1.3. Other Methods

In this subsection we describe three numerical methods which cannot be classified within the previously described framework. As for the Green's function method and the expansion method with orthogonal functions we present only brief descriptions because at present they are replaced by more efficient methods. And we describe the conformal mapping method in a rather detailed manner.

(1) *Green's function method.* The Grad-Shafranov equation, Eq. (3.22), is formally transformed into an integral equation,

$$\psi = \lambda A^{*-1} f(r, \psi). \quad (4.56)$$

The concrete form of the above integral equation is given by using the Green's function of a ring current as

$$A^{*-1} = \int G(r, z; r', z') dr' dz', \quad (4.57)$$

where the Green's function  $G(r, z; r', z')$  is given in 3.1. The equilibrium solver based on the Green's function is written according to the following numerical procedure [40, 41, 115]: (1) set initial values to mesh points  $(r_i, z_j)$ ; (2) calculate plasma current density  $J_{\phi,ij}$  at each mesh point; (3) iterate the eigenvalue appearing in the right-hand side of the Grad-Shafranov equation (the nonlinear eigenvalue problem) under the condition of constant total plasma current; (4) calculate  $\psi$  solution at the  $(n+1)$ th step,  $\psi_{p,ij}^{n+1}$ , using Eq. (4.56); (5) check convergence by comparing  $\psi_{p,ij}^n$  and  $\psi_{p,ij}^{n+1}$ ; (6) repeat the above process if not converged. This method is very simple and intelligible. The magnetic fields due to the plasma current and the external coil current are clearly separated, which is advantageous for the engineering applications. On the other hand, generally, it takes much computing time in comparison with other more efficient codes and one cannot attain a solution with higher resolution because of the appearance of dense singularities.

(2) *Expansion with orthogonal functions.* MHD equilibrium calculation based on toroidal multipolar expansion was first proposed by Feneberg and Lackner [36] and the scheme was tested for various plasma configuration with force-free equilibria with a simple sharp boundary distribution of volume currents. A numerical equilibrium code SPHEX using this method was reported in detail by Seki *et al.* [42] which is applicable to more general current profile. First, the magnetic flux function  $\psi$  is expressed by a sum of the flux function due to the plasma current  $\psi_p$  and the vacuum magnetic flux function  $\psi_0$  due to the external coil currents. Then the Grad-Shafranov equation (Eq. (2.7)) is rewritten as

$$\Delta^* \psi_p = S(\psi_p + \psi_0) \cdot f(r, \psi_p + \psi_0), \quad (4.58)$$

where the form factor  $S$  defined by Eqs. (3.2) and (3.3) is used and

$$f(r, \psi_p + \psi_0) \equiv -\mu_0 r J_\phi(r, \psi_p + \psi_0). \quad (4.59)$$

Then the flux function  $\psi_p$  is expanded by a set of the associated Legendre functions of the first type  $P_n^1(x)$  and by using the orthogonality condition the Grad-Shafranov equation is transformed into the equation which determines the coefficients of the expansion. Solving the equation we can easily derive the final solution as

$$\begin{aligned} \psi_p = \sum_{n=1}^{\infty} \frac{1}{2n+1} & \left[ -r^{n+1} \int_r^{\infty} \rho^{-n} g_n(\rho) d\rho \right. \\ & \left. - r^{-n} \int_0^r \rho^{n+1} g_n(\rho) d\rho \right] \sqrt{1-x^2} P_n^1(x), \end{aligned} \quad (4.60)$$

$$g_n(r) = \frac{2n+1}{2n(n+1)} \int_{-1}^1 \frac{P_n^1(x)}{\sqrt{1-x^2}} S(\psi_p + \psi_0) \cdot f(r \sqrt{1-x^2}, \psi_p + \psi_0) dx. \quad (4.61)$$

As the right-hand side of the equation contains  $\psi_p$  one must solve this equation iteratively in order to obtain the equilibrium solution.

Alladio and Crisanti [43] developed an equilibrium solver based on the toroidal multipolar expansion in the fully toroidal coordinate system  $(\theta, \tilde{\omega}, \phi)$  [116]. The method is advantageous especially when used for magnetic measurement [117] because it can easily provide various macroscopic quantities such as the current density weight center [72], the shape of the last magnetic surface [118], and the triangularity [117]. Especially, it is proved that the  $m$ -number spectrum of the internal multipolar moments contains information necessary for separation of  $\beta_p$  and  $I_i/2$  in the electromagnetic measurement.

(3) *Conformal mapping method.* Goedbloed [46] developed a conformal mapping method for solving the Grad-Shafranov equation, where two steps of conformal mappings from the original  $z$ -plane to the computational  $w$ -plane are considered: (I) the Moebius transformation ( $z \rightarrow \zeta$ ) of the unit disk  $|z| \leq 1$  onto the unit disk  $|\zeta| \leq 1$  such that  $z = \delta$  ( $\delta$ : position of the magnetic axis) corresponds to  $\zeta = 0$ ; and (II) the mapping ( $\zeta \rightarrow w$ ) of a simply-connected region enclosed by the curve  $\zeta(\Gamma_p)$  ( $\Gamma_p$ : curve of the plasma surface in the  $z$ -plane) onto the unit disk,  $|w| \leq 1$ . The resultant mapping  $w(\zeta(z))$  is also a conformal mapping which transforms the plasma boundary  $\Gamma_p$  in the  $z$ -plane onto a unit circle  $|w| = 1$  while shifting the magnetic axis  $x = \delta$  to the origin of the  $w$ -plane (Fig. 4.7). The Grad-Shafranov equation is solved in the  $w$ -plane by using Fourier representations. The advantage obtained by such a transformation is that the number of Fourier harmonics needed for accurate representation of an equilibrium can be reduced substantially by the Moebius transformation and that the inversion of the Laplace operator can be performed analytically in the cylindrical coordinates in the  $w$ -plane. As a natural consequence of the above mappings this method is suitable for solving the MHD equilibrium problems with a fixed boundary condition where the position of the magnetic axis,  $\delta$ , is substituted for the approximate poloidal beta,  $\beta_p$ , as an input parameter characterizing the equilibrium.

The explicit form of the Moebius transform is

$$\zeta = \frac{z - \delta}{1 - \delta z}. \quad (4.62)$$

The existence of the mapping (II) is guaranteed by the classical Riemann mapping

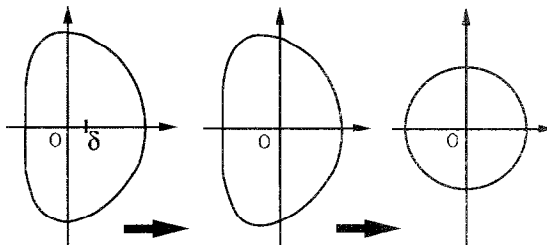


FIG. 4.7. Conformal mapping used for the equilibrium calculation [46].

theorem [119]. Such a mapping is expressed by a nonlinear integral equation of a type of Hilbert transform as shown in the following. We consider an analytic function,  $\zeta = g(w)$ , which transforms a unit disk,  $|w| \leq 1$ , to a simply-connected region in the  $\zeta$ -plane. By the Cauchy's integral theorem, the value of  $g(w)$  for  $w = re^{it}$  ( $r < 1$ ) is given by the integral of  $g(w)$  on  $|w| = 1$  as

$$g(w) = \frac{1}{2\pi} \int_0^{2\pi} \frac{g(e^{it'})}{1 - re^{i(t-t')}} dt'. \quad (4.63)$$

The boundary value of  $g$  can be expressed by

$$g(e^{it'}) = g_R(t') + ig_I(t'), \quad (4.64)$$

where  $g_R$  and  $g_I$  are periodic functions. By taking the limit,  $r \rightarrow 1$ , with  $r < 1$ , we obtain an integral relation between  $g_R$  and  $g_I$  (Hilbert transformation) as

$$g_R(t) = A - \frac{1}{2\pi} P \int_0^{2\pi} \frac{1}{2} \cot\left(\frac{t-t'}{2}\right) g_I(t') dt', \quad (4.65)$$

$$A = \frac{1}{2\pi} \int_0^{2\pi} g_R(t') dt', \quad (4.66)$$

where  $P$  denotes Cauchy's principal value, and  $A = 0$  if  $g(0) = 0$ . Due to its convolution form, Eq. (4.65) can be solved easily with respect to  $g_I(t)$  by using a fast Hilbert transform (FHT) [46] based on the fast Fourier transform technique. Next, the shape of the boundary in the  $\zeta$ -plane ( $\zeta = \rho e^{i\theta}$ ) is specified by the equation,

$$\rho = f(\theta), \quad (4.67)$$

and the following function is introduced to make correspondence between the angular variables,  $t$  and  $\theta$ ,

$$F(w) = \ln(\zeta(w)/w), \quad (4.68)$$

which takes the values at the boundary,  $|w| = 1$ ,

$$F(e^{it}) = \ln(f(\theta(t)) + i(\theta(t) - t)). \quad (4.69)$$

The real and imaginary parts of the right-hand side of Eq. (4.69) satisfy the relation expressed by the Hilbert transformation. From this relation one can derive a nonlinear integral equation for the unknown function  $\theta(t)$  as

$$\ln(f(\theta(t))) = -\frac{1}{2\pi} P \int_0^{2\pi} \frac{1}{2} \cot\left(\frac{t-t'}{2}\right) (\theta(t') - t') dt', \quad (4.70)$$

and this equation is solved iteratively by using FHT. In this way the complete mapping comprised of the two steps of the mappings is derived as

$$\begin{aligned} z(w) &= x + iy = \delta + (1 - \delta^2) \frac{g(w)}{1 + \delta g(w)} \\ &= \delta + \sum_{m=1}^{\infty} \phi_m s^m e^{imt}, \end{aligned} \quad (4.71)$$

where  $w = se^{it}$  and the  $\phi_m$ 's (real for up-down symmetric cases) are obtained from the Fourier expansion of the numerically obtained boundary function,

$$z(e^{it}) = \delta + \sum_{m=1}^{\infty} \phi_m e^{imt}. \quad (4.72)$$

After some cumbersome handling of equations, the Grad-Shafranov equation in the  $w$ -plane is derived as

$$\mathcal{A}_{\perp}^{(w)} \Psi = AH(\Psi), \quad (4.73)$$

where

$$\mathcal{A}_{\perp}^{(w)} = \frac{1}{s} \frac{\partial}{\partial s} \left( s \frac{\partial}{\partial s} \right) + \frac{1}{s^2} \frac{\partial^2}{\partial s^2}, \quad (4.74)$$

$$H(\Psi) = h^2 [\Gamma(\Psi) + Bx(2 + \varepsilon x) \Pi(\Psi)] + \frac{\varepsilon}{1 + \varepsilon x} \left( \frac{1}{s} \frac{\partial y}{\partial t} \frac{\partial \Psi}{\partial s} + \frac{1}{s^2} \frac{\partial x}{\partial t} \frac{\partial \Psi}{\partial t} \right), \quad (4.75)$$

$$h(s, t) \equiv \left| \frac{dz}{dw} \right| = \frac{1}{s} \sqrt{(\partial x / \partial t)^2 + (\partial y / \partial t)^2}. \quad (4.76)$$

$\Gamma(\Psi)$  and  $\Pi(\Psi)$  are the profile functions of  $dG/d\Psi$  and  $dP/d\Psi$ , respectively, defined as

$$\frac{dG}{d\Psi} = -A\Gamma(\Psi), \quad \frac{dP}{d\Psi} = -AB\Pi(\Psi), \quad (4.77)$$

and the other notations are the same as those in 2.7. Boundary conditions are imposed on  $\Psi$  as

$$\Psi = 1, \quad \text{at } s = 1, \quad (4.78)$$

$$\nabla \Psi = 0, \quad \text{at } s = 0, \quad (4.79)$$

to ensure the location of the magnetic axis at  $x = \delta$ ,  $y = 0$ . In Eqs. (4.73) and (4.75),  $A$  is an eigenvalue and  $B$  is determined corresponding to the value of  $\delta$ . Equation (4.73) is solved iteratively as

$$\mathcal{A}_{\perp}^{(w)} \Psi^{(n+1)} = AH(\Psi^{(n)}), \quad (4.80)$$

where the inversion of the operator  $A_{\perp}^{(w)}$  is easily carried out by the integration over the  $s$ -direction in terms of Fourier representation of  $\Psi(s, t)$  and  $H(\Psi)$  as

$$\Psi(s, t) = \frac{1}{2} \Psi_0(s) + \sum_{m=1}^{\infty} \Psi_m(s) \cos(mt), \quad (4.81)$$

$$H(\Psi) = \frac{1}{2} H_0(s) + \sum_{m=1}^{\infty} H_m(s) \cos(mt). \quad (4.82)$$

with the boundary conditions,

$$\Psi_m(1) = 2\delta_{m,0}, \quad (4.83)$$

and the regularity conditions,

$$\Psi_m(0) = 0, \quad \frac{d\Psi_m}{ds}(0) = 0, \quad (4.84)$$

for  $m = 0, 1, 2, \dots$ . From the regularity conditions for the  $m=0$  and the  $m=1$  components, equations determining  $B(n)$  and  $A(n)$  are derived, respectively, as

$$\int_0^1 (1-s^2) H_1^{(n)}(s) ds = 0. \quad (4.85)$$

$$A(n) = 2 \int_0^1 \left\{ \frac{1}{s} \int_0^s s' H_0^{(n)}(s') ds' \right\} ds. \quad (4.86)$$

This scheme is advantageous for its high efficiency because it uses only the FFT in the main part of the solver. Moreover, this scheme can provide not only the flux function  $\Psi(s, t)$  but also the first- and second-order derivatives, needed in the stability analysis in terms of the harmonics. However, because of the previously described reason it seems rather difficult to apply this method to a free boundary problem of the first type described in 3.1.

#### 4.2. Inverse Equilibrium Solver

Theoretical analysis of MHD stability requires equilibrium with a very high accuracy and an equilibrium solution based on magnetic flux coordinates is often necessary. Sometimes, this is also the case for a transport analysis code such as a 1.5D tokamak code (see 5.4). For these purposes several inverse equilibrium solvers in which the real space coordinates  $(r, z, \phi)$  are directly obtained as functions of the magnetic flux functions, have been developed. Moreover, in solving the MHD equilibrium by the inverse solver the poloidal angular coordinate is, inevitably, prescribed and a coordinate system is directly obtained by specifying an appropriate Jacobian. Solution methods so far developed are divided into two classes, i.e., iterative methods and expansion methods. The former is subdivided into the iterative metric method and the direct solution of the inverse equilibrium equation.

#### 4.2.1 Iterative Reconstruction of Metrics

The iterative methods are essentially based on iterative reconstruction of metrics defined on the magnetic flux coordinates. The most intuitive one of this type is employed in the SELENE equilibrium code by Takeda and Tsunematsu [48]. This code is developed on the basis of the iterative reconstruction of FEM meshes which are constructed so that two of edges of a rectangular FEM mesh always lie on magnetic surfaces (Fig. 4.3). On this FEM mesh structure the usual Grad-Shafranov equation is solved directly as a nonlinear eigenvalue problem and new mesh structure is reconstructed. This process is repeated until convergence is attained under some prescribed condition. The FEM formulation of the Grad-Shafranov equation is described in the previous section. The overall iteration procedure is summarized in Fig. 4.8. An inverse equilibrium is obtained by an outer iteration where the internal iteration procedures are repeated until the resulting  $\psi$  values coincide with the values of the mesh points. Figure 4.9 shows that the eigenvalue  $\lambda$  converges quadratically with respect to the mesh numbers.

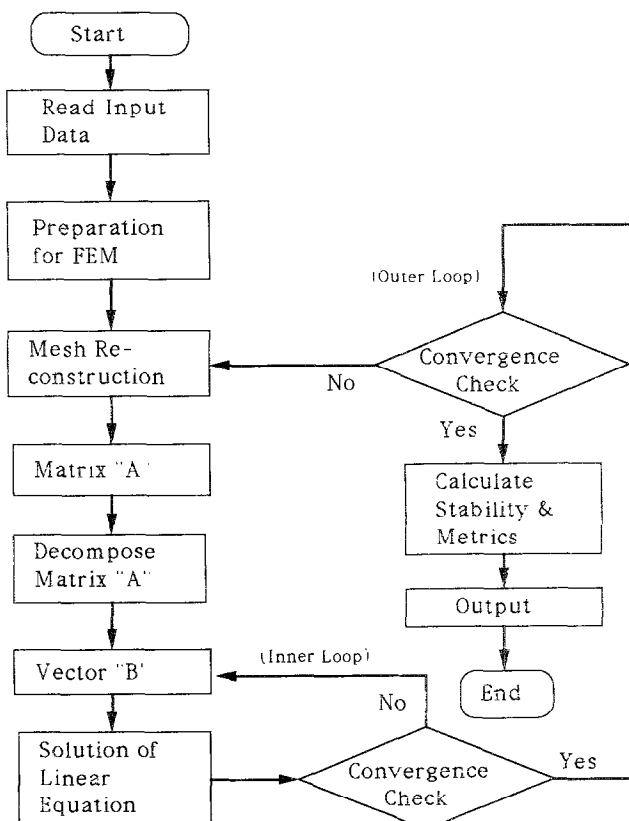


FIG. 4.8. Flow diagram of the iterative metric method employed for the SELENE code [48].

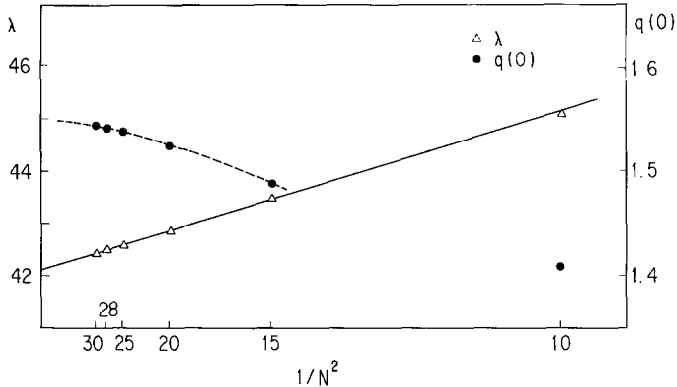


FIG. 4.9. An example of convergence of the eigenvalue  $\lambda$  of the inverse equilibrium code SELENE [48].  $q(0)$  is the safety factor at the magnetic axis.

The inverse equilibrium solver by DeLucia *et al.* [49] is somewhat similar to the above method but in this solver the procedure to iteratively determine metrics is clearly realized without the help of the numerical process. First, the Jacobian  $\mathcal{J}$  is given as

$$\mathcal{J} = (\nabla\psi \times \nabla\theta \cdot \nabla\phi) = \mu \left( \frac{r}{R_0} \right)^m \psi^n. \quad (4.87)$$

By using this Jacobian the inverse equilibrium equation is derived as

$$\Delta^* \chi(\psi) \equiv r^2 [\nabla r^{-2} \nabla \chi(\psi)] = r^2 \mathcal{J}^{-1} [(\chi_\psi h^{\psi\psi})_\psi + (\chi_\psi h^{\psi\theta})_\theta] = f(\psi, r), \quad (4.88)$$

$$\mathcal{J} = r(r_\psi z_\theta - r_\theta z_\psi) = \mu \left( \frac{r}{R_0} \right)^m \psi^n, \quad (4.89)$$

$$h^{\psi\psi} = (r_\theta^2 + z_\theta^2)/\mathcal{J}, \quad (4.90)$$

$$h^{\psi\theta} = -(r_\theta r_\psi + z_\theta z_\psi)/\mathcal{J}, \quad (4.91)$$

where  $r_\psi = \partial r / \partial \psi$ ,  $r_\theta = \partial r / \partial \theta$ ,  $z_\psi = \partial z / \partial \psi$ ,  $z_\theta = \partial z / \partial \theta$ , and  $\chi$  is the poloidal magnetic flux function, whereas  $\psi$  is a coordinate constructed as a different label of the magnetic flux function. The above equations are solved with respect to  $\chi$  for fixed metrics and this process is repeated. The effectiveness of the inverse equilibrium solver was demonstrated by analyzing the ideal internal and free surface mode instabilities of equilibria generated by the above code as shown in Fig. 4.10 and confirming a high  $\beta$  region of stability to internal modes and demonstrating high  $\beta$  saturation of the latter modes.

#### 4.2.2. Direct Solution of Inverse Equilibrium Equation

Both of the above methods solve the Grad-Shafranov equation and obtain the poloidal magnetic flux as the solution during the iteration process. However, in the

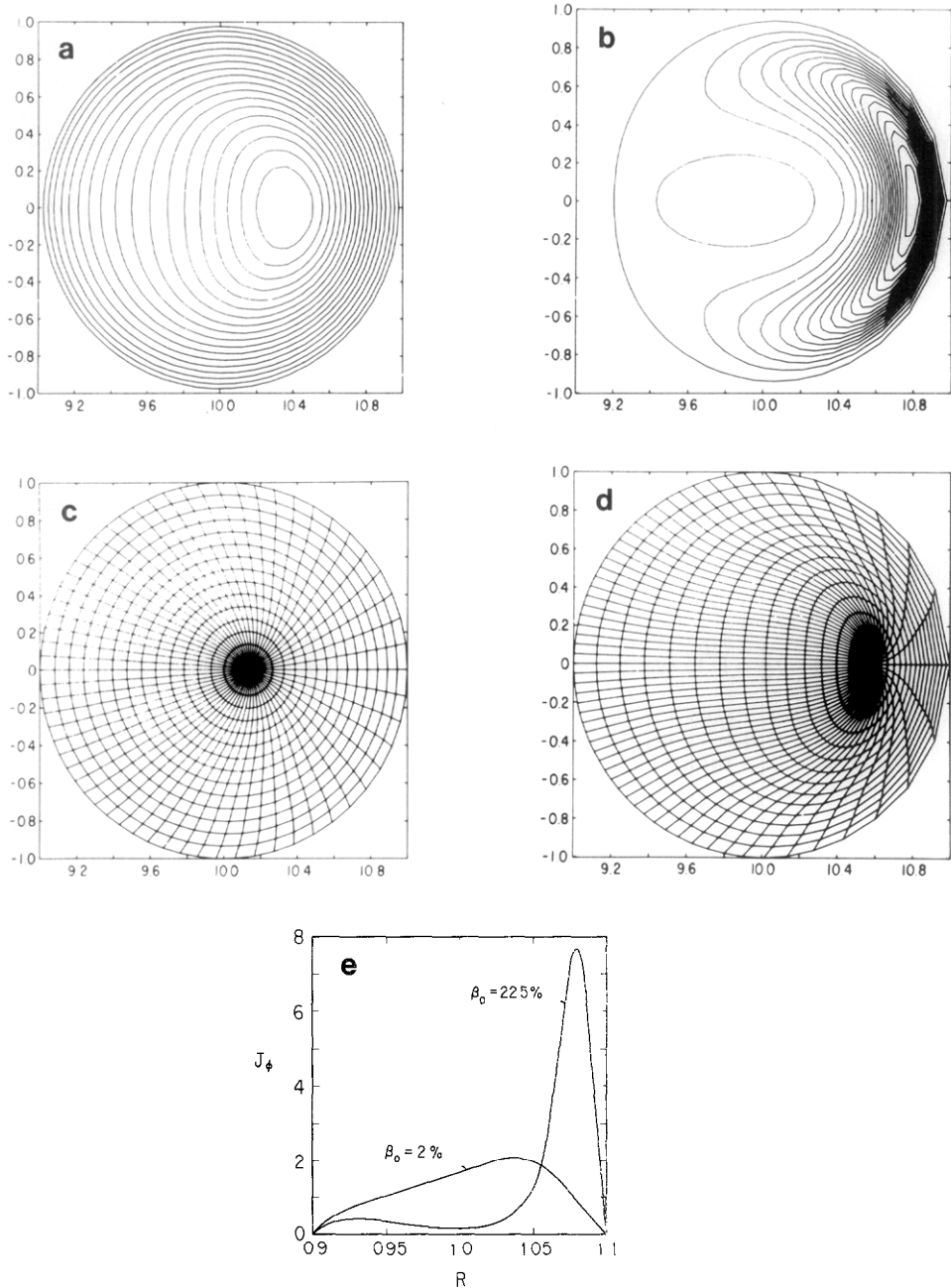


FIG. 4.10. An example of the equilibrium solutions by the iterative metric method of DeLucia *et al.* [49]: (a) and (b) are current contours for  $\beta = 0.020$  and  $\beta = 0.225$ , respectively; (c) and (d) are flux surfaces for  $\beta = 0.20$  and  $\beta = 0.225$ , respectively; (e) midplane current profiles.

methods by Hicks *et al.* [51] and Vabishchevich *et al.* [47] real space coordinates  $r$  and  $z$  are determined directly as dependent variables of the partial differential equations by iterating the metrics of the system. They started from the usual Grad-Shafranov equation and transformed the unknown variables from the magnetic flux function  $\psi$  and the poloidal angle  $\theta$  to the real space coordinates  $r$  and  $z$ .

In the equilibrium code AXE Hicks *et al.* adopt nonorthogonal coordinate system and assume a Jacobian of the form,

$$\mathcal{J} = J_0(\rho) r^l \rho, \quad (4.92)$$

where they used  $\rho$  as the magnetic surface label instead of the magnetic flux  $\psi$ . According to Hicks *et al.* the nonlinear equations to be solved are obtained from the Jacobian and the Grad-Shafranov equation as

$$J_0(\rho) r^l = r \left( \frac{\partial r}{\partial \rho} \frac{1}{\rho} \frac{\partial z}{\partial \theta} - \frac{1}{\rho} \frac{\partial r}{\partial \theta} \frac{\partial z}{\partial \rho} \right) \quad (4.93)$$

and

$$\begin{aligned} & \frac{r^{2(l-1)}}{J_0^2} \left\{ J_0 \rho \frac{d}{d\rho} \left( \frac{1}{J_0 \rho} \frac{d\psi}{d\rho} \right) \left[ \frac{1}{\rho^2} \left( \frac{\partial r}{\partial \theta} \right)^2 + \frac{1}{\rho^2} \left( \frac{\partial z}{\partial \theta} \right)^2 \right] \right. \\ & + \frac{d\psi}{d\rho} \left[ \frac{1}{\rho} \frac{\partial r}{\partial \theta} \frac{1}{\rho} \frac{\partial^2 r}{\partial \theta \partial \rho} + \frac{1}{\rho} \frac{\partial z}{\partial \theta} \frac{1}{\rho} \frac{\partial^2 z}{\partial \theta \partial \rho} - \frac{1}{\rho^2} \frac{\partial^2 r}{\partial \theta^2} \frac{\partial r}{\partial \rho} \right. \\ & \left. \left. - \frac{1}{\rho^2} \frac{\partial^2 z}{\partial \theta^2} \frac{\partial z}{\partial \rho} - l J_0 \frac{\partial z}{\partial \theta} r^{l-2} \right] \right\} + r^2 p' + F F' - A^* \psi_{\text{vac}} = 0, \end{aligned} \quad (4.94)$$

where the quantities  $F$ ,  $p$ , and  $\rho$  are taken as functions on a grid  $\rho_j$ . Several additional constraints are considered as boundary conditions at the plasma surface, plasma axis, and wall. The safety factor  $q$  and pressure function  $p$  are given as

$$q(\rho) = - \frac{J_0(\rho) \rho F(\rho)}{d\psi/d\rho} \langle r^{l-2} \rangle_{m=0} \quad (4.95)$$

$$p(\psi) = p_0 (\psi/\psi_0)^l. \quad (4.96)$$

The numerical solution of the above equations is obtained by using the Fourier transform as

$$r(\rho, \theta) = \sum_m r_m(\rho_j) \cos(m\theta), \quad (4.97)$$

$$z(\rho, \theta) = \sum_m z_m(\rho_j) \sin(m\theta). \quad (4.98)$$

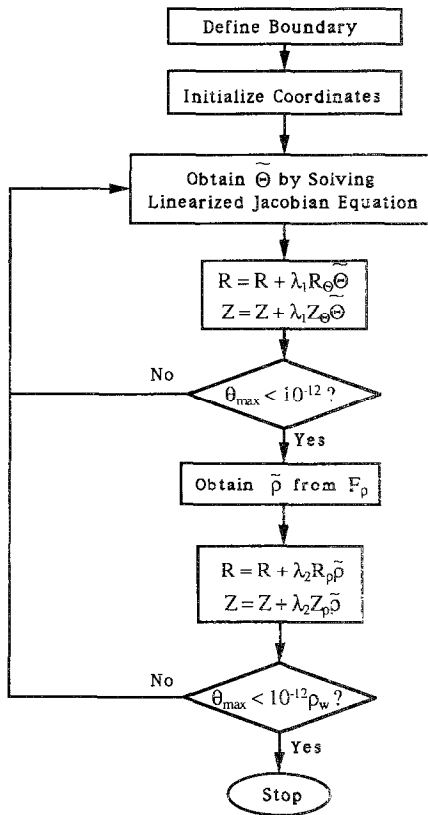


FIG. 4.11. Flow diagram of the AXE code [51].

The AXE code is constructed on the basis of the above equations as shown in the overall flowchart of Fig. 4.11, in which the Jacobian equation is solved by modifying the  $r$  and  $z$  coordinates as

$$\tilde{r} = r_\theta \tilde{\theta}, \quad \tilde{z} = z_\theta \tilde{\theta}. \quad (4.99)$$

It was concluded that the convergence of the Jacobian equation is extremely rapid when a sufficient number of  $m$  components is included (Fig. 4.12). The computational results were compared with a usual Cartesian equilibrium code RSTEQ [120] and it was concluded that the Fourier amplitudes are essentially the same for  $m \leq 7$ .

On the other hand, Vabishchevich *et al.* assume an orthogonality condition,

$$\frac{\partial \psi}{\partial r} \frac{\partial \theta}{\partial r} + \frac{\partial \psi}{\partial z} \frac{\partial \theta}{\partial z} = 0. \quad (4.100)$$

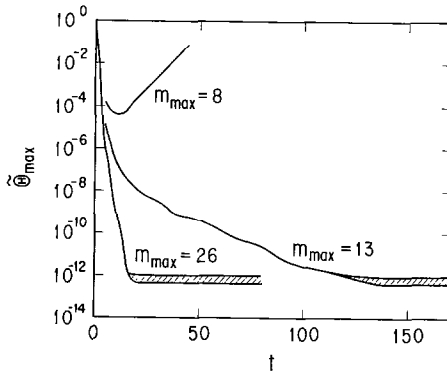


FIG. 4.12. Convergence of the equilibrium calculation by the AXE code with respect to the number of Fourier components [51].

On the basis of this condition they introduce a new variable  $\mu(\psi, \theta)$  as

$$\mu r \frac{\partial \theta}{\partial z} = \frac{\partial \psi}{\partial r}, \quad \mu r \frac{\partial \theta}{\partial r} = \frac{\partial \psi}{\partial z}. \quad (4.101)$$

These equations are transformed into the following two equations determining  $r$  and  $z$  as functions of  $\psi$  and  $\theta$  if the variable  $\mu$  is determined from the Grad-Shafranov equation as shown in the following third equation

$$\frac{\partial}{\partial \psi} \left( \mu r \frac{\partial r}{\partial \psi} \right) + \frac{\partial}{\partial \theta} \left( \frac{1}{\mu r} \frac{\partial r}{\partial \theta} \right) = 0, \quad (4.102)$$

$$\frac{\partial}{\partial \psi} \left( \mu r \frac{\partial z}{\partial \psi} \right) + \frac{\partial}{\partial \theta} \left( \frac{1}{\mu r} \frac{\partial z}{\partial \theta} \right) = 0, \quad (4.103)$$

and

$$\frac{\partial \mu}{\partial \psi} = -\mu r \left[ \left( \frac{\partial r}{\partial \psi} \right)^2 + \left( \frac{\partial z}{\partial \psi} \right)^2 \right] J_\phi(\psi, r). \quad (4.104)$$

Vabishchevich *et al.* show several examples of the calculation on fixed/free boundary, cylindrical/toroidal equilibria but details of the numerical procedure are not clearly described in their paper. In the case of this orthogonal coordinate system, stability analyses often suffer from the singularity at the magnetic axis and the method seems rather difficult to apply directly to the stability analyses.

#### 4.2.3. Methods of Expansion in Poloidal Angle

The inverse equilibrium solver based on the expansion method has been extensively studied in relation to three-dimensional MHD equilibria. This method originated from the analytical equilibrium solution [121, 122] in the early stage of

tokamak research. A practical inverse equilibrium code (VMOMS) based on a variational moment method in a general form was developed by Lao and co-workers [50]. First, the authors define a Lagrangian  $L$ , which corresponds to the integrand of the Lagrangian in the description of the FEM formalism (Eq. (4.38)), as

$$L = r \left( \frac{B_r^2}{2} - \frac{B_t^2}{2} - p \right), \quad (4.105)$$

where

$$B_r = \frac{|\nabla \psi|}{r}, \quad (4.106)$$

$$B_t = \frac{F}{r}. \quad (4.107)$$

The Grad-Shafranov equation is reproduced from the Euler equation of this Lagrangian  $L$  as

$$\frac{\partial L}{\partial \psi} - \frac{\partial}{\partial r} \frac{\partial L}{\partial \psi_r} - \frac{\partial}{\partial z} \frac{\partial L}{\partial \psi_z} = 0, \quad (4.108)$$

where  $\psi_r = \partial \psi / \partial r$ ,  $\psi_z = \partial \psi / \partial z$ . Next they define a volume integral of the Lagrangian as

$$Q = \iiint_V dr dz L(\psi, \psi_r, \psi_z, r). \quad (4.109)$$

By transforming the independent variables  $(r, z)$  to  $(\rho, \theta)$  the volume integral  $Q$  is represented as

$$Q = \iint d\rho d\theta \tilde{L}(r, r_\rho, r_\theta, z_\rho, z_\theta, \psi, \psi_\rho). \quad (4.110)$$

It should be noted that the value of the integral is invariant under a transformation of the coordinates. The variation of  $Q$  with respect to  $r$  and  $z$  under the boundary condition of  $\delta r(\text{boundary}) = 0$  or  $\delta z(\text{boundary}) = 0$  yields

$$\delta Q_r = - \iint d\rho d\theta \delta r r z_\theta \hat{G} \quad (4.111)$$

and

$$\delta Q_z = - \iint d\rho d\theta \delta z r r_\theta \hat{G}, \quad (4.112)$$

where

$$\hat{G} = \frac{\psi'(\rho)}{\mathcal{J}} \left[ \frac{\partial}{\partial \rho} \left( \frac{g_{\theta\theta}}{\mathcal{J}} \psi'(\rho) \right) - \frac{\partial}{\partial \theta} \left( \frac{g_{\rho\theta}}{\mathcal{J}} \psi'(\rho) \right) \right]. \quad (4.113)$$

By specifying a particular representation for the poloidal angle  $\theta$  as

$$r(\rho, \theta) = \sum_{n=0}^{n_r} r_n(\rho) \cos n\theta, \quad (4.114)$$

$$z(\rho, \theta) = \sum_{n=0}^{n_z} z_n(\rho) \sin n\theta. \quad (4.115)$$

Euler equations describing  $r_n(\rho)$  and  $z_n(\rho)$  are derived as

$$\langle M_{r_n} \hat{G} \rangle = 0, \quad n = 0, 1, \dots, n_r, \quad (4.116)$$

$$\langle M_{z_n} \hat{G} \rangle = 0, \quad n = 0, 1, \dots, n_z, \quad (4.117)$$

$$M_{r_n} = r z_\theta \cos n\theta, \quad (4.118)$$

$$M_{z_n} = r r_\theta \sin n\theta, \quad (4.119)$$

where the angle bracket is defined as

$$\langle A \rangle = \int_0^{2\pi} \frac{d\theta}{2\pi} A. \quad (4.120)$$

In this way the Fourier expansion coefficients  $r_n$  and  $z_n$  are determined by moments of the inverse equilibrium equation with respect to the weighting functions  $M_r$  and  $M_z$ . The above moment equations are second-order ordinary differential equations and each equation is supplemented by two boundary conditions. The second-order equations are rewritten as a system of first order differential equations of the form

$$\mathbf{u}' = f(x, \mathbf{u}), \quad (4.121)$$

where  $\mathbf{u}$  is a vector comprised of the Fourier amplitudes. To demonstrate the applicability of the moment method, comparisons of the results of this code with those of the fixed boundary two-dimensional code RSTEQ [120] were carried out for the ISX-B and INTOR/FER tokamaks. Figure 4.13 shows the flux contours and various profiles of the ISX-B tokamak, where the solid curves are obtained by the moment method and the broken ones are obtained by the RSTEQ code. In all cases

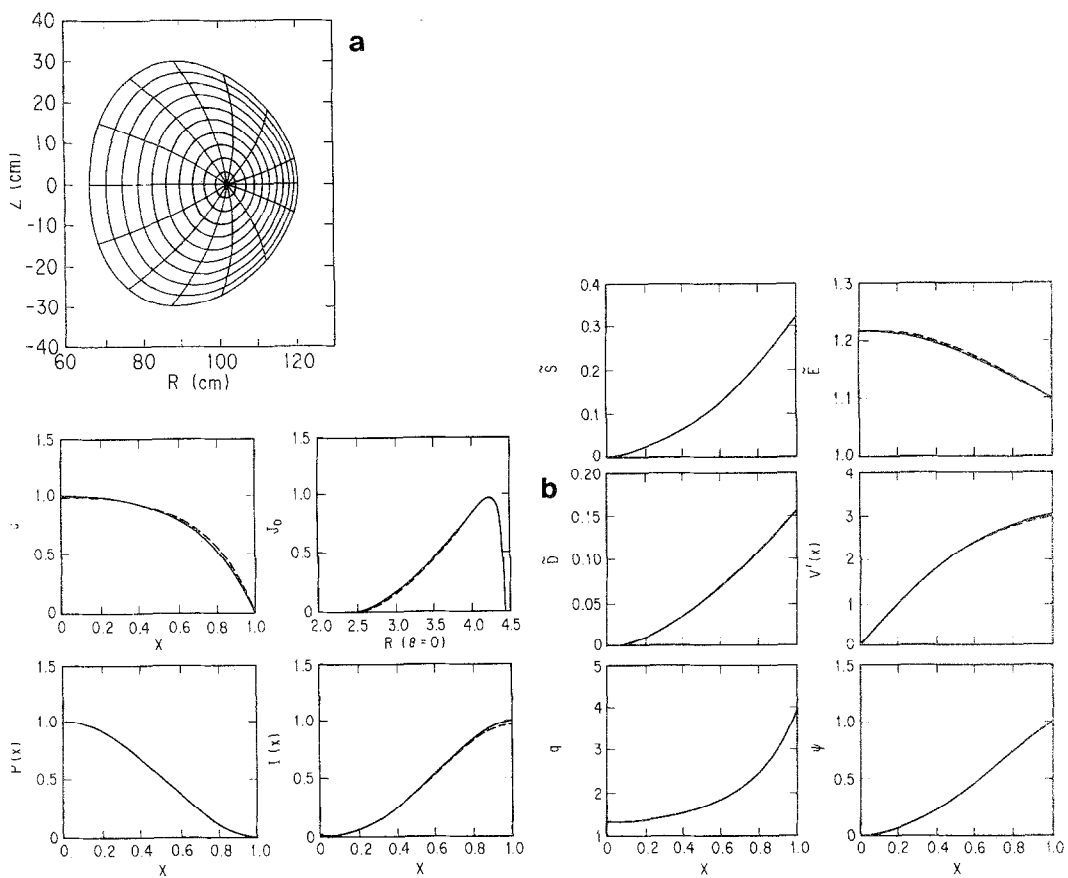


FIG. 4.13. An example of the flux surface contours (a) of the ISX-B tokamak by the inverse equilibrium code VMOMS (solid lines) and the conventional two-dimensional code RSTEQ (broken lines). Profiles of various equilibrium quantities of the ISX-B tokamak are shown in (b) [50].

there was close agreement between the results by the usual code and the inverse equilibrium code.

The FCT equilibrium is often desirable for theoretical analysis because the pressure and safety factor profiles can be prescribed before the calculation and the high beta equilibrium is obtained easily. However, as boundary condition for the FCT equilibrium cannot be assigned explicitly in the case of the full Grad-Shafranov equation, it is rather difficult to develop an inverse solver for the FCT equilibrium. To cope with this problem Tokuda *et al.* [123] developed an inverse solver SELENEHB for the FCT equilibrium on the basis of the moment method incorporated with a high beta tokamak ordering. The high beta tokamak ordering equation (Eq. (2.81)) is adopted as the equilibrium equation. The FCT

condition for the equation is derived explicitly as follows. First, the equation defining the safety factor  $q$  and the Jacobian  $\mathcal{J}$  are expanded as

$$q = \frac{\alpha}{2s} [1 - \varepsilon P(\Psi) + \dots] \left\langle \frac{1}{1 + \varepsilon x} \right\rangle, \quad (4.122)$$

$$\mathcal{J} = \mathcal{J}^{(0)} + \varepsilon \mathcal{J}^{(1)}, \quad (4.123)$$

where  $s = \sqrt{\Psi}$  and

$$\mathcal{J} = \mathcal{J}[x, y] \equiv \frac{\partial x}{\partial s} \frac{\partial y}{\partial \theta} - \frac{\partial x}{\partial \theta} \frac{\partial y}{\partial s}. \quad (4.124)$$

By assuming up-down symmetry the real space coordinates  $x$  and  $y$  are expressed by magnetic flux coordinates  $s$  and  $\theta$  as

$$x = A + s\rho \cos \theta + s \sum_{m=2} X_m \cos m\theta, \quad (4.125)$$

$$y = s\kappa \sin \theta + s \sum_{m=2} Y_m \sin m\theta. \quad (4.126)$$

The Grad-Shafranov equation is transformed to

$$A_\perp \Psi = \frac{1}{\mathcal{J}} \frac{\partial}{\partial s} \left[ \frac{d\Psi}{ds} \mathcal{J} |\nabla s|^2 \right] + \frac{1}{\mathcal{J}} \frac{d\Psi}{ds} \frac{\partial}{\partial \theta} [\mathcal{J} (\nabla s \cdot \nabla \theta)]. \quad (4.127)$$

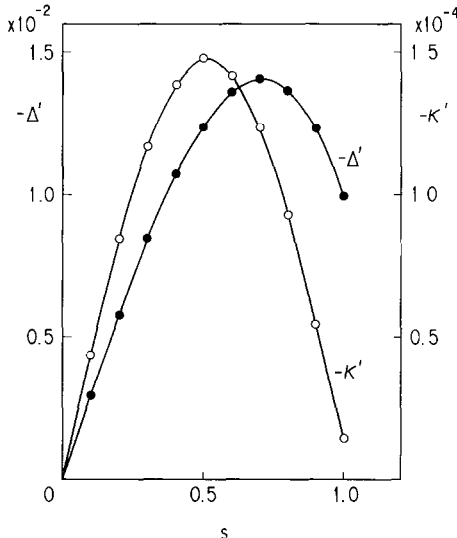


FIG. 4.14. Derivatives of the ellipticity  $\kappa'$  and the toroidal shift  $A'$  of a low beta tokamak plasma ( $\beta/\varepsilon = 10^{-2}$ ). Points are obtained by the inverse equilibrium solver and solid lines are obtained by an analytical expression [123].

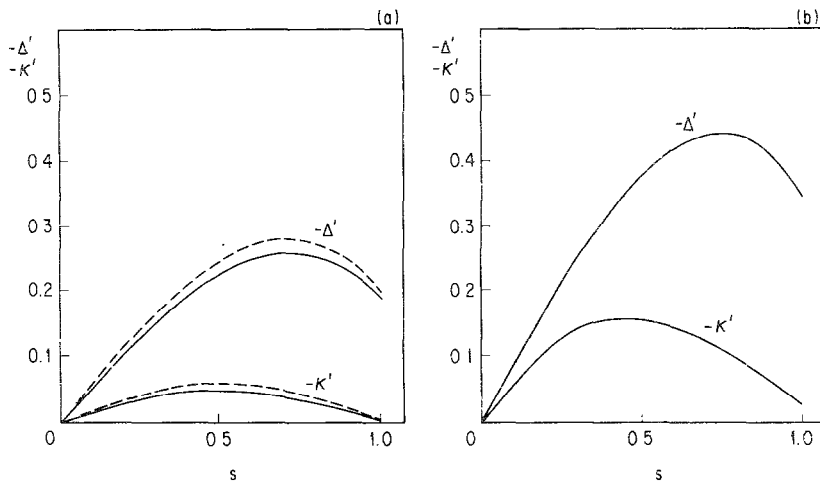


FIG. 4.15. Derivatives of the ellipticity  $\kappa'$  and the toroidal shift  $\Delta'$  of a higher beta tokamak plasmas ( $\beta/e = 0.2$  for (a),  $\beta/e = 0.4$  for (b)). Solid lines were obtained by the inverse equilibrium solver and the broken lines were obtained by an approximate analytical expression [123].

By truncating the series at  $m = M$  and averaging each term with a weight of  $\cos mq$  ( $m = 1, 2, 3, \dots, 2M$ ) the following  $2M$  ordinary differential equations are obtained:

$$\langle A_{\perp} \Psi \cos m\theta \rangle = -2\alpha^2 \frac{dP}{d\Psi} \langle x \cos m\theta \rangle. \quad (4.128)$$

With the constraining condition derived from the FCT condition and expansion of the Jacobian,

$$\left\langle x \frac{\partial y}{\partial \theta} \right\rangle = \frac{2}{x} \int sq ds, \quad (4.129)$$

a system of  $(2M + 1)$  ordinary differential equations with unknown variables ( $A$ ,  $\rho$ ,  $\kappa$ ,  $X_2$ ,  $Y_2$ , ...,  $X_M$ ,  $Y_M$ ) is obtained and by solving it an inverse equilibrium is obtained. Comparison with the analytical calculation of a low beta circular plasma showed excellent agreement for the ellipticity and the shift of the magnetic surfaces (Fig. 4.14). As for higher beta plasmas, the comparison was made with an approximate analytical result and also good agreement was attained (Fig. 4.15).

#### 4.3. Numerical Mapping to Flux Coordinates

Linear MHD stability codes such as PEST [124] and ERATO [125] are, usually, written by using a flux coordinate system and the various metric quantities necessary for the stability analyses are given at the mesh points defined on the flux coordinates. Therefore, if the equilibrium solution is given by a conventional real

space solver the solution should be mapped from the real space coordinates to the flux coordinates and finally the real space coordinates  $r$  and  $z$  should be expressed in terms of the flux coordinates  $\psi$  and  $\chi$ .

The angular coordinate  $\chi$  in the flux coordinate system is defined by a line integral on a contour of  $\psi$  as

$$\chi = 2\pi \int \frac{dl}{\mathcal{J}B_p} / \oint \frac{dl}{\mathcal{J}B_p}. \quad (4.130)$$

The metric quantities which should be calculated at the  $(\psi, \chi)$  mesh points are  $r(\psi, \chi)$ ,  $z(\psi, \chi)$ ,  $\partial r/\partial\psi$ ,  $\partial r/\partial\chi$ ,  $q(\psi)$ ,  $dq/d\psi$  and the non-orthogonality parameter  $\beta_\chi = \nabla\psi \cdot \nabla\chi / |\nabla\psi|^2$  [125].

A crude mapping method is to draw a set of contours by linear interpolation of  $\psi$  values given at the  $(r, z)$  mesh points and determine the angular coordinate  $\chi$  by calculating the line integral along the approximate contours. Afterwards various metric quantities are obtained by linear interpolation and numerical differentiation. In this method the following problems are encountered: (1) it is very difficult to obtain contour lines near the magnetic axis; (2) in general the error of the finite differentiation with respect to  $\psi$  and  $\chi$  becomes large even if the accuracy of the calculation of  $\psi(r, z)$  is high. For the stability calculation by PEST, Grimm *et al.* employed auxiliary quasi-cylindrical coordinates  $\rho$  and  $\theta$  defined as

$$r = R_0 + \rho \cos \theta, \quad (4.131)$$

$$z = \rho \sin \theta. \quad (4.132)$$

In terms of the auxiliary angular coordinate  $\theta$  the real space coordinates  $r$  and  $z$ , and the straight field line angular coordinate  $\chi$  are expressed as

$$\left. \frac{\partial r}{\partial \theta} \right|_{\psi} = -\rho \frac{\partial \psi}{\partial z} \left( \frac{\partial \psi}{\partial r} \cos \theta + \frac{\partial \psi}{\partial z} \sin \theta \right)^{-1}, \quad (4.133)$$

$$\left. \frac{\partial z}{\partial \theta} \right|_{\psi} = -\rho \frac{\partial \psi}{\partial r} \left( \frac{\partial \psi}{\partial r} \cos \theta + \frac{\partial \psi}{\partial z} \sin \theta \right)^{-1}, \quad (4.134)$$

$$\left. \frac{\partial \chi}{\partial \theta} \right|_{\psi} = \frac{F}{q} \frac{\rho}{r} \left( \frac{\partial \psi}{\partial r} \cos \theta + \frac{\partial \psi}{\partial z} \sin \theta \right)^{-1}, \quad (4.135)$$

where it should be noted that the definition of  $\theta$  and  $\mathcal{J}$  are different from the original paper by Grimm *et al.* The above differential equations are integrated by the Newton-Cotes predictor-corrector algorithm and the values of  $r$ ,  $z$ , and so on are determined accurately on the mesh points in the flux coordinate system, where the flux function  $\psi$  is interpolated by the cubic spline method. In this case the non-orthogonality parameter is expressed as

$$\beta_\chi(\psi, \chi) = -\frac{1}{\mathcal{J}^2 |\nabla\psi|^2} \left( \frac{\partial r}{\partial \psi} \frac{\partial r}{\partial \chi} + \frac{\partial z}{\partial \psi} \frac{\partial z}{\partial \chi} \right). \quad (4.136)$$

On the other hand, in order to resolve the problems appearing in the ERATO stability analysis Tokuda *et al.* [126] employed a two-dimensional spline interpolation [127] as the mapping method, which satisfies the following two conditions: (1) the value of the metric quantities are determined uniquely only by the set of the data  $(r_i, z_i, \psi_i)$  given on the  $(r, z)$  meshes and they are independent of the  $(\psi, \chi)$  meshes; (2) the derivatives with respect to  $\psi$  are determined uniquely even on the  $(\psi, \chi)$  meshes. The contour  $\psi(r, z) = \psi_i$  is calculated from the differential equations,

$$\frac{dr}{dl} = \frac{1}{|\nabla\psi|} \frac{\partial\psi}{\partial z}, \quad \frac{dz}{dl} = -\frac{1}{|\nabla\psi|} \frac{\partial\psi}{\partial r}, \quad (4.137)$$

where  $dl$  is a line element of a contour. To avoid a partial differentiation some quantities are represented by line integrals along the contours as

$$\beta_z(\psi, \chi) = \frac{F}{q} \left( \int \tilde{G}(l) dl - \frac{\chi}{2\pi} \oint \tilde{G}(l) dl \right), \quad (4.138)$$

$$\frac{dq}{d\psi} = \frac{F'}{2\pi} \oint \frac{dl}{r^2 B_p} + \frac{F}{2\pi} \oint \tilde{G}(l) dl, \quad (4.139)$$

$$\begin{aligned} \tilde{G} = & -\frac{B_p}{|\nabla\psi|} \left\{ \left[ \left( \frac{\partial\psi}{\partial z} \right)^2 - \left( \frac{\partial\psi}{\partial r} \right)^2 \right] \left[ \frac{\partial^2\psi}{\partial r^2} - \frac{\partial^2\psi}{\partial z^2} \right] \right. \\ & \left. + 4 \frac{\partial\psi}{\partial r} \frac{\partial\psi}{\partial z} \frac{\partial^2\psi}{\partial r \partial z} \right\} - \frac{1}{r^5 B_p^3} \frac{\partial\psi}{\partial r}. \end{aligned} \quad (4.140)$$

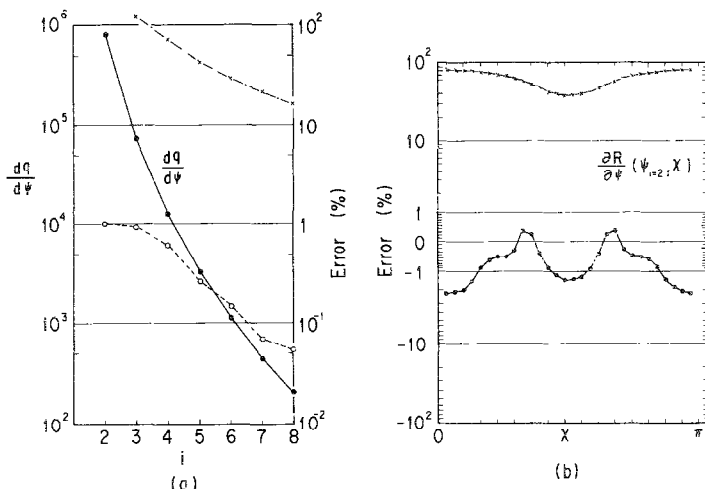


FIG. 4.16. Examples of relative errors of quantities  $dq/d\psi$  (a) and  $\partial R/\partial\psi$  (b) calculated by the two-dimensional spline mapping (lower curve) and a linear interpolation mapping (upper curve) [126]. The solid line in the subfigure (a) shows the analytical value of  $dq/d\psi$ .

The derivatives of  $\partial r/\partial\psi$  and  $\partial r/\partial\chi$  are given as

$$\frac{\partial r}{\partial\psi} = \frac{1}{|\nabla\psi|^2} \frac{\partial\psi}{\partial r} + \frac{qr}{F} \beta_x \frac{\partial\psi}{\partial z}, \quad (4.141)$$

$$\frac{\partial r}{\partial\chi} = -\frac{qr}{F} \frac{\partial\psi}{\partial z}. \quad (4.142)$$

Test calculations of the spline mapping method were carried out for a model equilibrium,

$$\psi(r, z) = 2\pi \left( r^2 + \frac{z^2}{4} \right)^2. \quad (4.143)$$

The error level of the numerical calculation of the metrics was obtained and compared with the analytically obtained metric quantities. Some examples are given in Fig. 4.16, which shows that extreme improvement is attained in comparison with a mapping method based on the linear interpolation.

#### 4.4. Numerical Technique for Vector Processor

Because the MHD equilibrium calculation is a basis of various analyses of the fusion plasma and it is required to calculate equilibria many times, one of the most

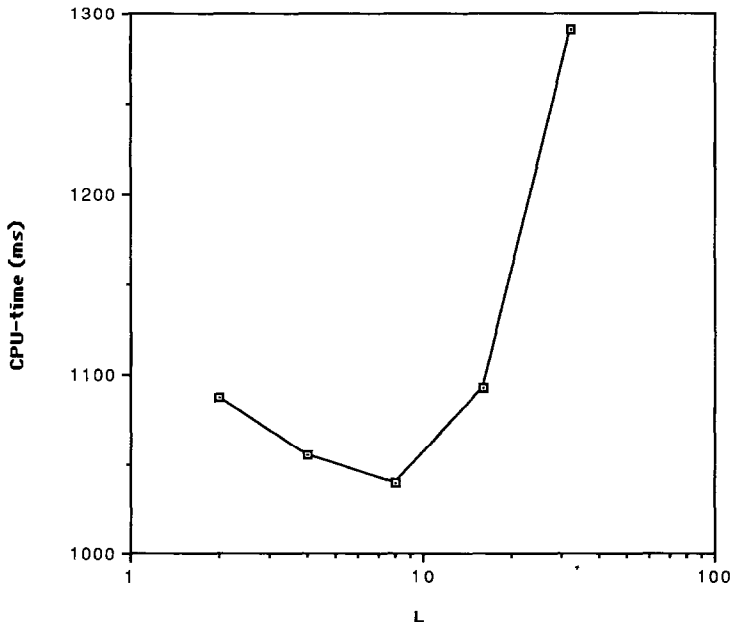


FIG. 4.17. Degradation of vector-processing efficiency at a short vector length region, observed in the calculation by the DCR code [129].  $L$  is the minimum vector length plus 1.

important requirements on numerical codes is high speed calculation. For this purpose, sometimes, we need improvement of the numerical algorithms to attain efficient calculation on a vector processor type super-computer.

When we solve an elliptic partial differential equation such as the Grad-Shafranov equation, algorithms using the cyclic reduction method and the fast Fourier transform (FFT) are very advantageous from the viewpoint of the total number of numerical operations as described in the previous section. These algorithms are highly sophisticated to match computations on a scalar computer and usually one cannot attain a high efficiency on a vector computer if one simply converts a code to a vector-oriented one. Matsuura *et al.* [128] investigated this problem in detail and implemented vector-oriented cyclic reduction methods into the MHD equilibrium code SELENE40.

As for the DCR, the length of the main vectorizable DO loop decreases, e.g., from 64 to 32, 16, 8, 4 during the reduction process. When the vector length is shorter than a certain critical value, the vector operation, in general, takes a longer time than a scalar operation. Therefore, one had better leave a shorter DO loop as a scalar DO loop. An example of the critical length of a DO loop is shown in Fig. 4.17 [129]. In the case of the FACR two approaches are considered. One is to employ a vectorized FFT algorithm and the other is to utilize the parallelism found

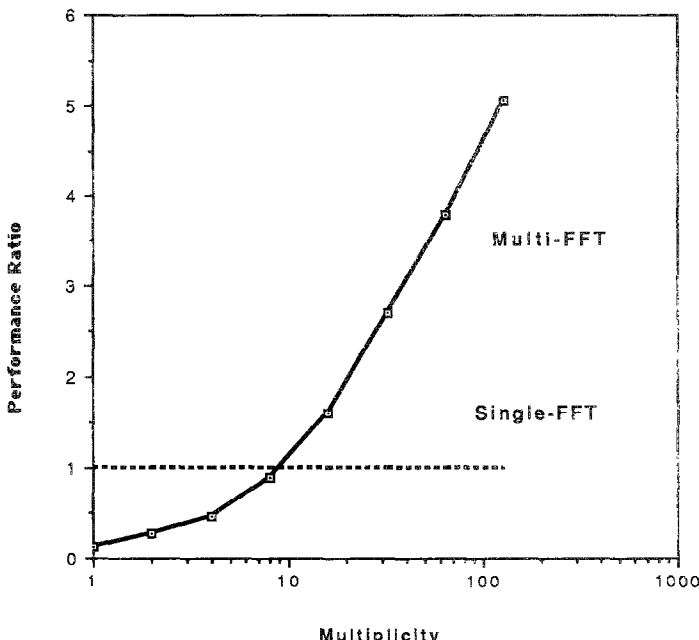


FIG. 4.18. Comparison of vector efficiencies of the multiple FFT and the single FFT [128]. Performance ratio of the vectorized multi-FFT with respect to the scalar FFT is shown as a function of the multiplicity.

TABLE II

Performance Ratio of a Vector Processor for Equilibrium Solvers by FACR and DCR Algorithms

| Algorithm for equilibrium solver | Scalar mode<br>(Fortran-H) in ms | Vector mode<br>(AP-Fortran) in ms | Performance ratio<br>(vector/scalar) |
|----------------------------------|----------------------------------|-----------------------------------|--------------------------------------|
| DCR method                       | 1668                             | 916                               | 1.82                                 |
| FACR method                      | 1119                             | 286                               | 3.91                                 |

in the calling sequence of the FFT subroutine. In the FACR procedure with  $NR \times NZ$  meshes, the FFT subroutine is called  $NR$  times on each  $Z$  mesh line. This FFT loop with the length of  $NR$  is easily vectorized and high vector performance is attained as shown in Fig. 4.18 [129]. A detailed description of the vector-parallel algorithm of the FACR method is given in Ref. [130]. The vector performance for both the DCR and FACR is summarized in Table II.

As for the future trend of high speed calculation, parallel processors will inevitably be used for MHD equilibrium calculation. In this case iterative solution methods are more advantageous than direct methods which are widely used for equilibrium calculation at present. In particular, the MGM described in Section 4.1.1 seems promising as an effective algorithm for parallel processors.

## 5. MORE GENERAL EQUILIBRIUM MODELS

In the descriptions of the previous sections we assumed implicitly that the plasma is in a static equilibrium with isotropic pressure. This assumption is not valid in a plasma subject to intense auxiliary heating. For example, neutral beam injection (NBI) heating causes plasma rotation (plasma flow) and strongly anisotropic pressure distribution. In order to apply the equilibrium solver to such a problem, therefore, it is necessary to extend the model to cover equilibria with flows and/or anisotropic pressure. Another important subject connected with MHD equilibria of a plasma with additional equations is the analysis of equilibria with non-ohmically driven currents. In the previous equilibrium code discussion on the current sources were not treated explicitly and, instead, we had to specify profiles of quantities which are difficult to determine experimentally, such as the toroidal field function and the safety factor. However, it is necessary to treat explicitly the current sources when we study MHD equilibria especially for a tokamak with non-ohmic current. For investigation of these problems it is no longer sufficient to stay in the framework of the MHD model and we must take into account transport processes based on the kinetic theory. In connection with this issue and equilibrium solver consistent with the transport process and an equilibrium evolution solver are considered.

### 5.1. Equilibrium with Steady Flow

In this subsection we consider the MHD equilibrium equation with flow for an axisymmetric plasma on the basis of the incompressible ideal single fluid MHD model [131]. The basic equations of the system are

$$\operatorname{div}(\rho \mathbf{V}) = 0, \quad (5.1)$$

$$\rho \mathbf{V} \cdot \nabla \mathbf{V} = -\nabla p + \mathbf{J} \times \mathbf{B}, \quad (5.2)$$

$$\operatorname{rot}(\mathbf{V} \times \mathbf{B}) = 0, \quad (5.3)$$

$$\operatorname{rot} \mathbf{B} = \mathbf{J}, \quad (5.4)$$

$$\mathbf{V} \cdot \nabla S = 0, \quad (5.5)$$

where  $S$  is the entropy. First, we derive two algebraic relations among the quantities characterizing the flow equilibrium. From the Maxwell–Ohm's law for an ideal fluid (Eq. (5.3)), it is shown that the electric field  $\mathbf{V} \times \mathbf{B}$  is expressed by an electrostatic potential  $\Psi_E$ , which is a surface quantity (a function of only a magnetic surface label), as

$$\mathbf{V} \times \mathbf{B} = -\nabla \Psi_E, \quad (5.6)$$

$$\nabla \Psi_E = \Omega(\psi) \nabla \psi. \quad (5.7)$$

It is easily seen from Eqs. (2.5) and (5.6) that the velocity vector lies on a magnetic surface and it is decomposed into the parallel and toroidal flow velocities as

$$\mathbf{V} = \frac{\Phi_M}{\rho} \mathbf{B} + u_r \nabla \phi, \quad (5.8)$$

where

$$u_r = r^2 \Omega(\psi). \quad (5.9)$$

As the system is axisymmetric and the plasma is incompressible it is shown that the function  $\Phi_M$  is also a surface quantity. When  $\Phi_M(\psi) \equiv 0$  the flow is purely toroidal; otherwise the flow has a poloidal component given by

$$\rho \mathbf{V} \cdot \nabla \theta = \frac{\Phi_M}{J}. \quad (5.10)$$

Therefore, the poloidal component of the flow divided by the poloidal magnetic field is the function  $\Phi_M$  itself. Equation (5.10) means that the poloidal variation of the poloidal (and parallel) flow is derived from the poloidal variation of the magnetic field. By using the above equation (Eq. (5.8)), the equation for entropy conservation (Eq. (5.5)) is rewritten as

$$\frac{\Phi_M}{\rho} \mathbf{B} \cdot \nabla S = 0, \quad (5.11)$$

which means that the entropy is also a surface quantity provided that  $\Phi_M$  is not identically zero. On the other hand, there is no constraint on the entropy for a purely toroidal flow ( $\Phi_M \equiv 0$ ); instead of the above equation (Eq. (5.11)) we use the isothermal condition on each magnetic surface in this case as

$$T = T(\psi). \quad (5.12)$$

Then, we obtain the following magnetic differential equations (Bernoulli-type equations) from the scalar product of the equation of motion (Eq. (5.2)) with  $\nabla\phi$  and  $\mathbf{B}$ , respectively, as

$$\mathbf{B} \cdot \nabla \left[ \left( \frac{\Phi_M^2}{\rho} - 1 \right) F + r^2 \Phi_M \Omega \right] = 0, \quad (5.13)$$

$$\mathbf{B} \cdot \nabla \left[ \frac{\Phi_M^2}{2\rho^2} B^2 - \frac{1}{2} r^2 \Omega^2 + \frac{\gamma}{\gamma-1} S(\psi) \rho^{\gamma-1} \right] = 0. \quad (5.14)$$

In the above equations the expressions for the pressure are assumed for the general case and the purely toroidal case, respectively, as

$$p = S(\psi) \rho^\gamma, \quad (5.15)$$

$$p = \frac{\rho T}{M}, \quad (5.16)$$

where  $M$  is the particle mass of the fluid. Integrals,  $I(\psi)$  and  $H(\psi)$ , of Eqs. (5.13) and (5.14) are obtained as

$$I(\psi) = \left( \frac{\Phi_M^2}{\rho} - 1 \right) F + r^2 \Phi_M \Omega, \quad (5.17)$$

$$H(\psi) = \frac{\Phi_M^2}{2\rho^2} B^2 - \frac{1}{2} r^2 \Omega^2 + \frac{\gamma}{\gamma-1} S(\psi) \rho^{\gamma-1}. \quad (5.18)$$

From Eq. (5.17) it is known that the toroidal field function is no longer a surface quantity except for the case of a purely toroidal flow. One can see, from Eq. (5.18), that the density, i.e., the pressure, is not an arbitrarily given surface quantity but a quantity obtained by solving Eq. (5.18) simultaneously with the Grad-Shafranov equation. Next, the equation for the general flow equilibrium which corresponds to the Grad-Shafranov equation of the static equilibrium is obtained as

$$\begin{aligned} & \operatorname{div} \left[ \left( 1 - \frac{F\Phi_M^2}{\rho} \right) \frac{\nabla\psi}{r^2} \right] + \mathbf{V} \cdot \mathbf{B} \frac{d\Phi_M}{d\psi} + \rho \left( r^2 \Omega + \frac{F\Phi_M}{\rho} \right) \frac{d\Omega}{d\psi} + \frac{F}{r^2} \frac{dI}{d\psi} \\ & + \rho \frac{dH}{d\psi} - \frac{1}{\rho-1} \rho^\gamma \frac{dS}{d\psi} = 0. \end{aligned} \quad (5.19)$$

For the case of a purely toroidal flow Eq. (5.18) is reduced to a much simpler form as

$$H(\psi) = -\frac{1}{2} r^2 \Omega^2 + \frac{T}{M} \ln \rho, \quad (5.20)$$

and the pressure can be expressed explicitly by the surface quantities  $\Omega$  and  $H$  as

$$p = \exp \left( H_0 + \Omega_0^2 \frac{r^2}{2} \right) = p_0(\psi) \exp \left( \Omega_0^2 \frac{r^2}{2} \right), \quad (5.21)$$

where

$$H_0 = \frac{M}{T} H + \ln \frac{T}{M} \quad (5.22)$$

and

$$\Omega_0 = \sqrt{\frac{M}{T}} \Omega. \quad (5.23)$$

Then, the equation for a purely toroidal flow corresponding to the Grad-Shafranov equation is derived from Eq. (5.19) as

$$\Delta^* \psi = -r^2 \frac{\partial p}{\partial \psi} \Big|_r - F \frac{dF}{d\psi}, \quad (5.24)$$

where the pressure gradient is obtained from Eq. (5.21) as

$$\frac{\partial p}{\partial \psi} \Big|_r = \left( \frac{dH_0}{d\psi} + \Omega_0^2 r^2 \frac{d\Omega_0}{d\psi} \right) p. \quad (5.25)$$

To solve Eq. (5.24) one should specify the functions  $F$ ,  $H_0$ , and  $\Omega_0$ . Numerical codes for this kind of equilibria were developed by Semanzato *et al.* [44], and Kerner and Jandl [45] for a fixed boundary plasma and by Kerner and Tokuda [132] for a semi-fixed boundary plasma. In the former two codes the FEM approach was adopted and in the latter the cyclic reduction method was adopted. An example of the numerical results by the latter code is shown in Fig. 5.1.

When one analyzes a more general flow equilibrium with both toroidal and the poloidal flows one must solve the partial differential equation (Eq. (5.19)) simultaneously with the associated equations (Eqs. (5.17) and (5.18)) by specifying the five functions,  $\Omega$ ,  $\Phi_M$ ,  $S$ ,  $I$ , and  $H$ . Also with the solution  $\psi$ , the toroidal field function  $F$  and the density  $\rho$  which are not surface quantities but functions of  $r$ ,  $\psi$ , and  $|\nabla \psi|^2$  are determined. The difficulty of this problem arises from the fact that the equilibrium equation (Eq. (5.19)) is not always an elliptic partial differential equation [133, 134]. This type of differential equation is classified by an investi-

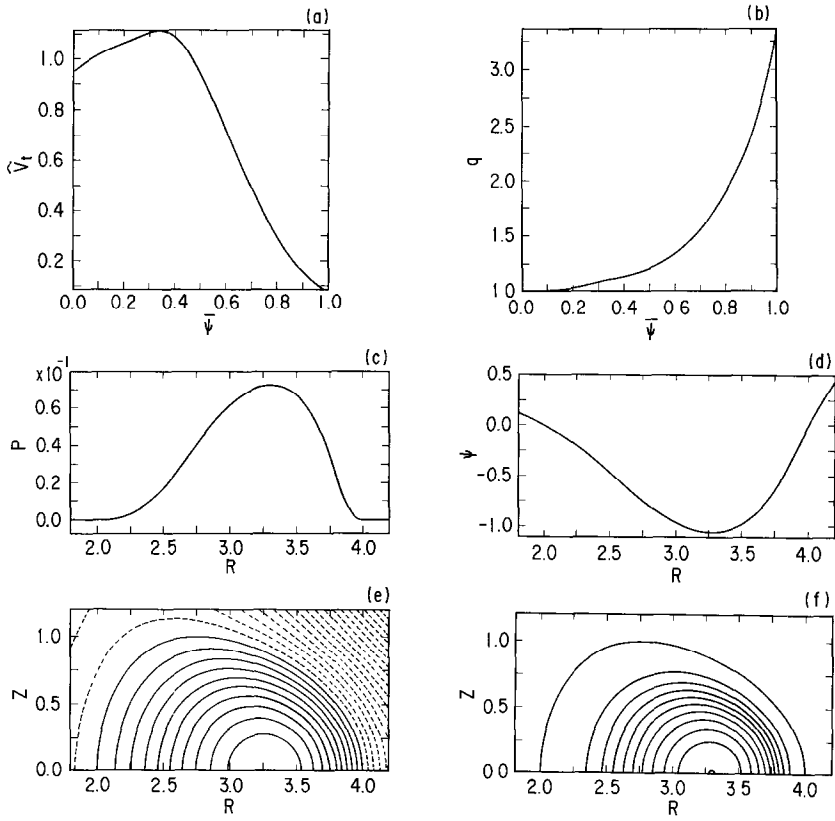


FIG. 5.1. An example of equilibria with toroidal flow: (a) flow velocity; (b) safety factor; (c) total pressure; (d) poloidal flux function are shown. It should be noted that the flux surface (e) and the constant pressure surface do not coincide with each other [132].

gation of the second-order derivatives of the equation,  $(1 - A^2 + \alpha\psi_r^2)\psi_{rr} + 2\alpha\psi_r\psi_z\psi_{rz} + (1 - A^2 + \alpha\psi_z^2)\psi_{zz}$ , where  $A = |\Phi_M|/\rho$  is the Alfvén Mach number of the poloidal flow with respect to the poloidal field and  $\alpha = (2A^2/\rho) \partial\rho/\partial(|\nabla\psi|^2)$ . From this analysis [133, 134], it is shown that the equation is elliptic in the intervals

$$0 \leq A^2 < \beta_s, \quad A_s^2 < A^2 < 1, \quad 1 < A^2 < A_f^2, \quad (5.26)$$

where

$$\begin{aligned} \beta_s &= \frac{\gamma p}{\gamma p + B^2}, \\ A_s^2 &= 1 - \left[ 1 - \frac{4\beta_s B_p^2}{\gamma p + B^2} \right]^{1/2} \frac{\gamma p + B^2}{2B_p^2}, \\ A_f^2 &= 1 + \left[ 1 - \frac{4\beta_s B_p^2}{\gamma p + B^2} \right]^{1/2} \frac{\gamma p + B^2}{2B_p^2}. \end{aligned} \quad (5.27)$$

When the ellipticity of the partial differential equation is violated, shock waves may cause a change of the topology of the flux surfaces [135] and the equilibrium problem may become complicated. From the viewpoint of the application, the solution of the equilibrium with general flow may explain the experimentally observed asymmetry of the density profile, which is usually too large to be explained by the effect of the toroidal flow. In general, however, the neoclassical transport theory shows that parallel viscous force associated with magnetic field modulation in a tokamak is apt to damp the poloidal flow within an ion-ion collision time scale [136–138], and there is still a question of whether the steady state with poloidal flow can exist or not.

### 5.2. Anisotropic Equilibria

The basic anisotropic equilibrium equation is given as

$$\mathbf{J} \times \mathbf{B} = \operatorname{div} \mathbb{P}. \quad (5.28)$$

On the basis of guiding center plasma theory [139] the tensor pressure  $\mathbb{P}$  is expressed only by the parallel pressure  $p_{||}$  and the perpendicular pressure  $p_{\perp}$  as

$$\mathbb{P} = p_{||} \mathbf{n} \otimes \mathbf{n} + p_{\perp} (\mathbb{I} - \mathbf{n} \otimes \mathbf{n}), \quad (5.29)$$

where  $\mathbf{n} = \mathbf{B}/B$ ,  $\mathbb{I}$  is the unit tensor, and  $\otimes$  denotes the tensor product. From the above equations we can derive the set of equations which governs the anisotropic equilibrium [140, 141],

$$p_{\perp} = p_{||} - B \left. \frac{\partial p_{||}}{\partial B} \right|_{\psi}, \quad (5.30)$$

$$\sigma F = I(\psi), \quad (5.31)$$

$$\Delta^* \psi = -\frac{r^2}{\sigma} \left. \frac{\partial p_{||}}{\partial \psi} \right|_B - \frac{1}{\sigma^2} \frac{d}{d\psi} I^2 - \frac{1}{\sigma} \nabla \psi \cdot \nabla \sigma, \quad (5.32)$$

where

$$\sigma = 1 - \frac{p_{\perp} - p_{||}}{B^2}. \quad (5.33)$$

As seen in Eq. (5.31)  $\sigma F$  is a surface quantity instead of the toroidal field function  $F$  for the case of isotropic equilibrium. Moreover, although in the isotropic case both the current ( $\mathbf{J}$ ) and the magnetic field ( $\mathbf{B}$ ) vectors lie on a magnetic surface and the natural coordinate system [10] is constructed so that both the  $\mathbf{J}$  and  $\mathbf{B}$  trajectories are straight lines, in the anisotropic case the  $\mathbf{J}$  vector no longer lies on a magnetic surface. Instead, a quantity,

$$\mathbf{K} = \operatorname{rot}(\sigma \mathbf{B}). \quad (5.34)$$

lies on the magnetic surface and the natural coordinate system is constructed so that the **J** and **K** trajectories are straight in this coordinate system [142]. There are additional constraining conditions on the parallel and perpendicular pressures, which come from the stability conditions against the mirror and firehose instabilities [140] as

$$\sigma = 1 - \frac{1}{B} \left. \frac{\partial p_{\parallel}}{\partial B} \right|_{\psi} > 0, \quad (5.35)$$

$$\tau = 1 + \frac{1}{B} \left. \frac{\partial p_{\perp}}{\partial B} \right|_{\psi} > 0. \quad (5.36)$$

The conditions are consistent with the condition that the equilibrium equation is elliptic, and these are satisfied for a usual tokamak plasma.

Equation (5.32) can be solved numerically by the same methods applied to the solution of the scalar pressure equilibrium. First, the parallel pressure profile is specified in the two-dimensional space  $(\psi, B)$ , and then the perpendicular pressure is determined by using Eq. (5.30). One of the most important applications of the anisotropic equilibrium solver is the analysis of equilibrium and/or stability of intensely heated plasmas by, for example, neutral beam injection. In this case the parallel beam pressure is calculated from the beam distribution function  $f_b(\mu, E, \psi)$  ( $\mu$ : the magnetic moment,  $E$ : particle energy), which is the solution of the Fokker–Planck equation. Cooper *et al.* [143] use an analytical solution where the pitch-angle scattering operator has been ignored. Figure 5.2 shows an example of the numerical results of the anisotropic equilibria calculated by Cooper *et al.* [143].

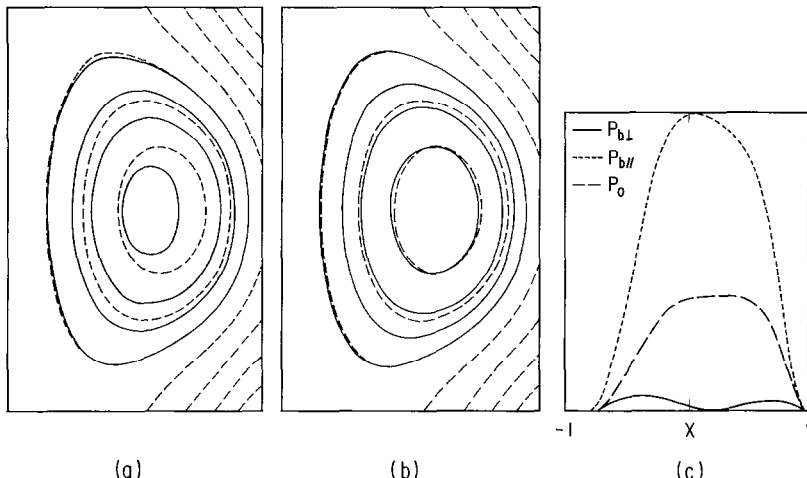


FIG. 5.2. Parallel (a) and perpendicular (b) pressure profiles overlayed on flux surfaces (broken lines) for a broad-profile tensor pressure equilibrium induced by parallel beam injection [143]. Background pressure profile (coarse broken line), parallel beam pressure profile (fine broken line), and perpendicular beam pressure profile (solid line) are also shown in (c).

Salberta *et al.* [144] employ the solution,  $f_b(\mu, E, \psi)$ , of a radial one-dimensional version of the Fokker–Planck equation where the radial convection term, as well as pitch-angle scattering operator, are retained.

### 5.3. Equilibria with Specified Current Sources

The previous sections are devoted to the description of numerical solutions of the Grad–Shafranov equation by specifying the functions  $p$  and  $F$  (or  $p$  and  $q$ ). When we use the surface-averaged parallel current  $\langle \mathbf{J} \cdot \mathbf{B} \rangle$ , instead of  $F$  or  $q$ , we can treat explicitly the sources of currents confining a plasma. Within the framework of the neoclassical transport theory the surface-averaged parallel current [145] is expressed by

$$\langle \mathbf{J} \cdot \mathbf{B} \rangle = \langle \mathbf{J} \cdot \mathbf{B} \rangle_E + \langle \mathbf{J} \cdot \mathbf{B} \rangle_B + \langle \mathbf{J} \cdot \mathbf{B} \rangle_S, \quad (5.37)$$

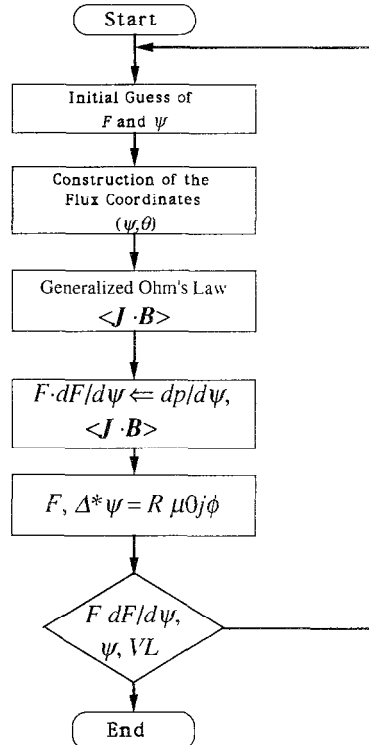


FIG. 5.3. Flow diagram of an equilibrium code with specified current source [152].

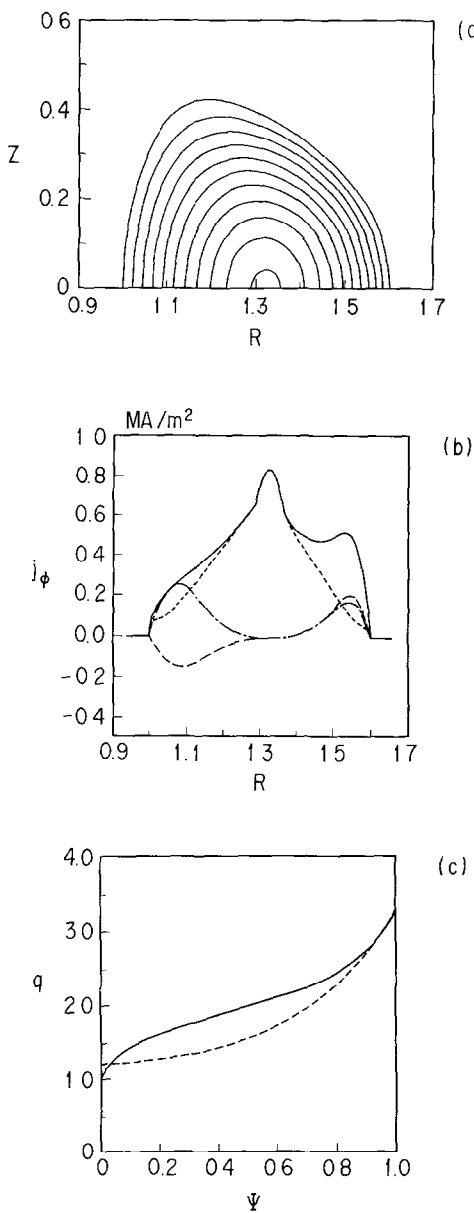


FIG. 5.4. An example of equilibria with broad pressure profile which is consistent with the neoclassical transport process, where  $I_p = 140\text{kA}$  [152]. (a) Contours of poloidal flux function  $\psi$ , where  $\psi_{\text{axis}} = -2.24 \times 10^{-2}$  weber. (b) Toroidal current on the midplane. Total current, ohmic current, Phirsch-Schlüter current, and bootstrap current are shown by solid line, dotted line, dashed line, and dotted dashed line, respectively. (c) Safety factor for neoclassical equilibrium (solid line) and classical equilibrium (dotted line).

where  $\langle \mathbf{J} \cdot \mathbf{B} \rangle_E$ ,  $\langle \mathbf{J} \cdot \mathbf{B} \rangle_B$  are ohmic current and bootstrap current given by

$$\langle \mathbf{J} \cdot \mathbf{B} \rangle_E = \sigma_{NC} \langle \mathbf{E} \cdot \mathbf{B} \rangle, \quad (5.38)$$

$$\langle \mathbf{J} \cdot \mathbf{B} \rangle_B = -F \left( L_{31}^e \frac{dp_e}{d\psi} + L_{31}^i \frac{dp_i}{d\psi} + L_{32}^e \frac{dT_e}{d\psi} + L_{32}^i \frac{dT_i}{d\psi} \right), \quad (5.39)$$

and  $\langle \mathbf{J} \cdot \mathbf{B} \rangle_S$  stands for the non-ohmically driven current. The neoclassical transport coefficients,  $\sigma_{NC}$ ,  $L_{31}^e$ ,  $L_{31}^i$ ,  $L_{32}^e$ , and  $L_{32}^i$  are given in neoclassical transport theory review papers [69, 146]. The equation for the toroidal field function  $F$  is related to the parallel current as

$$F \frac{dF}{d\psi} = - \left[ \frac{F^2}{\langle B^2 \rangle} \frac{dp}{d\psi} + F \frac{\langle \mathbf{J} \cdot \mathbf{B} \rangle}{\langle B^2 \rangle} \right]. \quad (5.40)$$

By solving the above equation and the Grad-Shafranov equation simultaneously one can obtain an MHD equilibrium self-consistently within the neoclassical transport theory and the employed theory of the non-ohmically driven current [147]. This set of differential equations is solved iteratively. Figure 5.3 shows an example of the iterative processes, where the non-ohmically driven current is not considered and the problem is formulated as a nonlinear eigenvalue problem with the one turn voltage  $V_t$  in a quasi-steady state as the eigenvalue,

$$\langle \mathbf{E} \cdot \mathbf{B} \rangle = \frac{V_t}{2\pi R_0} B_t. \quad (5.41)$$

Ehst *et al.* [148] obtained self-consistent equilibria with the current driven by fast wave excitation. In this calculation  $\langle \mathbf{J} \cdot \mathbf{B} \rangle_S$  is given by a ray-tracing calculation for a fast wave. Okano *et al.* [149] and Tani *et al.* [150] computed equilibria sustained by beam driven current. Tokuda *et al.* [151] developed a numerical code SELENENEON on the basis of the iteration scheme shown in Fig. 5.3 and computed equilibria for a non-circular tokamak with ohmic current and bootstrap current calculated self-consistently, where the neoclassical coefficients derived by a simple rational approximation given by Eq. (4.75) of Ref. [146] were employed (see also [152]). The neoclassical effects on the electric conductivity and the deformation of the plasma current profile due to the bootstrap current in a high beta tokamak are clearly demonstrated by this calculation (Fig. 5.4).

#### 5.4. Equilibrium Evolution

Calculation of the evolution of equilibria in a tokamak plasma plays an important role from the viewpoint of the transport property. Transport analyses are indispensable in the studies of the confinement properties of the tokamak plasma and various one-dimensional (1D) transport codes, called “tokamak codes” have been developed [153–158]. With the evolution of the equilibrium, however, the

transport property, especially the energy balance in the plasma, changes, which is not taken into account in a usual 1D tokamak code. Therefore, the transport process of the tokamak plasma should be analyzed in a two-dimensional (2D) space by taking into account the change of field geometry [159]. In other words, the resulting transport such as the diffusion is a non-local process which depends on the global nature of the boundary value problem. Moreover, although a tokamak equilibrium is usually determined by assigning profiles of plasma pressure and magnetic field, these profiles should not be given a priori, but they are determined from the transport process and the initial profile. For some applications the conventional procedure of equilibrium solution may be satisfactory but, for other applications, self-consistent determination of the current profile is required. In the previous subsection (5.3) we described the time independent method of self-consistent determination of equilibrium with transport process. Another method for the self-consistent determination is solving the equilibrium evolution on the resistive time scale and a 1.5D tokamak transport code is favorably used for this purpose.

An equilibrium evolution solver (a 1.5D tokamak transport code) is, essentially, composed of a two-dimensional equilibrium solver and a solver of the one-dimensional transport equations averaged on magnetic surfaces; this was called an alternating dimensional method by Grad. What should be remarked is that there are no equations which advance in time the metric quantities included in the above transport equations. To resolve this issue the metric quantities are transferred to the transport code from the equilibrium code and the information on the current profile necessary for the equilibrium calculation is fed back from the transport solver

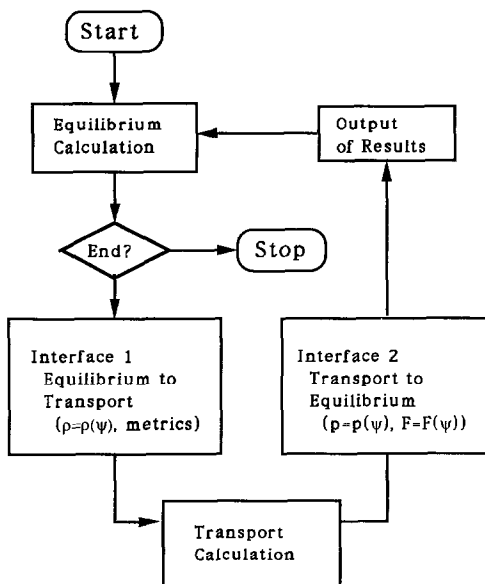


FIG. 5.5. Overall flow diagram of an equilibrium evolution code.

(Fig. 5.5). This scheme of equilibrium evolution solver was first proposed by Grad and Hogan [160] and afterward various numerical codes were developed by many authors [161–166]. In this kind of solver time scale for change of the plasma shape and its topology is comparable with the transport time scale and it is much slower than the Alfvén transit time. Within this time scale plasma flows are generated so that the force balance equation,  $\nabla p - \mathbf{J} \times \mathbf{B} = 0$ , is always satisfied [161]. This condition constrains the “grid velocities” of the flux coordinates, which follow a linear integro-differential equation [167, 168]. In tokamaks, however, the toroidal flux,  $\Phi$ , is virtually unchanging and one can eliminate the grid velocities by adopting the toroidal flux as the independent (grid) variable, by which a “conservation equation” for the safety factor  $q$  is derived [166, 167]. This model is suitable for practical applications. The FCT algorithm is, therefore, inevitably employed for solving the Grad–Shafranov equation in this model. As described later Jardin adopted another approach in the TSC code [169] to treat the plasma motion, in which artificial forces are introduced and the equilibrium equation is converted to an equation of motion.

As for the transport process of the equilibrium evolution code, the density and energy equations are given from the flux surface average of the conservation equations for particles and energy. Closure relations are needed to determine the relations among the particle/energy fluxes and the radial derivatives of density/temperature as well as the electric field. Though the neoclassical theory gives a complete set of equations, in an actual plasma, anomalous transport processes seem to dominate and the behavior of the tokamak plasma cannot be recovered by only including neoclassical process. At present, it is necessary to adopt a semi-empirical set of transport equations for theoretical understanding of an actual tokamak plasma on the basis of computation. As there is no reliable semi-empirical transport model applicable to comprehensive understanding of all tokamaks, we only describe a simple but a typical transport model where the particle (heat) flux of species is derived only from its density (temperature) gradient (diagonal model) and the plasma obeys a classical Ohm’s law [166].

As mentioned above, the “radial” coordinate is defined from the toroidal magnetic flux as

$$\rho = \sqrt{\Phi/\pi B_0}, \quad (5.42)$$

where  $B_0$  is a typical (for example, externally applied) toroidal field. The equations of density and energy of the plasma with ion charge number  $Z_i$  are

$$\frac{\partial N_e}{\partial t} - \frac{\partial}{\partial \rho} \left( D C_1 \frac{\partial n_e}{\partial \rho} \right) = \langle S_1 \rangle V', \quad (5.43)$$

$$\begin{aligned} & \frac{3}{2(V')^{1/2}} \frac{\partial \sigma_e}{\partial t} - \frac{\partial}{\partial \rho} \left( K_e C_1 \frac{\partial T_e}{\partial \rho} \right) - \frac{5k}{2} \left( D C_1 T_e \frac{\partial n_e}{\partial \rho} \right) \\ &= \left( \frac{B_0}{\mu_0} \right)^2 \frac{\eta \rho}{C_3^2} \frac{\partial}{\partial \rho} \left( \frac{C_2 \rho}{q} \right) \frac{\partial}{\partial \rho} \left( \frac{C_2 C_3}{q} \right) + \frac{D C_1}{n_e} \frac{\partial p_i}{\partial \rho} \frac{\partial n_e}{\partial \rho} - Q_{,i} V' + \langle S_2 \rangle V', \end{aligned} \quad (5.44)$$

$$\begin{aligned} & \frac{3}{2(V')^{3/2}} \frac{\partial \sigma_i}{\partial t} - \frac{\partial}{\partial \rho} \left( K_i C_1 \frac{\partial T_i}{\partial \rho} \right) - \frac{5k}{2} \left( D C_1 T_i \frac{\partial n_i}{\partial \rho} \right) \\ &= - \frac{D C_1}{n_e} \frac{\partial p_i}{\partial \rho} \frac{\partial n_e}{\partial \rho} + Q_A V' + \langle S_3 \rangle V', \end{aligned} \quad (5.45)$$

$$\frac{\partial}{\partial t} \left( \frac{\rho}{q} \right) = \frac{1}{\mu_0} \frac{\partial}{\partial \rho} \left[ \frac{\eta \rho}{C_3^2} \frac{\partial}{\partial \rho} \left( \frac{C_2 C_3}{q} \right) \right], \quad (5.46)$$

$$Q_A = \frac{3m_e}{m_i} \frac{n_e}{\tau_e} (T_e - T_i), \quad (5.47)$$

where

$$N_e = n_e V', \quad \sigma_e = p_e (V')^{5/3}, \quad \sigma_i = p_i (V')^{5/3}, \quad V' = dV/d\rho, \quad n_i = n_e/Z_i, \quad (5.48)$$

$$C_1 = V' \langle |\nabla \rho|^2 \rangle, \quad C_2 = V' \langle (|\nabla \rho|/r)^2 \rangle, \quad C_3 = V' \langle (1/r)^2 \rangle, \quad (5.49)$$

and  $D$  is the electron diffusion coefficient,  $K_e$  and  $K_i$  are the electron and ion thermal conductivities;  $\langle S_1 \rangle$  stands for the particle source, and  $\langle S_2 \rangle$  and  $\langle S_3 \rangle$  stand for electron and ion heat sources, respectively. To solve Eqs. (5.43), (5.44), and (5.45) the values of  $n_e$ ,  $T_e$ , and  $T_i$  must be specified. The constraint that the total toroidal current  $I_p$  is given is the appropriate boundary condition for Eq. (5.46).

In the 1.5D code of the above type, concerns are more in the transport process than in the equilibrium itself and the equilibrium calculation is rather simplified as restricted to the fixed boundary problem. On the other hand, when one uses the 1.5D tokamak code for an engineering purpose the plasma motion subject to the transport process and the electrical property of the system is the main object to be analyzed. In this case it is necessary to solve a free boundary equilibrium with the electric circuit and realistically positioned external conductors. The TSC code is suitable for this kind of applications. This code analyzed the time evolution of the free boundary equilibrium of the axisymmetric toroidal plasma subject to the resistive diffusion, the additional heating, and the electric current in the set of the poloidal magnetic field coils. The basic equations of the code are the equation of the 2D motion, the equations of the poloidal and the toroidal magnetic fluxes, the surface-averaged entropy equations for the ions and the electrons, and the surface-averaged equation of the plasma density. The essential feature of the code is that the equation of motion is derived from the equilibrium condition and the artificial viscous forces as

$$\frac{\partial \mathbf{m}}{\partial t} + \mathbf{F}_v(\mathbf{m}) = \mathbf{J} \times \mathbf{B} - \nabla p, \quad (5.50)$$

$$\mathbf{F}_v = -v_1 [\nabla^2 \mathbf{m} - \nabla(\nabla \cdot \mathbf{m})] - v_2 \nabla(\nabla \cdot \mathbf{m}), \quad (5.51)$$

where  $\mathbf{m}$  is the plasma momentum,  $v_1$  and  $v_2$  are the viscosities. In the above equation the convective term is neglected. By enhancing the viscosity terms artificially, plasma is always made in approximate equilibrium which mitigates the computational difficulty, due to the large difference of time scales of the MHD wave motion and diffusion process. The free boundary solution is obtained by replacing the vacuum with the low temperature, null pressure gradient plasma.

Various kinds of applications of the equilibrium evolution solvers have been reported. Examples of the former equilibrium evolution calculation subject to realistic transport processes are found in the paper by Hogan [163], where the author presents several calculations concerning the accessibility of high beta tokamak states. Figure 5.6 shows the change of the Mercier and resistive interchange criteria of the PDX tokamak due to equilibrium evolution according to different transport models [163]. Miller [164] applied the equilibrium evolution code to an analysis of shape control of the doublet tokamak. The doublet shape is determined by the plasma current profile and the current flowing in the field shaping coils. Therefore, as the plasma current evolves, the field shaping coils

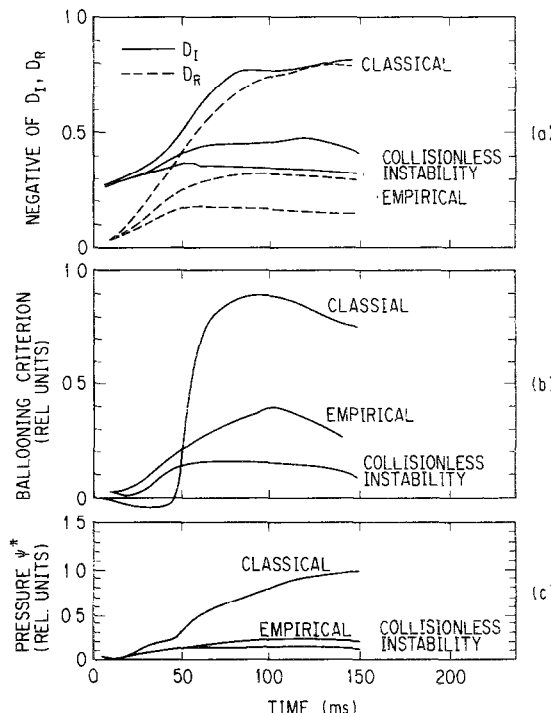


FIG. 5.6. Evolution of Mercier and resistive interchange criteria for a PDX model calculation [163]: (a) Mercier (solid line) and resistive interchange (dotted line) for three transport models. The criteria are evaluated at  $\psi = 0.8\psi_{\max} = \psi^*$ . (b) Evolution of the ballooning figure-of-merit for the three transport models of  $\psi^*$ . (c) Evolution of  $P(\psi^*)$  for the three transport models.

must be actively programmed to preserve a desired plasma shape. It was found possible to control the doublet shape by appropriately adjusting the current in the field shaping coils. As for the TSC code, applications in the field of plasma control such as the simulations of plasma shaping in the PBX tokamak [170] and relaxation process of the spheromac [171] were reported. Applications of this kind of codes are found in the experimental analysis codes or reactor designing codes, where they incorporate two-dimensional phenomena in a real space, such as the neutral particle diffusion or phenomena in a velocity space.

### *5.5. Comments on Three-Dimensional Equilibrium Solvers*

Though the tokamak plasma is basically axisymmetric, in some cases three-dimensional (3D) equilibrium analysis is necessary. In this section we summarize briefly the purposes and the methods of the 3D equilibrium solvers for the analyses of the fusion plasma.

The purposes of the 3D equilibrium analyses are considerably different between the non-axisymmetric system such as stellarators [172] and the axisymmetric system as tokamaks. For the research of the former system the 3D equilibrium analysis is essential. The determination of the finite beta equilibrium itself is the main purpose of the 3D equilibrium calculation of the system. By this calculation the maximum beta value governed by the condition for the existence of the equilibrium with well-defined magnetic surfaces is determined and the formation processes of magnetic islands and/or stochastic regions appearing with increasing beta value are analyzed. On the other hand, in the research of the tokamak, analyses are made concerning the three dimensionality attributed to the imperfection of the system and to the symmetry-breaking process by a nonlinear evolution of an instability. An example of the imperfection is the ripple magnetic field arising from the discreteness of the toroidal magnetic field coils. At present the main concern on this issue is the degradation of the alpha-particle confinement [173], and the effect of the non-axisymmetry to the neoclassical transport is also studied [174]. Up to now the non-axisymmetric state appearing in a tokamak is mainly analyzed from the viewpoint of the nonlinear evolution of instabilities [175], but the non-axisymmetric equilibrium itself is also studied by some authors [176].

Methods for the solution of 3D equilibrium are divided into two classes, i.e., the variational approach and the non-variational approach. Numerical codes based on the variational approach are further subdivided depending on whether existence of the 3D magnetic surfaces are assumed or not. In the codes by Chodura and Schlüter [177], Bauer, Betancourt, and Garabedian [178], and Hender *et al.* [179] belong to the category where the existence of the magnetic surfaces is not assumed *a priori*. On the other hand, in the 3D inverse equilibrium solvers based on the moment method [180–183] the positions of the magnetic surfaces are Fourier-analyzed in both the toroidal and the poloidal directions, which is possible only when the existence of the magnetic surfaces is assumed *a priori*. Equilibrium solvers based on both the above methods are used for design studies of the non-

axisymmetric tori such as ATF [179] but the latter method is by far advantageous from the viewpoint of the cost performance [184].

The non-variational approach is also subdivided into two groups, i.e., the direct iteration method and the averaging method. In the direct iteration code the MHD equilibrium equations (Eqs. (2.1)–(2.3)) are directly solved by using an iterative procedure [185]. This method was originated by Spitzer [186] and on the basis of the idea a 3D equilibrium code was developed by Greenside *et al.* [187, 188]. This method is effective for computing accurately an equilibrium with magnetic islands and/or stochastic regions [189], and for self-consistent calculation of the tokamak equilibrium with ripple magnetic field [190]. The averaging method is an approximate solution method used for the analysis of the stellarator equilibrium and stability, where the magnetic field is composed of a strong axisymmetric field and a weak one varying rapidly along the magnetic field lines. To derive the averaged MHD equation the original equations are expanded on the assumption that the inverse aspect ratio and the nonaxisymmetric quantities are small (stellarator expansion) [191–193]. Sometimes the assumption of the small inverse aspect ratio is not used [194–200] then the resultant averaged equilibrium equation becomes similar to the axisymmetric Grad–Shafranov equation and the various numerical methods described in this article can be used effectively. Good agreement of results of the averaging method with those of full 3D calculation is obtained [196–201].

## 6. APPLICATIONS

### 6.1. Beta Limit Optimization

As well as the studies of the numerical procedure of the equilibrium solution and the development of the equilibrium solvers a lot of effort was put on the development of optimization methods necessary from the viewpoint of the fusion reactor development programs. Though the early tokamaks were circular cross-sectional, later many theoretical and experimental studies were carried out for non-circular cross-sectional tokamaks in order to attain high plasma current density necessary for good energy confinement and intense ohmic heating under the condition of reasonably high safety factor  $q_a$  [2]. Solving the Grad–Shafranov equation numerically and calculating the beta limit from the Mercier criterion Peng *et al.* [92] showed that a D-shaped tokamak is advantageous to attain a stable high beta equilibrium. Afterward investigation of optimized high beta equilibrium stable with respect to the ideal MHD modes such as the ballooning mode and the kink mode were carried out [202–205]. In the optimization studies two different equilibrium groups were investigated; one was a group of strongly-shaped tokamaks such as a bean-shaped tokamak [206–209], crescent-shaped tokamak [210], and an ellipsoidally shaped tokamak [211], and the other was a group of the low-aspect-ratio tokamaks [92, 212–214] which are advantageous of their compactness [212]. All

these studies are based on the calculation of the beta limit determined by the ideal MHD stability and the results are summarized in terms of the Troyon factor [205],  $g_T = \beta/(I/aB_r)$ . On the other hand, the equilibrium optimization aiming at improvement of the plasma confinement is also pursued. In this case suppression of the trapped particle instability is the key issue [215] and the equilibrium was optimized so that the  $\psi$  derivative of the second adiabatic invariant  $J = \oint v_{||} dl$  or the velocity-space average value of the invariant over the trapped particles is negative or as low as possible [216, 217] (see also [218] for the related topics).

As a typical example of the application of the high resolution equilibrium calculation in this subsection we present a beta limit optimization with respect to the high- $n$  ( $n$ : toroidal mode number) ballooning mode. Strictly speaking the beta limit optimization should be carried out with respect to all possible modes of instabilities but the high- $n$  ballooning mode is often the most stringent mode [219] which imposes a beta limit on a tokamak plasma. This mode can be analyzed on each magnetic surface independently, which makes the stability calculation extremely easy in comparison with other instabilities.

The equation for the high- $n$  ballooning mode instability was derived by Connor *et al.* [220] as

$$\frac{d}{dy} \left( f(y) \frac{dg}{dy} \right) + \frac{dp}{d\psi} h(y) g = \omega^2 k(y) g, \quad (6.1)$$

where  $g$  is the slowly varying part of the instability amplitude of the so-called ballooning representation with respect to the extended poloidal angle  $y$  defined in an infinite region ( $-\infty < y < \infty$ ). The other quantities are expressed as

$$f(y) = \frac{1}{\mathcal{J} |\nabla \psi|^2} \left\{ 1 + \left( \frac{|\nabla \psi|^2}{B} \frac{\partial z}{\partial \psi_\perp} \right)^2 \right\}, \quad (6.2)$$

$$h(y) = \frac{\mathcal{J}}{B^2} \frac{\partial}{\partial \psi_\perp} (2p + B^2) - \frac{f}{B^4} \frac{\partial z}{\partial \psi_\perp} \frac{\partial B^2}{\partial y}, \quad (6.3)$$

$$k(y) = \frac{1}{|\nabla \psi|^2} \left\{ 1 + \left( \frac{|\nabla \psi|^2}{B} \frac{\partial z}{\partial \psi_\perp} \right)^2 \right\}, \quad (6.4)$$

$$z(y) = \int_{y_0}^y \frac{\mathcal{J} F}{r^2} dy, \quad (6.5)$$

where

$$\frac{\partial}{\partial \psi_\perp} \equiv \frac{\nabla \psi \cdot \nabla}{|\nabla \psi|^2}. \quad (6.6)$$

The boundary condition for  $g(y)$  is

$$g(y = \infty) = g(y = -\infty) = 0. \quad (6.7)$$

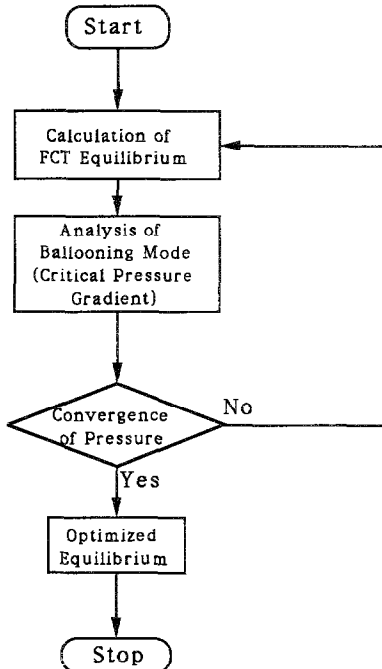


FIG. 6.1. Flowchart of calculation of the beta limit optimization.

By letting  $\omega^2 = 0$  the critical pressure gradient  $(dp/d\psi)_{cr}$  is obtained as the eigenvalue,  $dp/d\psi$ , of Eq. (6.1). The numerical procedure of the beta limit optimization is a combination of the FCT equilibrium calculation and the stability calculation as shown in Fig. 6.1, where the pressure distribution is determined by the above critical pressure gradient analysis. In the actual calculation the ballooning equation (Eq. (6.1)) is solved in a bounded domain of  $y[0, 2\pi N]$  for an up-down-symmetric case by assuming that the profile of the safety factor is fixed during the optimization process, where  $N$  is the parameter determining the approximate boundary of the integration. The marginal equation (Eq. (6.1) with  $\omega^2 = 0$ ) is numerically solved by using the Runge-Kutta method or the matrix method with the boundary conditions,

$$g(0) = \text{finite} \quad \text{and} \quad g(2\pi N) = 0. \quad (6.8)$$

An example of the beta limit optimization with respect to the high- $n$  ballooning mode is shown in Fig. 6.2 [221, 222].

Since the behavior of  $g(y)$  in Eq. (6.1) is determined in the limit of large  $y$  by the Mercier criterion [223], this criterion always predicts stability if the ballooning criterion does. However, it is often convenient to evaluate it, since this requires only an averaging of equilibrium quantities along magnetic field lines, rather than solving a differential equation along the line, as

$$M = M_s + M_w + M_p > 0, \quad (6.9)$$

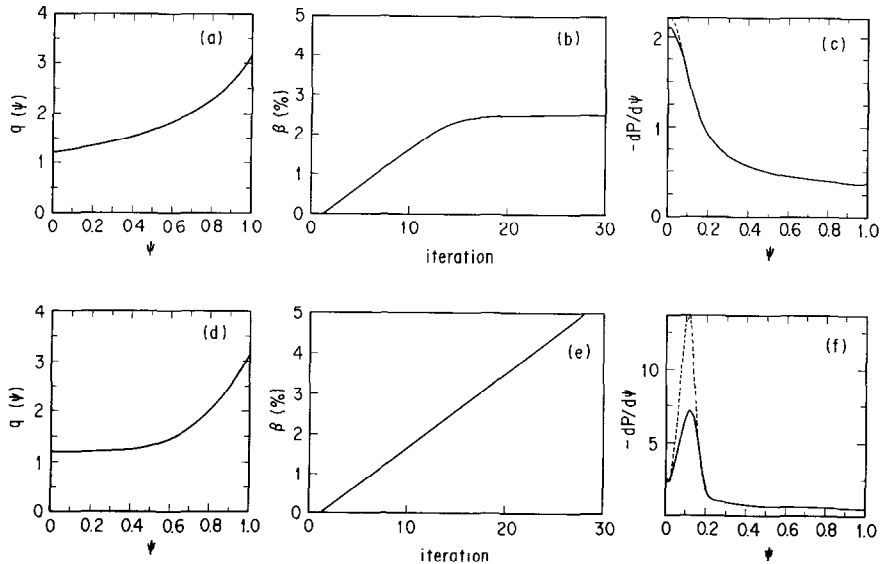


FIG. 6.2. Example of calculation of the beta limit optimization. Subfigures (a), (b), and (c) are for the case with moderate shear, whereas subfigures (d), (e), and (f) are for the case with high shear at the plasma surface.

where

$$M_s = \frac{1}{4} \left( 4\pi^2 \frac{dq}{d\psi} \right)^2, \quad (6.10)$$

$$M_w = - \frac{dp}{d\psi} \left\{ 4\pi^2 \frac{dq}{d\psi} Q_1 - \frac{d^2 V}{d\psi^2} \left( F^2 Q_2 + 4\pi^2 \frac{q}{F} \right) \right\}, \quad (6.11)$$

$$M_p = - \left( \frac{dp}{d\psi} \right)^2 \left\{ \left( F^2 (Q_2 Q_3 - Q_1^2) + 4\pi^2 \frac{q}{F} \right) \right\}, \quad (6.12)$$

$$Q_1 = 2\pi \oint \frac{dl}{r^2 B_p^3}, \quad (6.13)$$

$$Q_2 = 2\pi \oint \frac{dl}{r^4 B_p^3}, \quad (6.14)$$

$$Q_3 = 2\pi \oint \frac{dl}{B_p^3}. \quad (6.15)$$

When the local interchange instability is the limiting instability, the critical pressure is obtained from the Mercier criterion [221] as

$$\left( \frac{dp}{d\psi} \right)_{cr} = - \frac{C_2 + \sqrt{C_2^2 + 4C_1 C_3}}{2C_3}, \quad (6.16)$$

where

$$C_1 = M_s, \quad C_2 = -\frac{M_n}{dp/d\psi}, \quad C_3 = -\frac{M_p}{(dp/d\psi)^2}. \quad (6.17)$$

## 6.2. Engineering Applications

MHD equilibrium calculations give basic data which are necessary for designing a tokamak device. The confinement properties of a tokamak plasma is determined on the basis of the MHD equilibrium. Therefore, the MHD equilibrium calculations of a tokamak plasma are directly related to engineering applications as well as other applications. More specifically, the determination of a desired external magnetic field configuration and coil system, and analyses of the positional instability properties are two major engineering applications of MHD equilibrium calculations. There are also other engineering applications as analyses of shape control by using the equilibrium evolution code incorporated with the external circuit equation [164] mentioned in the previous section. This problem is a rather complicated one from the engineering viewpoint which includes the MHD equilibrium, transport process in the plasma, eddy current problem in the external conductors, and electrical circuit outside plasma. In the following we describe the former two applications.

The design of a external magnetic field configuration is formulated as follows. The external confining magnetic field is determined from the equilibrium solution by separating the confining field and the self-field from the composite magnetic field. The simplest way to carry out this process is to calculate the self-field by integrating the plasma current density over the whole plasma cross section and subtracting the self-field from the composite field. However, this process is very cumbersome and impractical for the usual equilibrium calculation. To cope with this difficulty Shafranov and Zakharov [87] proposed the virtual casing principle in which the surface integral of the plasma current in the previous calculation is replaced by a line integral along a magnetic surface. To apply the virtual casing principle one assumes an equilibrium configuration surrounded by a closed superconducting sheath  $S$  coinciding a magnetic surface. Outside this sheath the magnetic field is zero, because the magnetic field due to the plasma current is completely cancelled by the surface current  $i$  induced in the super-conductor,

$$\mathbf{i} = \frac{1}{\mu_0} \mathbf{B}_s \times \mathbf{n}, \quad (6.18)$$

where  $\mathbf{B}_s$  is the magnetic field of the equilibrium configuration at the surface  $S$  and  $\mathbf{n}$  is the normal unit vector perpendicular to the surface. Thus the magnetic field due to the current in the virtual casing coincides with the confining field inside the casing and outside the casing it coincides with the magnetic field due to the plasma current with opposite direction. Therefore, by using the virtual casing principle one

can calculate the external confining magnetic field inside the virtual casing [72] as: (1) determine a fixed boundary equilibrium by assigning the plasma boundary shape; (2) calculate the magnetic field tangential to the boundary at the inner surface of the virtual casing; (3) calculate the surface current density in the virtual casing from Eq. (6.18); (4) calculate the magnetic field  $B_\tau(s)$  due to the above surface current. Calculation of the current distribution in external field coils is an inverse problem from the magnetic field. This problem is reduced to a first type Fredholm integral equation as

$$\hat{C}\mathbf{i}_1 \equiv \oint_l \mathbf{i}_1(l) b_\tau(s; l) dl = \mathbf{B}_\tau(s), \quad (6.19)$$

where

$$\mathbf{b}_\tau(s; l) = \mathbf{b}(s; l) \cdot [\mathbf{e}_\phi \times \mathbf{n}(s)], \quad (6.20)$$

and  $l$ ,  $\mathbf{i}_1(l)$ , and  $\mathbf{b}_\tau(s; l)$  are the position along an arbitrarily chosen contour surrounding the virtual casing, current density at  $l$ , and the magnetic field at  $s$  by unit current at  $l$ , respectively. The above integral equation is an ill-posed problem in the sense of Hadamard, and Zakharov used the regularization method of Tikhonov [224] which minimizes the functional

$$F = \oint_\Gamma (\hat{C}\mathbf{i}_1 - \mathbf{B}_\tau)^2 ds + \alpha \oint \left[ k_1(l) \left( \frac{di_1}{dl} \right)^2 + k_2(l) i_1^2 \right] dl, \quad (6.21)$$

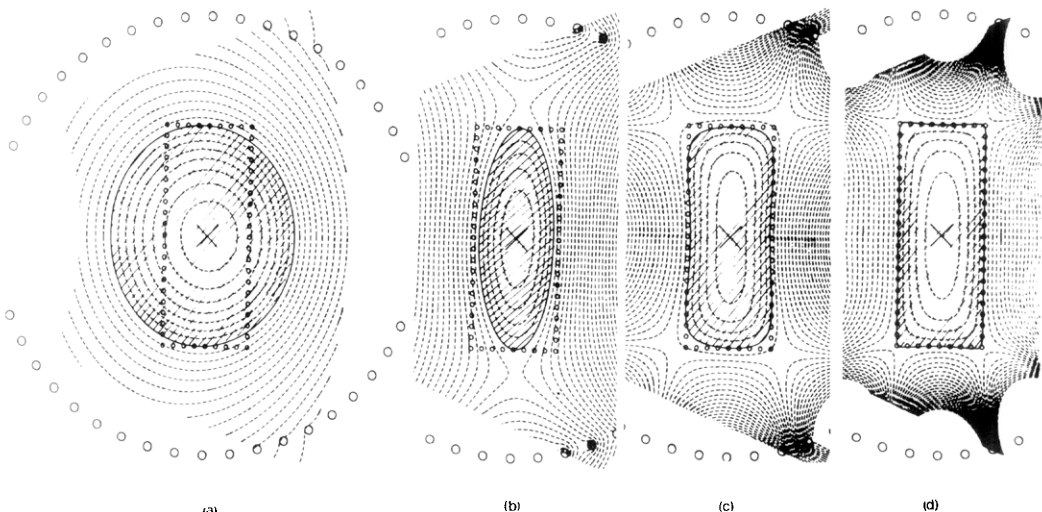


FIG. 6.3. Dependence of the approximation of the external coil currents on the cutoff Fourier number  $K$  [4]: (a)  $K=1$ ; (b)  $K=3$ ; (c)  $K=5$ ; (d)  $K=7$ .

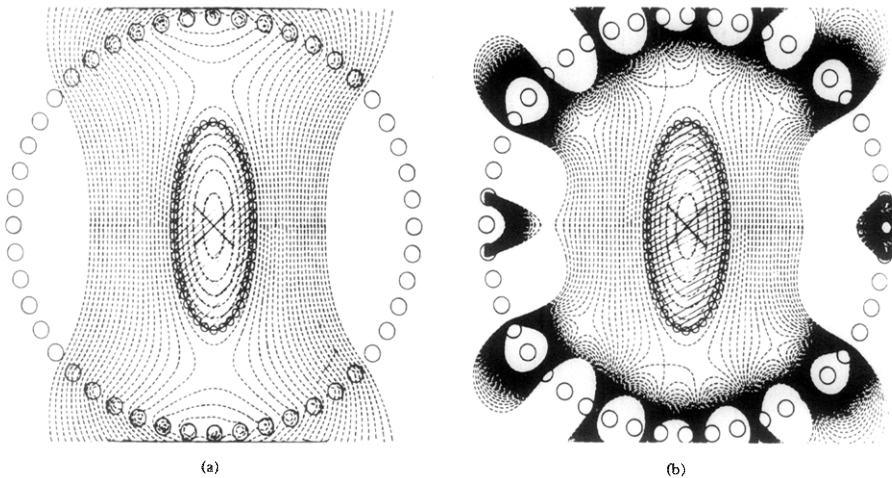


FIG. 6.4. Effect of using too many Fourier components for the external current distribution [7] using: (a)  $K=5$ , or (b)  $K=11$ , gives practically the same approximation to the prescribed plasma surface.

where  $k_1$  and  $k_2$  are positive functions,  $\alpha$  is the regularization parameter. Modifications of the above method have been proposed by many authors. Basically the problem is made numerically tractable by dropping the requirement that the actual plasma boundary should coincide exactly with the prescribed one, while posing restrictions on the location and current in the external conductors. Lackner [7] represented the external current on the closed surface by a Fourier series truncated at a given order  $K$  to enforce a controllable degree of smoothness, and expressed the total field at the  $n$ th cycle as

$$\psi^n = \psi_p^n + \sum_{i=0}^K \alpha_i \psi_{e,i}, \quad (6.22)$$

where  $\psi_{e,i}$  is the field produced by the  $i$ th Fourier component of the external current. The  $K+1$  Fourier coefficients  $\alpha_i$ 's were then determined at each iteration to minimize the deviation of the flux function (Fig. 6.3). Too many Fourier components result in a strongly oscillating external current distribution (Fig. 6.4). Instead of optimizing the current distribution in external coil systems Toi and Takeda [225] proposed optimization of the positions of external coils carrying prescribed currents. In this method the position of a coil is restricted to a prescribed curve and is represented by a single parameter such as a poloidal angle along the curve and the objective function made of the square of the difference of the desired magnetic fields is minimized with respect to the poloidal angles by using an appropriate nonlinear programming algorithm. Due to the discreteness of the coil currents unnecessary strong oscillation is suppressed and the solution is regularized as shown in Fig. 6.5.

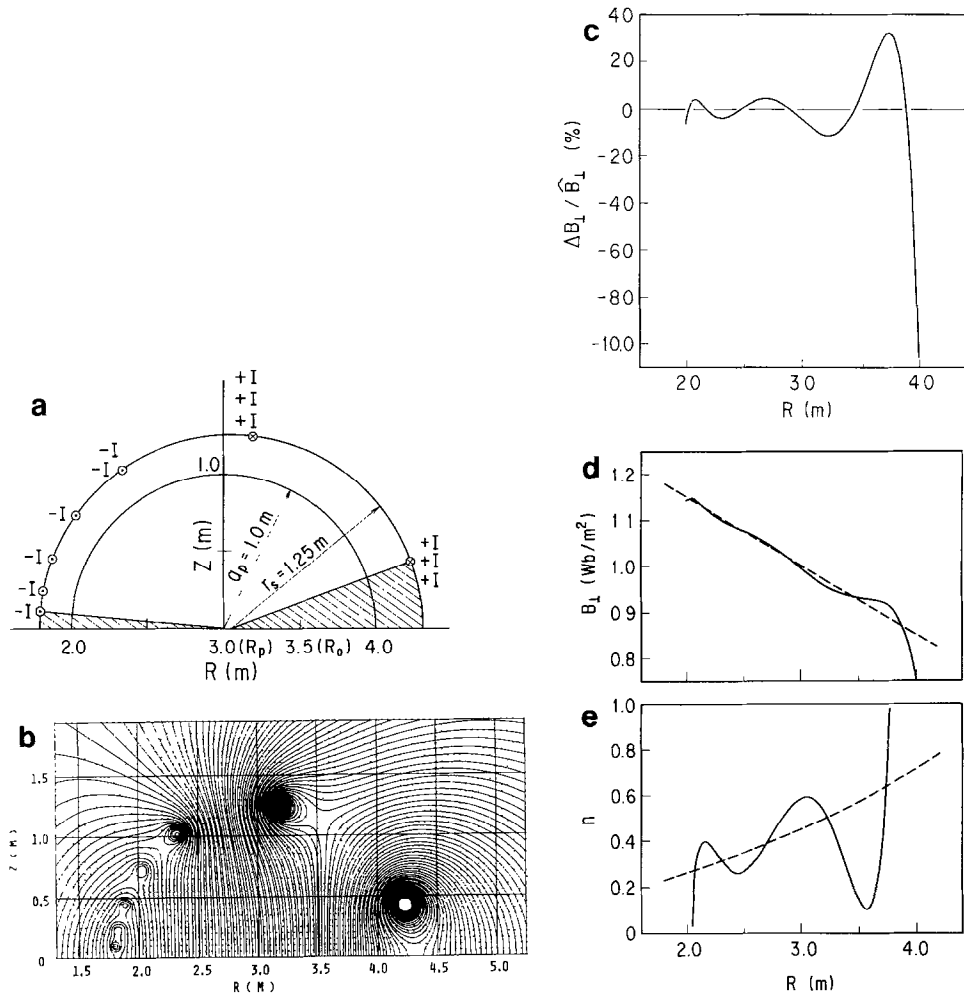


FIG. 6.5. Example of the external coil design by using the nonlinear optimization algorithm [225]. The subfigure (a) shows a constraining circle with radius of 1.25 m, on which the coils with currents  $\pm I$  move during the optimization process. The coils are inhibited to enter the shaded angular regions. The subfigure (b) shows the map of the magnetic field lines due to the optimized coil configuration. The subfigures (c), (d), and (e) show the deviation of the realized magnetic field from the desired one, the vertical magnetic field on the median plane, and the realized  $n$ -index.

The positional instability of a tokamak is primarily related to the gradient of the external magnetic field and usually only a few parameters are sufficient to identify the stability condition for this instability. Representative models used for analyses of this instability are (1) rigid model, (2) rigid displacement model, and (3) general linearized ideal MHD model. In the rigid model a toroidal plasma is represented by a current carrying rigid conductor and the instability is analyzed electrodynamic-

cally, where plasma deformation is neglected. The stability condition [97] is expressed by the gradient of the magnetic field ( $n_i$ :  $n$ -index) for a circular cross-sectional tokamak as

$$0 < n_i < \frac{3}{2}, \quad (6.23)$$

where

$$n_i \equiv -\frac{r}{B_z} \frac{\partial B_z}{\partial r}. \quad (6.24)$$

By a slightly more complicated formula the stability condition for an elliptical cross-sectional tokamak is also obtained on the basis of this model [226]. In the

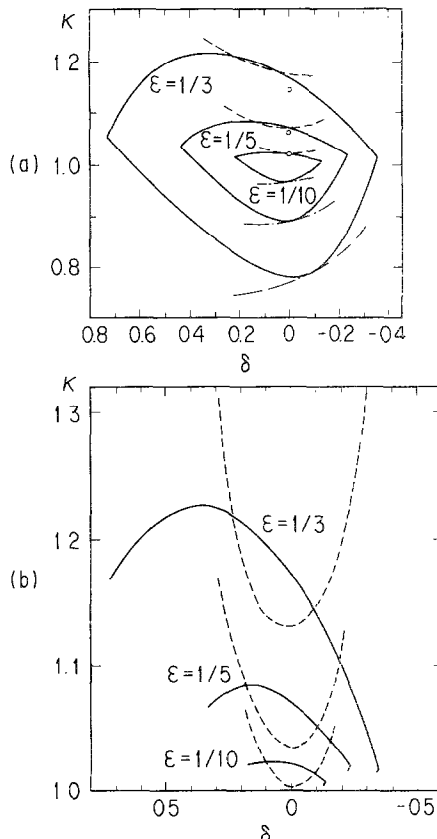


FIG. 6.6. Stability diagram for the positional instability of the Solov'ev equilibrium on the basis of various models [228]. Broken line and dotted-broken line in (a) show the decay index  $n_i = 0.0$  and  $n_i = 1.5$ , respectively. Broken lines in the subfigure (b) are the stability boundary calculated by the solid displacement model. Solid lines in both the subfigures show the stability boundaries calculated by the general MHD model.

rigid displacement model, uniform plasma displacement over the whole plasma cross section is assumed and the variational principle is applied for this uniform displacement [227]. In the general MHD model no such assumption is introduced to the plasma displacement and the instability is analyzed by using a general linearized ideal MHD code such as ERATO [125] or PEST [124]. Kumagai *et al.* [228] analyzed the positional instability for the Solov'ev equilibrium [20] on the basis of the above three models. They found that the stability conditions obtained for these three models are rather different from each other, especially when the non-circularity is large and/or the aspect ratio is small, as shown in Fig. 6.6. By using the rigid model the stability condition is easily calculated because it is not necessary to solve an MHD equilibrium. It is, however, concluded that the general MHD model is indispensable to analyze the positional instability in a present day large tokamak with highly shaped cross section and/or small aspect ratio. The importance of calculation of the MHD equilibrium is remarkable when one analyzes the positional instability of a tokamak with a magnetic limiter or divertor. When a tokamak has a poloidal divertor on the median plane as in the case of the JT-60 tokamak [229], the external magnetic field changes its sign at the stagnation point ( $X$ -point) of the separatrix magnetic surface. Consequently, the  $n$ -index varies from plus infinity to minus infinity at the  $X$ -point (Fig. 6.7), which makes the widely used rigid model useless for identification of the stability condition of this

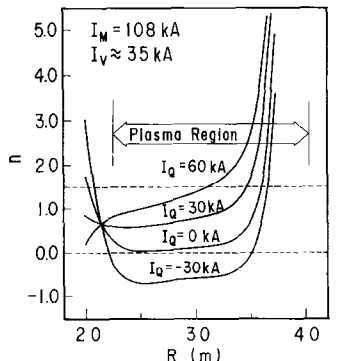
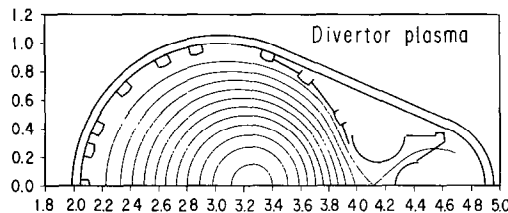


FIG. 6.7. Spatial variation of the  $n$ -index in a plasma with a separatrix magnetic surface [229]. The external coil currents are adjusted to fix the  $X$ -point at the prescribed position.

system and the general linearized ideal MHD model is indispensable. For a tokamak equilibrium where the plasma surface coincides with the separatrix magnetic surface we must be very careful to calculate metric quantities which diverge at the  $X$ -point. In the calculation of Ref. [229] a magnetic surface separated inwards by  $\delta\psi_{sep}$  from the separatrix was chosen as the plasma surface. The difference of the magnetic flux  $\delta\psi_{sep}$  is defined as

$$\delta\psi_{sep} = |\psi_{sur} - \psi_{sep}| = \delta |\psi_{sep} - \psi_{axil}|, \quad (6.25)$$

where  $\delta$  of 0.001 is employed as a typical value of separation. To ensure high accuracy, fine meshes with  $N_r = 512$  and  $N_z = 256$  were chosen and mesh accumulation near the plasma surface was adopted in the stability calculation. The main

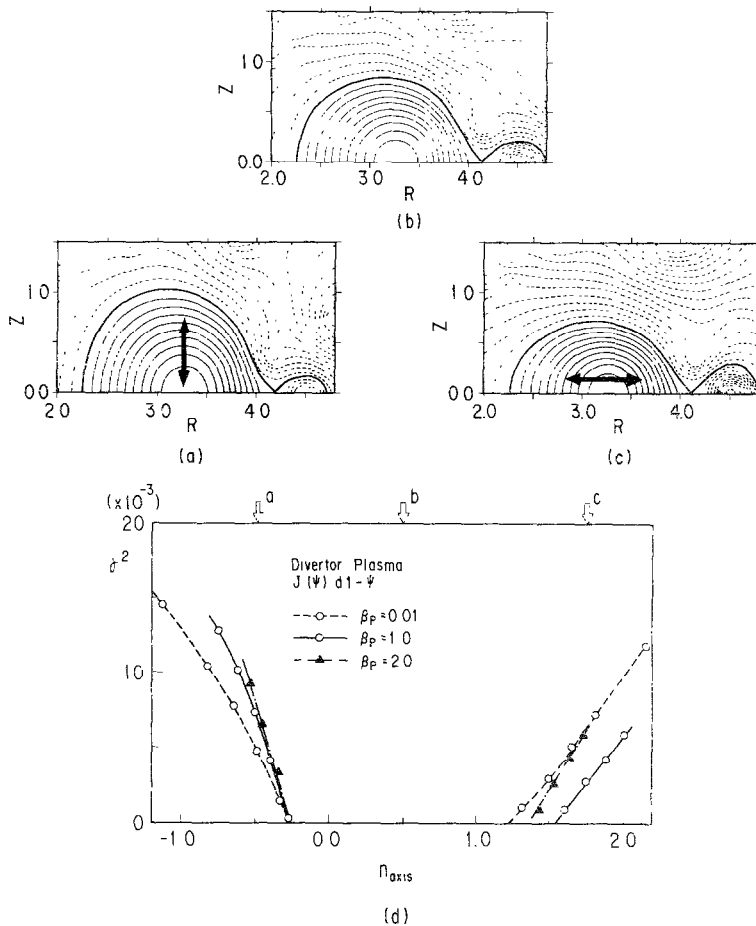


FIG. 6.8. Stability window of a positional instability (the lower subfigure) in a plasma with a separatrix magnetic surface [229]. The upper subfigures show the vertically-unstable, stable, and horizontally-unstable equilibria from the left to the right.

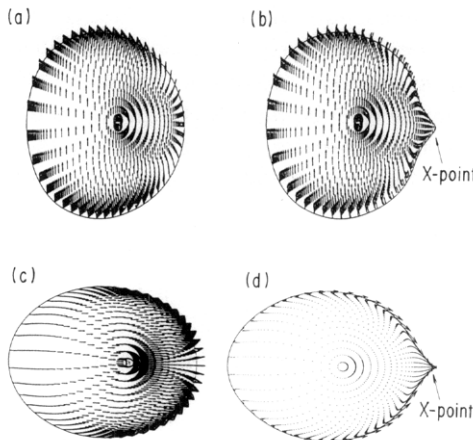


FIG. 6.9. Plasma displacement due to the positional instability [229]. Subfigures (a) and (b) show the vertical positional instability, and subfigures (c) and (d) show the horizontal positional instability. Subfigures (a) and (c) and subfigures (b) and (d) are the limiter case and the divertor case, respectively.

results of the analyses of the positional instability in the JT-60 plasma are summarized as follows: (1) Even in the case of a tokamak plasma with an  $X$ -point, positional stability is assured in a wide range of the  $n$ -index,  $0.25 < n_i < 1.2$  (Fig. 6.8). This result, however, contradicts the result of the rigid displacement model which gives wider stability window [230]. (2) The vertical displacement is well described as a rotation around the  $X$ -point and the horizontal displacement is described as a radial flow into the  $X$ -point (Fig. 6.9). Both flow patterns differ considerably from those corresponding to the rigid model or rigid displacement model. (3) The current distribution affects the stability considerably. If the current profile is peaked the stability window widens to the high  $n_i$  side. All of these results indicate that the MHD equilibrium calculation is very important even for the calculation of global instabilities such as the positional instability.

### 6.3. Experimental Analyses

In a tokamak experiment basic information on the MHD equilibrium of the plasma is obtained by measurement of electromagnetic signal. Needless to say, detailed equilibrium can be obtained by using additional information by other diagnostics but we can reconstruct a fairly satisfactory equilibrium configuration of a tokamak plasma only by measurement of the electromagnetic signal from the plasma. In most tokamak devices magnetic probes and flux loops are installed as a system of the electromagnetic measurement. The usual magnetic probes are small coils to sense the local magnetic field, and a long densely wound coil surrounding the minor circumference of the plasma, called a Rogowski coil, is used to measure the toroidal plasma current. Sometimes, a set of partial Rogowski coils which do

not cover the complete minor circumference is used as in the case of the Dcublet-III tokamak [231]. A flux loop is a loop wound along the major circumference of the toroidal plasma that senses the change of the poloidal magnetic flux  $\psi$  inside the flux loop. A flux loop surrounding the plasma minor cross section is called a diamagnetic loop and it senses the change of toroidal flux, which is related to the plasma pressure. In this section we use a set of data from the Rogowski coil, magnetic probes, and flux loops as input data for the equilibrium analyses.

Christiansen and Taylor [232] have shown that the current distribution in an axisymmetric toroidal discharge can, in principle, be completely determined from purely geometric information about the shape of the magnetic surfaces. Determination of current distribution based on this procedure was carried out by Christiansen *et al.* [233] by using the X-ray tomography technique [234]. The electromagnetic signals are only obtained outside the plasma that do not give information on the shape of the inner magnetic surfaces and it is interesting to know to what extent we can determine the plasma equilibrium configuration by using such a limited set of information. In the following we describe a method to determine the equilibrium, especially the  $\beta_p$ ,  $I_i$ , shape, and position, from the input data of the magnetic field and the magnetic flux at several points outside the plasma. This kind of analyses is indispensable for experiments in a large tokamak and various numerical codes have been developed by many authors [235–240]. Generally this procedure is divided into two steps; i.e., the first step determines the plasma position and cross-sectional shape, and then a more detailed equilibrium is obtained by solving the Grad-Shafranov equation as a semi-fixed boundary problem by using the data of the plasma shape obtained in the first step. In the second step an assumption is made that the current distribution is given by a simple function with a few parameters.

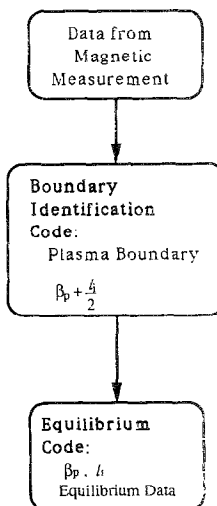


FIG. 6.10. Overall flow diagram to determine an equilibrium from a set of experimental data.

The overall procedure to determine the equilibrium is shown in Fig. 6.10. We describe the two steps in more detail:

(1) The result of this step is not only used as the input data for the second step but also used independently for the on-line control of the plasma position and a fast and simple calculation method is required for this step. The toroidal multipole method of Zakharov is one of the direct methods used to determine the position and shape of the plasma [72, 117]. In this method the moments of the current are defined as

$$u_m = \int \chi_m(r, z) J_\phi(r, z) dr dz, \quad (6.26)$$

where the  $\chi_m$ 's are solutions of the differential equation,

$$\nabla \frac{1}{r^2} \nabla \chi_m = 0. \quad (6.27)$$

The surface integrals over the cross section of the plasma are reduced to line integrals surrounding the plasma cross section, and the multipole moments are obtained from the electromagnetic signals measured outside the plasma. Thus the plasma position, ellipticity, and triangularity are derived from the first, second, and third moments,  $u_1$ ,  $u_2$ , and  $u_3$ , respectively. This is an elegant method but in an actual situation applicability of this method is limited due to the hardware restriction.

On the other hand, the practical method of this step, widely used for the experimental analyses of large tokamaks, is based on the least square matching of the measured magnetic field and the calculated magnetic field which is produced by filament currents or surface currents located inside the plasma. It is not possible to determine completely the plasma current distribution from any external measurement but it is possible to determine the multipole moments  $u_m$ 's and we can expand the flux  $\psi_p$  due to the plasma current as

$$\psi_p = \sum_{m=1}^M u_m \chi_m. \quad (6.28)$$

It should be remarked, however, that current distribution which realize a particular set of moments,  $u_1, \dots, u_M$ , cannot be determined uniquely. This fact enables us to fit the outside magnetic field by varying the currents in the filaments or surface at fixed positions. In the filament current method [237-239], typically, six filament currents are located inside the plasma region and magnetic field fitting is carried out for six parameters, i.e., the currents in the six filaments. The location of the plasma current filaments are arbitrarily chosen because the calculated boundary position is rather insensitive to the positions of the filaments unless they are too close to the boundary or they are located too closely to each other. The least square

matching of the magnetic fields is carried out by minimizing the object function,  $\Xi$ , defined as

$$\Xi = \sum_i^M w_i (\hat{b}_i - b_i)^2, \quad (6.29)$$

where  $\hat{b}_i$ 's are measured magnetic fields and  $b_i$ 's are the calculated fields expressed as

$$b_i = \sum Q_{ij}^c I_j^c + \sum Q_{ij}^p I_j^p, \quad (6.30)$$

where  $I_j^c$  and  $I_j^p$  are the currents flowing in the external conductors and filament currents in the plasma region.  $Q_{ij}$  is the response matrix expressed in terms of the complete elliptic integrals. There are several variations of this method, especially concerning the treatment of external conductors and constraining conditions such as a fixed plasma current. When the tokamak device has an iron core and/or the effects of eddy current in the external conductors play an important role, the system should be analyzed very carefully. In this case currents in the external conductors should be treated as unknown variables and the surface current model is more suitable for the equilibrium analysis.

After the plasma position and the poloidal field strength on the plasma surface are determined we can calculate the surface integrals  $S_1$  and  $S_2$  (Eqs. (2.62) and (2.63)). Then, the current beta  $\beta_j$  and the internal inductance  $l_i$  can be evaluated using the measurement of the diamagnetic flux. In an actual experiment, however, the current beta determined from Eq. (2.60) does not coincide with the current beta from Eq. (2.61) because of the unavoidable experimental error. The beta value calculated from the former current beta is called the diamagnetic beta  $\beta^{\text{dia}}$  and that from the latter is called MHD beta  $\beta^{\text{MHD}}$  conventionally. In the tokamak research these beta values, as well as the kinetic beta  $\beta^{\text{kin}}$ , evaluated from the measurement of the density, the temperature, and so on, are used in experimental data analyses [235, 240]. Generalization of the definition of the above betas to the anisotropic pressure equilibrium was given by Lao *et al.* [238]. In order to determine the MHD beta by Eq. (2.61) it is necessary to evaluate the internal inductance  $l_i$  independently from the calculation of  $S_1$  and  $S_2$ . One expedient is use of a fitting formula by which the internal inductance is expressed as a function of the parameters specifying the current profile and the plasma shape, current beta, and so on [235]. Another method is to calculate the equilibrium by parametrizing the plasma current profile, which is described minutely in the following.

(2) On the basis of the information obtained from the first step one can obtain more detailed information of the equilibrium by solving the Grad-Shafranov equation in the second step. Numerical codes for this kind of analyses are also developed by many authors [231, 239]. As the plasma boundary is already determined by the first step calculation, in this step one solves the Grad-Shafranov equation as a fixed boundary problem or a semi-fixed boundary value problem. The

plasma current distribution is expressed by several parameters and the parameters are determined through a nonlinear optimization procedure of the object function composed of the sum of squares of the magnetic field differences. The number of parameters is usually chosen as one or two. A key issue of this kind of problem is whether it can properly determine the poloidal beta  $\beta_p$  and the internal inductance  $l_i$ . In the analyses of the Doublet III tokamak [231] and JT-60 [239] the current density is expressed as

$$J_\phi(r, \tilde{\psi}) = J_0 \left[ \beta_{p0} \frac{r}{R_0} + (1 - \beta_{p0}) \frac{R_0}{r} \right] g_\phi(\tilde{\psi}), \quad (6.31)$$

$$g_\phi(\tilde{\psi}) = (1 - \tilde{\psi}^\alpha)^\gamma. \quad (6.32)$$

The parameters  $\alpha$  and  $\gamma$  correspond to the parameters with clearer physical meanings,  $q_{\text{axis}}$  and  $l_i$ . Therefore, the free parameters of this system are  $(I_p, \beta_p, q_{\text{axis}}, l_i)$ . In an actual situation one uses the plasma current measured by the Rogowski coil, and on the assumption that  $q_{\text{axis}} = 1$ , which is considered to be good for the case with sawtooth oscillations, determines the parameters  $\beta_p$  and  $l_i$ . In this analysis the Grad-Shafranov equation should be solved many times, even to determine one set of unknown parameters in the optimization procedure, and this series of calculations must be repeated many times to obtain the time-resolved experimental results.

Luxon and Brown claimed that, in plasmas with significant non-circularity, the internal inductance can be determined independently of the poloidal beta by this method [231]. According to them the ability to separate the internal inductance from the poloidal beta is dependent on non-circularity, where for the circular case

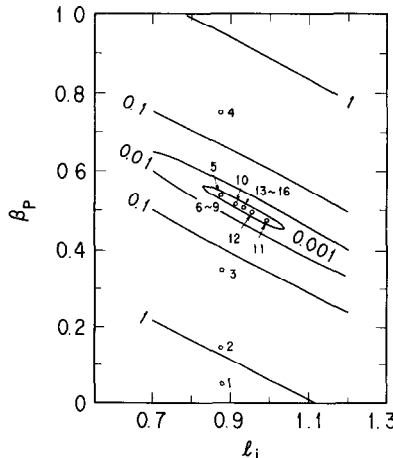


FIG. 6.11. Separation of  $\beta_p$  and  $l_i$  by sufficiently accurate equilibrium calculation [239]. The square of deviation between the observed and calculated magnetic field  $\Xi$  (contours) is minimized in the  $\beta_p - l_i$  space.

they cannot be separated. On the other hand, Tsuji *et al.* analyzed the experimental data of JT-60, a nearly circular cross-sectional tokamak [239], and they concluded that separation of  $\beta_p$  and  $l_i$  is possible if the resolution of the equilibrium calculation is high enough. In their calculation the outboard and inboard radii of the plasma ( $R_{\text{out}}$  and  $R_{\text{in}}$ ), determined by the filament current approximation, are used to define the plasma position and the SELENE40 code based on the DCR algorithm is used to solve the Grad-Shafranov equation. The values of  $\beta_p$  and  $l_i$  are determined by nonlinear optimization of  $\Xi$  in the  $\beta_p - l_i$  space by applying the Coggins method [241]. The contours of  $\Xi$  are almost parallel lines in the  $\beta_p - l_i$  plane, which means that  $\beta_p$  and  $l_i$  degenerate in the case of the circular cross-sectional tokamak (Fig. 6.11). The detailed structure of the contours shows, however, that the contours in the vicinity of the minimum are of extremely elongated elliptical shape and a single minimum exists. It was also concluded that even if there is an experimental error separation of  $\beta_p$  and  $l_i$  is possible by solving the Grad-Shafranov equation with very high resolution.

Another method for separation of  $\beta_p$  and  $l_i$  is to solve the equilibrium with toroidal multipolar expansions [43]. This method utilizes the fact that the multipolar spectrum carries the complete information on the MHD characteristics of the plasma. The multipolar spectrum at the plasma surface is calculated for a fixed boundary plasma and the dependence of the multipolar components on the poloidal beta value is obtained for a parameter of  $\beta_p + l_i/2$ . Separation of  $\beta_p$  is rather difficult for a circular cross-sectional tokamak as previously described. And because of existence of unavoidable random error there is a threshold value for the parameter  $\beta_p + l_i/2$ , under which separation is impossible.

Recently reconstruction of the current distribution from the externally measured magnetic signals on the basis of the solution methods of the mathematical inverse problem [242, 243] is being studied extensively by several authors [244, 246].

## 7. SUMMARY AND DISCUSSION

A lot of equilibrium solvers for a tokamak plasma have been developed and used for various objectives such as the MHD stability analysis, the experimental analysis, and the design of new devices. From the viewpoint of the numerical algorithm to solve the Grad-Shafranov equation with a free boundary condition the equilibrium solvers based on the cyclic reduction methods with the Green's function formula seem most efficient. As one can utilize a large memory space in a modern computer, equilibrium calculation with extremely high resolution becomes possible by using this algorithm. Inverse equilibrium solvers have been developed to attain a high resolution calculation but due to the above fact, recently, such an approach is not necessarily an indispensable one. A variety of solution methods of the Grad-Shafranov equation is, however, still necessary because there is room for choosing the best algorithm for different applications. Especially, it is quite probable that

some iterative algorithms such as the multi-grid method will be the most effective with the advancement of parallel processing computers.

In the field of theoretical analysis of the tokamak plasma the MHD equilibrium analysis was successfully used for the beta limit calculation concerning the beta limit scaling, the shape optimization, identification of the second stability region of the ballooning instability, and so on. An early stage tokamak with a circular cross section was a low beta device, at least experimentally. But in recent tokamaks higher beta value as more than 5% is attainable, even experimentally. For calculation of the higher beta equilibrium the FCT algorithm plays an important role. As for the physics implication of the MHD equilibrium, self-consistent determination of the plasma current including neoclassical current effects becomes important and efforts are paid to the studies of equilibrium with non-ohmic current source and equilibrium evolution by using a 1.5D tokamak transport code. This is because current sustainment by NBI/RF-wave seems indispensable for future tokamaks and current drive techniques are also effective for direct control of the current profile of a confined plasma, which may be used for the stabilization of unstable MHD modes. Study of anisotropic tokamak equilibria with or without toroidal/poloidal flows is another important subject for such tokamak plasmas. The effects of  $\alpha$  particles should be considered for analyses of fusion plasmas. Numerical codes for such problems have been developed but a lot of problems remain to be analyzed. Another important problem which has not been studied extensively up to now is the search for an equilibrium optimized with respect to the confinement property of the tokamak plasma. The transport process in the tokamak is governed by anomalous ones due to electrostatic and/or electromagnetic microinstabilities. These instabilities may be suppressed by the control of the macroscopic quantities such as the shaping of the plasma cross section, the profiles of the density, temperature, and electric current. This possibility was pointed out by several authors but details still remain to be analyzed [247]. With the progress of tokamak experiments large efforts are directed to develop techniques for reconstruction of the MHD equilibrium from the experimentally measured electromagnetic data. This kind of techniques will become more and more important in the future reactor-scale devices where various kinds of measurement of the plasma behavior may be suffered from the irradiation of fusion neutrons.

Throughout this review we assumed that a tokamak has complete axisymmetry. We presented only a brief comment on the three-dimensional MHD equilibrium. However, a real tokamak device is not completely axisymmetric for various reasons, such as the existence of the rippling magnetic field. Even if a tokamak is completely axisymmetric, the symmetry of the MHD equilibrium may be broken by the occurrence of instabilities and equilibrium bifurcation with lower symmetry may be observed. Such a steady state with less symmetry may, sometimes, have a strong influence on the property of plasma confinement in a tokamak. For this kind of problems three-dimensional equilibrium/steady-state analysis is essential, for which the three-dimensional MHD equilibrium theory developed in stellarator research may be effectively used.

## ACKNOWLEDGMENTS

The authors would like to express their sincere gratitude to Drs. M. Azumi and T. Tsunematsu for valuable suggestions and discussions on various problems throughout this review article. Professor J. Todoroki is acknowledged for suggestive comments on the three-dimensional MHD equilibrium. Thanks are also due to Dr. T. Matsuura for a fruitful discussion on algorithms for a vector processor. Dr. M. Tanaka is greatly acknowledged for encouragement throughout this work.

## REFERENCES

1. L. A. ARTSIMOVICH, *Nucl. Fusion* **12**, 215 (1972).
2. H. P. FURTH, *Nucl. Fusion* **15**, 487 (1975).
3. J. A. WESSON, *Tokamaks* (Oxford Univ. Press, Oxford, 1987).
4. J. KILLEEN, *Nucl. Fusion* **16**, 841 (1976).
5. T. TAKEDA, T. TSUNEMATSU, S. TOKUDA, G. KURITA, AND T. TAKIZUKA, "MHD Computations in Tokamak Fusion Research," in *Computational Mechanics '86* (Springer-Verlag, Tokyo, 1986), Vol. 2, IX-3.
6. B. McNAMARA, *Proc. IEEE* **69**, 1043 (1981).
7. K. LACKNER, *Comput. Phys. Commun.* **12**, 33 (1976).
8. B. McNAMARA, "Equilibria of Magnetically Confined Plasmas," in *Methods in Computational Physics* (Academic Press, New York, 1976), Vol. 16, p. 211.
9. V. D. SHAFRANOV, "Plasma Equilibrium in a Magnetic Field," in *Reviews of Plasma Physics*, Vol. 2, edited by M. A. Leontovich (Consultants Bureau, New York, 1966), p. 103.
10. L. S. SOLOV'EV AND V. D. SHAFRANOV, "Plasma Confinement in Closed Magnetic Systems," in *Reviews of Plasma Physics*, Vol. 5, edited by M. A. Leontovich (Consultant Bureau, New York, 1970), p. 1.
11. G. BATEMAN, *MHD Instabilities* (MIT Press, Cambridge, MA, 1978).
12. J. P. FREIDBERG, *Rev. Mod. Phys.* **54**, 801 (1982).
13. J. P. FREIDBERG, *Ideal Magneto-Hydro-Dynamics* (Plenum, New York, 1987).
14. J. BLUM, *Numerical Simulation and Optimal Control in Plasma Physics with Applications to Tokamaks* (Wiley, Chichester, UK, 1989).
15. J. P. GOEDBLOED, FOM-Instituut voor Plasmaphysica. Rijnhuizen Report 83-145, 1979 (unpublished).
16. H. GRAD AND H. RUBIN, "Hydromagnetic Equilibria and Force-free Fields," in *United Nations Conference on the Peaceful Uses of Atomic Energy, Geneva, 1958*, Vol. 31, p. 190.
17. V. D. SHAFRANOV, *Sov. Phys. JETP* **6**, 545 (1958).
18. R. LÜST AND A. SCHLÜTER, *Z. Naturforsch.* **12B**, 850 (1957).
19. E. W. LAING, J. L. ROBERTS, AND R. T. P. WHIPPLE, *J. Nucl. Energy: Part C* **1**, 49 (1959).
20. L. S. SOLOV'EV, *Sov. Phys. JETP* **26**, 400 (1968).
21. E. MAZZUCATO, *Phys. Fluids* **18**, 536 (1975).
22. V. D. SHAFRANOV AND E. I. YURCHENKO, *Sov. Phys. JETP* **26**, 682 (1968).
23. V. D. SHAFRANOV AND E. I. YURCHENKO, *Nucl. Fusion* **8**, 329 (1968).
24. L. S. SOLOV'EV, "Hydromagnetic Stability of Closed Plasma Configurations," in *Reviews of Plasma Physics*, Vol. 6, edited by M. A. Leontovich (Consultant Bureau, New York, 1975), p. 239.
25. V. D. SHAFRANOV, *Nucl. Fusion* **3**, 183 (1963).
26. A. A. WARE AND F. A. HASS, *Phys. Fluids* **9**, 956 (1966).
27. J. M. GREENE, J. L. JOHNSON, AND K. E. WEIMER, *Phys. Fluids* **14**, 671 (1971).
28. H. R. STRAUSS, *Phys. Rev. Lett.* **26**, 616 (1971).
29. F. A. HASS, *Phys. Fluids* **15**, 141 (1972).
30. J. P. FREIDBERG AND F. A. HASS, *Phys. Fluids* **16**, 1909 (1973).
31. J. KILLEEN AND K. J. WHITEMAN, *Phys. Fluids* **9**, 1846 (1966).
32. J. D. CALLEN AND R. A. DORY, *Phys. Fluids* **15**, 1523 (1972).

33. K. LACKNER, *J. Geophys. Res.* **75**, 16 (1970).
34. B. MARDER AND H. WEITZNER, *Plasma Phys.* **12**, 435 (1970).
35. S. FISHER, *Phys. Fluids* **14**, 962 (1971).
36. W. FENEBERG AND K. LACKNER, *Nucl. Fusion* **13**, 549 (1973).
37. K. V. HAGENOW AND K. LACKNER, in *Proceedings, 7th Conference on the Numerical Simulation of Plasmas, New York, 1975*, p. 140.
38. J. L. JOHNSON, H. E. DALHED, J. M. GREENE, R. C. GRIMM, Y. Y. HSIEH, S. C. JARDIN, J. MANICKAM, M. OKABAYASHI, R. C. STORER, A. M. M. TODD, D. E. VOSS, AND K. E. WEIMER, *J. Comput. Phys.* **32**, 212 (1979).
39. Y. SUZUKI, *Nucl. Fusion* **14**, 345 (1974).
40. H. NINOMIYA, Y. SUZUKI, AND A. KAMEARI, Japan Atomic Energy Research Institute Report JAERI-M 6026, 1975 (unpublished). [Japanese]
41. H. NINOMIYA, A. KAMEARI, AND K. SHINYA, Japan Atomic Energy Research Institute Report JAERI-M 9127, 1980 (unpublished). [Japanese]
42. S. SEKI, H. MAEDA, A. KITSUNEZAKI, AND R. SAITO, Japan Atomic Energy Research Institute Report JAERI-M 6734, 1976 (unpublished). [Japanese]
43. F. ALLADIO AND F. CRISANTI, *Nucl. Fusion* **26**, 1143 (1986).
44. S. SEMENZATO, R. GRUBER, AND H. P. ZEHRFELD, *Comput. Phys. Rep.* **1**, 389 (1984).
45. W. KERNER AND O. JANDL, *Comput. Phys. Commun.* **31**, 269 (1984).
46. J. P. GOEDBLOED, *Comput. Phys. Commun.* **24**, 311 (1981).
47. P. N. VABISHCHEVICH, L. M. DEGTYAREV, AND A. P. FAVOSKII, *Sov. J. Plasma Phys.* **4**, 554 (1978).
48. T. TAKEDA AND T. TSUNEMATSU, Japan Atomic Energy Research Institute Report JAERI-M 8042, 1979 (unpublished).
49. J. DELUCIA, S. C. JARDIN, AND A. M. M. TODD, *J. Comput. Phys.* **37**, 183 (1980).
50. L. L. LAO, S. P. HIRSHMAN, AND R. M. WIELAND, *Phys. Fluids* **24**, 1431 (1981).
51. H. R. HICKS, R. A. DORY, AND J. A. HOLMES, *Comput. Phys. Rep.* **1**, 373 (1984).
52. S. H. HANEY, thesis, Massachusetts Institute of Technology Report PFC/RR-88-12, 1988 (unpublished).
53. R. A. DORY AND Y.-K. M. PENG, *Nucl. Fusion* **17**, 21 (1977).
54. J. F. CLARKE AND D. J. SIGMAR, *Phys. Rev. Lett.* **38**, 70 (1977).
55. T. MIZOGUCHI, T. KAMMASHI, AND D. J. SIGMAR, *Phys. Fluids* **21**, 2986 (1978).
56. G. O. SPIES, Max-Planck Institut für Plasmaphysik Report IPP 6/181, 1979 (unpublished).
57. D. B. NELSON, "Intense Neutral Beam Heating in the Adiabatic Approximation," in *Proceedings, Workshop on High Beta Plasma, Varenna, Italy 1977*, CONF-7709167, p. 173.
58. D. B. ALBERT, *Nucl. Fusion* **20**, 939 (1980).
59. L. A. CHARLTON, R. A. DORY, Y.-K. M. PENG, D. J. STRICKLER, S. J. LINCH, D. K. R. LEE, R. GRUBER, AND F. TROYON, *Phys. Rev. Lett.* **43**, 1395 (1979).
60. M. AZUMI, T. TSUNEMATSU, K. ITOH, T. TUDA, G. KURITA, T. TAKEDA, T. TAKIZUKA, S. TOKUDA, T. MATSUURA, Y. TANAKA, S. INOUE, AND M. TANAKA, "Evolution of Stable High Beta Tokamak Equilibria," in *Plasma Physics and Controlled Nuclear Fusion Research, 1980* (IAEA, Vienna, 1981), Vol. 1, p. 293.
61. L. A. CHARLTON, D. B. NELSON, AND R. A. DORY, *Phys. Rev. Lett.* **45**, 24 (1980).
62. D. DOBROTT, M. S. CHU, AND T. OHKAWA, *Phys. Fluids* **16**, 1870 (1973).
63. H. A. B. BODIN AND A. A. NEWTON, *Nucl. Fusion* **20**, 1255 (1980).
64. T. OHKAWA AND W. D. KERST, *Phys. Rev. Lett.* **7**, 41 (1961).
65. S. A. COLGATE AND H. P. FURTH, *Phys. Fluids* **3**, 982 (1960).
66. S. YOSHIKAWA AND U. CHRISTENSEN, *Phys. Fluids* **9**, 2295 (1966).
67. J. M. GREENE AND J. L. JOHNSON, *Plasma Phys.* **9**, 611 (1967).
68. J. M. GREENE AND J. L. JOHNSON, *Plasma Phys.* **10**, 729 (1968).
69. F. L. HINTON AND R. D. HAZELTINE, *Rev. Mod. Phys.* **48**, 239 (1976).
70. M. D. KRUSKAL, J. L. JOHNSON, M. B. GOTTLIEB, AND L. M. GOLDMAN, *Phys. Fluids* **1**, 421 (1958).
71. V. D. SHAFRANOV, *Plasma Phys.* **13**, 757 (1971).

72. L. E. ZAKHAROV AND V. D. SHAFRANOV, *Sov. Phys. Tech. Phys.* **18**, 151 (1973).
73. L. E. ZAKHAROV AND V. D. SHAFRANOV, "Equilibrium of Current-Carrying Plasmas in Toroidal Configurations," in *Reviews of Plasma Physics*, Vol. 11, edited by M. A. Leontovich (Consultant Bureau, New York, 1986), p. 153.
74. V. D. SHAFRANOV, *Plasma Phys. (J. Nucl. Energy Part C)* **5**, 251 (1963).
75. V. D. SHAFRANOV, *Nucl. Fusion* **4**, 232 (1964).
76. R. TEMAM, *Arch. Rat. Mech. Anal.* **60**, 51 (1975).
77. H. BERESTYCKI AND H. C. R. BRÉZIS, *Acad. Sci. Paris Ser. A* **283**, 1091 (1976).
78. R. COURANT AND D. HILBERT, *Methoden der Mathematischen Physik II* (Springer-Verlag, Berlin, 1937).
79. D. KINDERLEHRER AND G. STAMPACCHIA, *An Introduction to Variational Inequalities and Their Applications* (Academic Press, New York, 1980).
80. F. KIKUCHI, *Theor. Appl. Mech.* **29**, 319 (1981).
81. J. RAPPAZ, *Numer. Math.* **45**, 117 (1984).
82. F. KIKUCHI, K. NAKAZATO, AND T. USHIJIMA, *Japan J. Appl. Math.* **1**, 369 (1984).
83. J. DIEUDONNÉ, *Foundations of Modern Analysis* (Academic Press, New York, 1969).
84. M. REED AND B. SIMON, *Methods of Modern Mathematical Physics. Vol. I. Functional Analysis* (Academic Press, New York, 1980).
85. F. KIKUCHI AND T. AIZAWA, "Finite Element Analysis of Equilibria of Ideal MHD Plasmas in Torus Regions," in *Finite Elements in Fluids*. Vol. 5, edited by R. H. Gallagher, J. T. Oden, O. C. Zienkiewicz, T. Kawai, and M. Kawahara (Wiley, New York, 1984), p. 311.
86. G. CALOZ AND J. RAPAZ, *Comput. Phys. Commun.* **31**, 137 (1984).
87. V. D. SHAFRANOV AND L. E. ZAKHAROV, *Nucl. Fusion* **12**, 599 (1972).
88. L. E. ZAKHAROV, *Nucl. Fusion* **13**, 595 (1973).
89. H. YOSHIDA, H. NINOMIYA, M. AZUMI, AND S. SEKI, *J. Comput. Phys.* **63**, 477 (1986).
90. J. BLUM, J. LE FOLL, AND B. THOORIS, *Comput. Phys. Commun.* **24**, 235 (1981).
91. H. GRAD, P. N. HU, AND D. C. STEVENS, *Proc. Nat. Acad. Sci. USA* **72**, 3789 (1975).
92. Y.-K. M. PENG, R. A. DORY, D. B. NELSON, AND R. O. SAYER, *Phys. Fluids* **21**, 467 (1978).
93. J. P. PUEL, "Un problème de valeur propre nonlinéaire et de frontière libre," in *Journées d'Analyse Nonlinéaire*, (Springer-Verlag, Berlin, 1978), p. 188.
94. K. GEORG, *Numer. Math.* **32**, 69 (1978).
95. R. MEYER-SPASCHE, *Numer. Math.* **33**, 303 (1979).
96. M. SEMANGE, *Appl. Math. Optim.* **5**, 127 (1979).
97. V. S. MUKHOVATOV AND V. D. SHAFRANOV, *Nucl. Fusion* **11**, 605 (1971).
98. F. J. HELTON AND T. S. WANG, *Nucl. Fusion* **18**, 1523 (1978).
99. R. W. HOCKNEY, "The Potential Calculation and Some Applications," in *Methods in Computational Physics* (Academic Press, New York, 1970), Vol. 9, p. 135.
100. J. P. CHRISTIANSEN AND R. W. HOCKNEY, *Comput. Phys. Commun.* **2**, 129 (1971).
101. O. BUNEMAN, Stanford University Report SUITPR-294, 1968 (unpublished).
102. R. D. RICHTMYER AND K. W. MORTON, *Difference Methods for Initial-Value Problems*. 2nd ed. (Interscience, New York, 1967).
103. R. S. VARGA, *Matrix Iterative Analysis* (Prince-Hall, Englewood Cliffs, NJ, 1962).
104. G. STRANG, *Linear Algebra and Its Applications* (Academic Press, New York, 1976).
105. L. A. HAGEMAN AND D. M. YOUNG, *Applied Iterative Methods* (Academic Press, New York, 1981).
106. D. M. YOUNG, *Comput. Phys. Commun.* **53**, 1 (1989).
107. A. BRANDT, *Math. Comput.* **31**, 333 (1977).
108. W. HACKBUSCH AND U. TROTTERBERG (Eds.), *Multigrid Methods, Proceedings Köln-Forz, 1981*, Lecture Notes in Math., Vol. 960 (Springer-Verlag, Berlin, 1982).
109. W. L. BRIGGS, *A Multigrid Tutorial* (SIAM, Philadelphia, 1987).
110. W. HACKBUSCH, *Multi-Grid Methods and Applications* (Springer-Verlag, Berlin, 1985).
111. W. HACKBUSCH, *SIAM J. Numer. Anal.* **16**, 201 (1979).
112. B. J. BRAAMS, Max-Planck-Institut für Plasmaphysik Report IPP 5-6, 1985 (unpublished).

113. C. A. FELIPPA, thesis, University of California at Berkeley, 1966 (unpublished).
114. R. J. MELOSH, *AIA Aerospace J.* **1**, 1631 (1963).
115. H. NINOMIYA, Y. SUZUKI, AND A. KAMEARI, Japan Atomic Energy Research Institute Report JAERI-M 6025, 1975 (unpublished). [Japanese]
116. P. M. MORSE AND H. FESHBACH, *Methods of Theoretical Physics* (McGraw-Hill, New York, 1953).
117. A. J. WOOTTON, *Nucl. Fusion* **19**, 987 (1979).
118. D. K. LEE AND Y.-K. M. PENG, *J. Plasma Phys.* **25**, 161 (1981).
119. L. V. AHLFORS, *Complex Analysis* (McGraw-Hill, Auckland, 1985).
120. J. A. HOLMES, Y.-K. M. PENG, AND S. J. LYNCH, *J. Comput. Phys.* **36**, 35 (1980).
121. V. D. SHAFRANOV, *Nucl. Fusion* **8**, 253 (1968).
122. J. M. GREENE, J. L. JOHNSON, AND K. E. WEIMER, *Phys. Fluids* **14**, 43 (1971).
123. S. TOKUDA, T. TSUNEMATSU, AND T. TAKEDA, Japan Atomic Energy Research Institute Report JAERI-M 86-171, 1986 (unpublished). [Japanese]
124. R. C. GRIMM, J. M. GREENE, AND J. L. JOHNSON, "Computation of the Magnetohydrodynamic Spectrum in Axisymmetric Toroidal Confinement System," in *Methods in Computational Physics*, Vol. 16 (Academic Press, New York, 1976), p. 253.
125. R. GRUBER, F. TROYON, D. BERGER, L. C. BERNARD, S. ROUSSET, R. SCHREIBER, W. KERNER, W. SCHNEIDER, AND K. V. ROBERTS, *Comput. Phys. Commun.* **21**, 323 (1981).
126. S. TOKUDA, T. TSUNEMATSU, M. AZUMI, T. TAKIZUKA, K. NARAOKA, AND T. TAKEDA, Japan Atomic Energy Research Institute Report JAERI-M 9899, 1982 (unpublished). [Japanese]
127. T. N.E. GREVILLE, "Spline Functions, Interpolation and Numerical Quadrature," in *Mathematical Methods for Digital Computers*, Vol. 2 (Wiley, New York, 1967).
128. T. MATSUURA, Y. TANAKA, K. NARAOKA, T. TAKIZUKA, T. TSUNEMATSU, S. TOKUDA, M. AZUMI, G. KURITA, AND T. TAKEDA, *Comput. Phys. Commun.* **26**, 377 (1982).
129. T. MATSUURA, Fujitsu, Tokyo, private communications.
130. R. W. HOCKNEY AND C. R. JESSHOPE, *Parallel Computers* (Adam Hilger, Bristol, 1981), p. 342.
131. H. P. ZEHRFELD AND B. J. GREEN, *Nucl. Fusion* **12**, 569 (1972).
132. W. KERNER AND S. TOKUDA, *Z. Naturforsch.* **42a**, 1154 (1987).
133. B. J. GREEN AND H. P. ZEHRFELD, *Nucl. Fusion* **13**, 750 (1973).
134. E. J. HAMEIRI, *Phys. Fluids* **26**, 230 (1983).
135. E. J. HAMEIRI, *Plasma Phys.* **22**, 245 (1979).
136. A. B. HASSAM AND R. M. KULSRUD, *Phys. Fluids* **21**, 2271 (1978).
137. J. W. CONNOR, S. C. COWLEY, R. J. HASTIE, AND L. R. PAN, *Plasma Phys. Controlled Fusion* **29**, 919 (1987).
138. S. P. HIRSHMAN, *Nucl. Fusion* **18**, 917 (1978).
139. G. F. CHEW, M. L. GOLDBERGER, AND F. E. LOW, *Proc. Roy. Soc. London A* **236**, 112 (1956).
140. H. GRAD, *Phys. Fluids* **10**, 137 (1967).
141. G. O. SPIES AND D. B. NELSON, *Phys. Fluids* **17**, 1879 (1974).
142. G. O. SPIES AND D. B. NELSON, *Phys. Fluids* **17**, 1865 (1974).
143. W. A. COOPER, G. BATEMAN, D. B. NELSON, AND T. KAMMASH, *Nucl. Fusion* **20**, 985 (1980).
144. E. R. SALBERTA, R. C. GRIMM, J. L. JOHNSON, J. MANICKAM, AND W. M. TANG, *Phys. Fluids* **30**, 2796 (1987).
145. S. P. HIRSHMAN, *Phys. Fluids* **21**, 1295 (1978).
146. S. P. HIRSHMAN AND D. J. SIGMAR, *Nucl. Fusion* **21**, 1079 (1981).
147. N. J. FISCH, *Rev. Mod. Phys.* **59**, 175 (1987).
148. D. A. EHST, K. EVANS, JR., AND D. W. IGNAT, *Nucl. Fusion* **26**, 461 (1986).
149. K. OKANO, Y. OGAWA, AND H. NAITOU, Institute for Plasma Physics Report IPPJ-878, 1988 (unpublished).
150. K. TANI AND M. AZUMI, private communication; see also K. TANI, M. SUZUKI, S. YAMAMOTO, AND M. AZUMI, Japan Atomic Energy Research Institute Report JAERI-M 88-042, 1988 (unpublished).
151. S. TOKUDA, T. TAKEDA, AND M. OKAMOTO, *J. Phys. Soc. Japan* **58**, 871 (1989).
152. Y. B. KIM, University of Wisconsin Plasma Report UWPR 88-2, 1988 (unpublished).

153. C. MERCIER AND SOUBBARAMAYER, in *Proceedings, 4th European Conference on Controlled Fusion and Plasma Physics, 1970*, p. 16.
154. Y. N. DNESTROVSKII, D. P. KOSTMAROV, AND N. L. PAVLOVA, in *Proceedings, 4th European Conference on Controlled Fusion and Plasma Physics, 1970*, p. 17.
155. D. F. DUCHS, D. E. POST, AND P. H. RUTHERFORD, *Nucl. Fusion* **17**, 565 (1977).
156. C. MERCIER, J. P. BOUJOT, AND F. WERKOFF, *Comput. Phys. Commun.* **12**, 109 (1976).
157. J. T. HOGAN, "Multifluid Tokamak Transport Models," in *Methods in Computational Physics*, Vol. 16, edited by B. Alder, S. Fernbach, and M. Rotenberg (Academic Press, New York, 1976), p. 131.
158. C. E. SINGER, D. E. POST, D. R. MIKKELSEN, M. H. REDI, A. MCKENNEY, A. SILVERMAN, F. G. P. SEIDL, P. H. RUTHERFORD, R. J. HAWRYLUK, W. D. LARGER, L. FOOTE, D. B. HEIFETZ, W. A. HOULBERG, M. H. HUGHES, R. V. JENSEN, G. LISTER, AND J. OGDEN, *Comput. Phys. Commun.* **49**, 275 (1988).
159. H. GRAD, P. N. HU, D. C. STEVENS, AND E. TURKEL, "Classical Plasma Diffusion," in *Plasma Physics and Controlled Nuclear Fusion Research 1976* (IAEA, Vienna, 1977), Vol. II, p. 355.
160. H. GRAD AND J. T. HOGAN, *Phys. Rev. Lett.* **24**, 1337 (1970).
161. Y.-P. PAO, *Phys. Fluids* **19**, 1177 (1976).
162. F. J. HELTON, R. L. MILLER, AND J. M. J. RAWLS, *Comput. Phys.* **24**, 117 (1977).
163. J. T. HOGAN, *Nucl. Fusion* **19**, 753 (1979).
164. R. L. MILLER, *Nucl. Fusion* **20**, 133 (1980).
165. M. AZUMI, G. KURITA, T. MATSUURA, T. TAKEDA, Y. TANAKA, AND T. TSUNAMATSU, "A Fluid Model Numerical Code System for Tokamak Fusion Research," in *Computing Methods in Applied Sciences and Engineering*, edited by R. Glowinski and J. L. Lions (North-Holland, Amsterdam, 1980), p. 335.
166. J. BLUM AND J. LE FOLL, *Comput. Phys. Rep.* **1**, 465 (1984).
167. S. P. HIRSHMAN AND S. C. JARDIN, *Phys. Fluids* **22**, 731 (1979).
168. A. D. TURNBULL AND R. G. STORER, *J. Comput. Phys.* **50**, 409 (1983).
169. S. C. JARDIN, N. POMPHREY, AND J. DELUCIA, *J. Comput. Phys.* **66**, 481 (1986).
170. S. C. JARDIN, J. DELUCIA, M. OKABAYASHI, N. POMPHREY, M. REUSCH, S. KAYE, AND H. TAKAHASHI, *Nucl. Fusion* **27**, 569 (1987).
171. S. C. JARDIN, A. JANOS, AND M. YAMADA, *Nucl. Fusion* **26**, 647 (1986).
172. L. M. KOVRIZHNYKH AND S. V. SHCHEPETOV, *Sov. Phys. Usp. Engl. Transl.* **29**, 343 (1986).
173. K. TANI, T. TAKIZUKA, M. AZUMI, AND H. KISHIMOTO, *Nucl. Fusion* **23**, 657 (1983).
174. L. M. KOVRIZHNYKH, *Nucl. Fusion* **24**, 851 (1984).
175. R. B. WHITE, "Resistive Instabilities and Field Line Reconnection," in *Handbook of Plasma Physics*, edited by A. A. Galeev and R. N. Sudan (North-Holland, Amsterdam, 1983), Vol. 1.
176. K. KOTSCHENREUTHER, R. D. HAZELTINE, AND P. J. MORRISON, *Phys. Fluids* **28**, 294 (1985).
177. R. CHODURA AND A. SCHLÜTER, *J. Comput. Phys.* **41**, 68 (1981).
178. F. BAUER, O. BETANCOURT, AND P. GARABEDIAN, *A Computational Method in Plasma Physics* (Springer-Verlag, New York, 1978).
179. T. C. HENDER, B. A. CARRERAS, L. GARCIA, J. A. ROME, AND V. E. LYNCH, *J. Comput. Phys.* **50**, 76 (1985).
180. S. P. HIRSHMAN AND J. C. WHITSON, *Phys. Fluids* **26**, 3553 (1983).
181. S. P. HIRSHMAN AND H. K. MEIER, *Phys. Fluids* **28**, 1387 (1985).
182. L. L. LAO, J. M. GREENE, T. S. WANG, F. J. HELTON, AND E. M. ZAWADZKI, *Phys. Fluids* **28**, 869 (1985).
183. S. P. HIRSHMAN AND D. K. LEE, *Comput. Phys. Commun.* **39**, 161 (1986).
184. M. WAKATANI, *Kakuyugo Kenkyu* **54**, 175 (1985).
185. A. H. BOOZER, *Phys. Fluids* **27**, 2110 (1984).
186. L. SPITZER, *Phys. Fluids* **1**, 253 (1958).
187. A. H. REIMAN AND H. S. GREENSIDE, *Comput. Phys. Commun.* **43**, 157 (1986).
188. H. S. GREENSIDE, A. H. REIMAN, AND A. SALAS, *J. Comput. Phys.* **81**, 102 (1989).

189. A. H. REIMAN AND A. H. BOOZER, *Phys. Fluids* **27**, 2446 (1984).
190. J. L. JOHNSON AND A. H. REIMAN, *Nucl. Fusion* **28**, 1116 (1988).
191. J. M. GREENE AND J. L. JOHNSON, *Phys. Fluids* **4**, 875 (1961).
192. M. WAKATANI, *Nucl. Fusion* **18**, 1499 (1978).
193. H. R. STRAUSS, *Plasma Phys.* **22**, 733 (1980).
194. L. M. KOVRIZHNYKH AND S. V. SHCHEPETOV, *Sov. J. Plasma Phys.* **6**, 533 (1980).
195. V. D. PUSTOVITOV, *Nucl. Fusion* **23**, 1079 (1983).
196. B. A. CARRERAS, H. R. HICKS, J. A. HOLMES, V. E. LYNCH, L. GARCIA, J. H. HARRIS, T. C. HENDER, AND B. F. MASDEN, *Phys. Fluids* **26**, 3569 (1983).
197. L. M. KOVRIZHNYKH AND S. V. SHCHEPETOV, *Nucl. Fusion* **23**, 859 (1983).
198. M. I. MIKHAILOV, V. D. PUSTOVITOV, AND V. D. SHAFRANOV, *JETP Lett.* **35**, 186 (1982).
199. J. TODOROKI, *J. Phys. Soc. Japan* **56**, 128 (1987).
200. J. TODOROKI, *J. Phys. Soc. Japan* **58**, 3979 (1989).
201. T. C. HENDER, B. A. CARRERAS, L. A. CHARLTON, L. GARCIA, H. R. HICKS, J. A. HOLMES, AND V. E. LYNCH, *Nucl. Fusion* **25**, 1463 (1985).
202. A. M. M. TODD, J. MANICKAM, M. OKABAYASHI, M. S. CHANCE, R. C. GRIMM, J. M. GREENE, AND J. L. JOHNSON, *Nucl. Fusion* **19**, 743 (1979).
203. L. C. BERNARD, D. DOBROTT, F. J. HELTON, AND R. W. MOORE, *Nucl. Fusion* **20**, 1199 (1980).
204. T. TUDA, M. AZUMI, K. ITOH, G. KURITA, T. TAKEDA, T. TAKIZUKA, S. TOKUDA, T. TSUNEMATSU, M. ADACHI, Y. TANAKA, M. WATANABE, AND S.-I. ITOH, "Accessible Beta Values of Tokamaks," in *Plasma Physics and Controlled Nuclear Fusion Research 1984* (IAEA, Vienna, 1985), Vol. 2, p. 173.
205. F. TROYON, R. GRUBER, H. SAURENMANN, S. SEMENZATO, AND S. SUCCI, *Plasma Phys. Controlled Fusion* **26**, 209 (1984).
206. R. L. MILLER AND R. W. MOORE, *Phys. Rev. Lett.* **43**, 765 (1979).
207. J. MANICKAM, R. C. GRIMM, AND M. OKABAYASHI, *Phys. Rev. Lett.* **51**, 1959 (1983).
208. M. S. CHANCE, S. C. JARDIN, AND T. H. STIX, *Phys. Rev. Lett.* **51**, 1963 (1983).
209. R. C. GRIMM, M. S. CHANCE, A. M. M. TODD, J. MANICKAM, M. OKABAYASHI, W. M. TANG, R. L. DEWAR, H. FISHMAN, S. L. MENDELSON, D. A. MONTICELLO, M. W. PHILLIPS, AND M. REUSCH, *Nucl. Fusion* **25**, 805 (1985).
210. K. YAMAZAKI, T. AMANO, H. NAITOU, AND M. AZUMI, *Nucl. Fusion* **25**, 1543 (1985).
211. F. J. HELTON, M. S. CHU, J. M. GREENE, R. W. HARVEY, J. K. LEE, T. OHKAWA, AND P. A. POLITZER, "Ellipsoidal Shell Tokamak," in *Plasma Physics and Controlled Nuclear Fusion Research 1986* (IAEA, Vienna, 1987), Vol. 2, p. 45.
212. Y.-K. M. PENG AND D. J. STRICKLER, *Nucl. Fusion* **26**, 769 (1986).
213. B. A. CARRERAS, L. A. CHARLTON, J. T. HOGAN, J. A. HOLMES, E. A. LAZARUS, W. A. COOPER, AND T. C. HENDER, "MHD Stability in Low-Aspect-Ratio Tokamaks," in *Plasma Physics and Controlled Nuclear Fusion Research 1986* (IAEA, Vienna, 1987), Vol. 2, p. 53.
214. J. A. HOLMES, L. A. CHARLTON, J. T. HOGAN, B. A. CARRERAS, AND E. A. LAZARUS, *Phys. Fluids B* **1**, 358 (1989).
215. B. B. KADOMTSEV AND O. P. POGUTSE, *Nucl. Fusion* **11**, 67 (1971).
216. A. H. GLASSER, E. A. FREEMAN, AND S. YOSHIKAWA, *Phys. Fluids* **17**, 181 (1974).
217. R. L. MILLER, M. S. CHU, R. R. DOMINGUEZ, AND T. OHKAWA, *Comments Plasma Phys. Controlled Fusion* **12**, 125 (1989).
218. C. M. BISHOP AND J. B. TAYLOR, *Phys. Fluids* **29**, 1144 (1986).
219. L. L. LAO, E. J. STRAIT, T. S. TAYLOR, M. S. CHU, T. OZEKI, W. HOWL, R. D. STAMBAUGH, K. H. BURREL, M. S. CHANCE, J. C. DEBOO, P. GOHIL, J. M. GREENE, R. J. GROEBNER, A. G. KELLMAN, M. ALI MAHDavi, T. H. OSBORNE, G. PORTER, AND A. D. TURNBULL, *Plasma Phys. Controlled Fusion* **31**, 509 (1989).
220. J. W. CONNOR, R. J. HASTIE, AND J. B. TAYLOR, *Proc. Roy. Soc. A* **365**, 1, (1979).
221. T. TSUNEMATSU, S. TOKUDA, T. NEMOTO, M. AZUMI, AND T. TAKEDA, Japan Atomic Energy Research Institute Report JAERI-M 86-172, 1986 (unpublished).

222. S. SEKI, T. TSUNEMATSU, M. AZUMI, AND T. NEMOTO, *Nucl. Fusion* **27**, 330 (1987).
223. C. MERCIER, *Nucl. Fusion* **1**, 47 (1960).
224. A. N. TIKHONOV, *Dokl. Akad. Nauk SSSR* **151**, 501 (1963).
225. K. TOI AND T. TAKEDA, *Japan. J. Appl. Phys.* **16**, 325 (1977).
226. J. A. WESSON, *Nucl. Fusion* **18**, 87 (1978).
227. E. REBMAN, *Nucl. Fusion* **15**, 277 (1975).
228. M. KUMAGAI, T. TSUNEMATSU, S. TOKUDA, AND T. TAKEDA, Japan Atomic Energy Research Institute Report JAERI-M 83-085, 1983 (unpublished). [Japanese]
229. T. OZEKI, M. AZUMI, H. NINOMIYA, S. TOKUDA, T. TSUNEMATSU, AND S. SEKI, *Nucl. Fusion* **28**, 1859 (1988).
230. H. NINOMIYA, Y. SUZUKI, AND A. KAMEARI, *Japan. J. Appl. Phys.* **15**, 2201 (1976).
231. J. L. LUXON AND B. B. BROWN, *Nucl. Fusion* **22**, 813 (1982).
232. J. P. CHRISTIANSEN AND J. B. TAYLOR, *Nucl. Fusion* **22**, 111 (1982).
233. J. P. CHRISTIANSEN, J. D. CALLEN, J. J. ELLIS, AND R. S. GRANETZ, *Nucl. Fusion* **29**, 703 (1989).
234. R. S. GRANETZ AND P. SMEULDERS, *Nucl. Fusion* **28**, 457 (1988).
235. M. BRUSATI, J. P. CHRISTIANSEN, J. G. CODEY, K. JARRETT, E. LAZZARO, AND R. T. ROSS, *Comput. Phys. Rep.* **1**, 345 (1984).
236. W. FENEBERG, K. LACKNER, AND P. MARTIN, *Comput. Phys. Commun.* **31**, 143 (1984).
237. D. W. SWAIN AND G. H. NEILSON, *Nucl. Fusion* **22**, 1015 (1982).
238. L. L. LAO, H. ST. JOHN, R. D. STAMBAUGH, AND W. PFEIFFER, *Nucl. Fusion* **25**, 1421 (1985).
239. S. TSUJI, K. HAYASHI, H. YOSHIDA, N. HOSOGANE, M. KIKUCHI, R. YOSHINO, H. NINOMIYA, AND S. SEKI, Japan Atomic Energy Research Institute Report JAERI-M 86-006, 1986 (unpublished). [Japanese]
240. J. P. CHRISTIANSEN, *J. Comput. Phys.* **73**, 85 (1987).
241. G. F. COGGINS, Central Instruments Laboratory, ICI Research Note 64/11, 1964 (unpublished).
242. A. N. TIKHONOV AND V. Y. ARSENIN, *Solutions of Ill-Posed Problems*, translated by F. John (Winston/Wiley, Washington, DC, 1977).
243. *Inverse Problems*, edited by G. TALENTI, Lecture Notes in Mathematics (Springer-Verlag, Berlin, 1986).
244. YU. K. KUZNETSOV, V. N. RYUTOV, AND I. V. YASIN, *Sov. J. Plasma Phys.* **13**, 75 (1987).
245. P. N. VABISCHCHEVICH AND I. V. ZOTOV, *Sov. J. Plasma Phys.* **13**, 373 (1987).
246. P. N. VABISCHCHEVICH AND I. V. ZOTOV, *Sov. J. Plasma Phys.* **14**, 759 (1988).
247. K. ITOH AND S-I. ITOH, National Institute for Fusion Studies, Nagoya, private communication.